A Study on Turn-to-Turn Insulation of Medium Voltage Motors Fed by Variable Frequency Drives

by

Ibrahim Marwan Jarrar

A thesis

presented to the University of Waterloo

in fulfillment of the

thesis requirement for the degree of

Doctor of Philosophy

in

Electrical and Computer Engineering

Waterloo, Ontario, Canada, 2022

Examining Committee Membership

The following served on the Examining Committee for this thesis. The decision of the Examining Committee is by majority vote.

External Examiner	Behzad Kordi Professor
Supervisor(s)	Shesha Jayaram Professor Edward A. Cherney Adjunct Professor
Internal Member	Sahar Pirooz Azad Assistant Professor
Internal Member	Ayman El-Hag Definite Term Lecturer
Internal-external Member	Alexander Penlidis Professor

Author's Declaration

I hereby declare that I am the sole author of this thesis. This is a true copy of the thesis, including any required final revisions, as accepted by my examiners.

I understand that my thesis may be made electronically available to the public.

Abstract

The use of inverter drives in machine applications is expanding rapidly due to their advantages in terms of energy savings and speed control. Advances in the inverter drive industry have made it possible for inverter drives to be used in medium and high voltage applications. The pulse width modulation (PWM) approach, which is often employed in motor inverter drives, is one of the most popular techniques used to generate the output waveform. Unlike AC-fed machines, the voltage waveform generated through PWM is comprised of multi-width square shape impulses of short rise time and high repetition rate to generate the final AC voltage at the targeted fundamental frequency. The downside is that these drives cause extra stresses on machine insulation that AC-fed machines do not experience. These inherited stresses that accompany the PWM waveform accelerate the ageing of machine insulation and have led to premature failures. As a result, recognizing these stresses is critical for evaluating the endurance of machines turn insulation.

In this research, therefore, the impact of the waveform switching frequency, overshoot and rise time on the time-to-failure and the endurance of Type II machine insulation is investigated. Reference life curves at 1 kHz and 4 kHz are derived utilizing unipolar repetitive square-impulses of 15% overshoot and 300 ns rise time. The effects of the impulse overshoot and rise time in the ranges of 0% to 30% and 400 ns to 1000 ns are also evaluated and reflected on the established reference life plots. Moreover, an antenna-based partial discharge (PD) measurement system is utilized to record and investigate the significant factors affecting the life performance of the insulation systems. Two types of samples are used in this work; a back-to-back turn insulation sample and a single cavity layered insulation. The influence of varying the switching frequency, the rise time, and the overshoot components on the characteristics of the PDs during ageing are investigated to identify the effect of each factor while relating their influence on the life of turn insulation. The interaction between these factors is highlighted and examined utilizing the design of experiment principles. Finite element method simulation using COMSOL® Multiphysics is also utilized to explain and support the experimental findings and to suggest and describe the ageing and failure mechanism associated with the test samples.

Based on the endurance test results, the analysis of PD measurements, and the reported time-to-failure data, it is evident that turn insulation is subjected to additional stress factors when energized by an inverter supply as opposed to the stresses exhibited by sinusoidal waves. This indicates an

incomparable ageing rate between the two types of waveforms, even at similar peak voltages applied, resulting in inadequate use of sinusoidal supply to qualify inverter-fed machines. The overshoot component of the waveform is found to have a substantial impact on the endurance of turn insulation apart from the jump voltage impact, and therefore, is identified as a significant factor influencing the life of turn insulation independent from other factors. Moreover, the reported results of the time-to-failure analysis and the PD measurements advocate a non-linear relationship between the switching frequency and the life of turn insulation, whereas the waveform rise time is found to have a negligible but consistent impact within the considered range.

Acknowledgements

I want to start by thanking God for providing me with this chance to pursue my Ph.D. degree and for giving me the stamina and strength to complete it.

I would like to thank my supervisors, Prof. Edward Cherney and Prof. Shesha Jayaram for their assistance, support, and guidance throughout this work.

I wish to express my gratitude to the members of my Ph.D. committee; Prof. Behzad Kordi, Prof. Alexander Penlidis, Prof. Ayman El-Hag, Prof. Sahar Pirooz Azad, and Prof. Magdy Salama who honoured me by being on the committee of my thesis examination.

My special thanks go to Dr. Greg Stone from Iris Power and Prof. Kazimierz Adamiak from the University of Western for their guidance and valuable comments and discussions during this work. I would like also to thank Mr. Ashish Trivedi from Motion Electric for all of his help in providing the material and preparing the turn insulation samples.

I am also grateful to all my colleagues and friends from the high voltage engineering laboratory; you all have contributed to my learning experience. A special thanks to Amin and Anurag for all the productive discussions and the wonderful times experienced throughout these challenging times.

My deepest gratitude goes to all the members of my family: my dear mother, whose love and prayers are with me in whatever I pursue, my darling wife and sons for their understanding and support throughout this journey, and my wonderful brothers and sisters for all the support and inspiration they provided to complete this important milestone in my life

I gratefully acknowledge the financial support provided by the University of Waterloo and the Natural Sciences and Engineering Research Council of Canada (NSERC).

Dedication

To my father,

though you never got to see this, you were in my mind and heart during every moment of it. You are, and will be always, alive in my heart. May God almighty have mercy on your soul.

Table of Contents

List of Figures

List of Tables

Chapter 1
Introduction

Rotating machines account for more than one-half of today's electrical loads and energy consumption [1], [2]. Due to their extensive application, more than 90% of these machines are induction motors. With the introduction of variable frequency drives (VFDs), also known as adjustable speed drives (ASDs), more and more induction motors are being retrofitted to be used with these drives. Nearly all of these motors were originally designed to work at power frequency. However, with VFDs, the voltage that supplies these motors is a synthesized sinusoidal voltage that contains many harmonics [2]. One of the most popular techniques for generating this kind of supply is the pulse width modulation (PWM) technique used in voltage source converters (VSCs). Although the supply of these converters may have a variable fundamental frequency that can extend beyond the 50/60 Hz standard AC supply, it still consists of multi-width square impulses applied at a much higher frequency, commonly referred to as switching frequency (f_{sw}), to produce the output sinusoidal supply. The use of VFD has introduced several advantages to industries in terms of applications, power efficiency, and motor control to name a few; however, these advantages come with an additional cost. The PWM supply imposes new stresses on motor insulation that were not accounted for during sinusoidal-fed motor testing. These stresses include the fast repetitive impulses of short rise time (t_r), and a significant jump voltage (U_j) and overshoot (OS) [3], [4]. There is evidence to confirm that these additional stresses have caused severe degradation to different parts of the motor insulation system, leading to premature failures [2], [5]. Hence, the International Electrotechnical Commission (IEC) has developed two specific standards for qualifying rotating machines for VFD use: IEC 60034-18-41 and IEC 60034-18-42. The former deals with the qualification tests for insulation systems of machines that are not expected to experience partial discharge (PD) during their normal operating conditions (Type I machines), while the other one covers those which are expected to experience and withstand PD during their lifecycle (Type II machines) [3], [4]. Type II machines usually have a form-wound stator and an operating voltage of up to 15 kV. These Type II machines are the focus of this research.

In 2017, the IEC published an update to their Type II standard (amended in 2020) that encompassed many improvements over the earlier versions; however, several assumptions made in the standard have raised many questions, especially in terms of the linear effect of the supply switching frequency and the direct impact of the rise time on ageing [4], [6]. Currently, the IEC committee is in the process of updating the standard to address some of the assumptions made in their earlier editions. However, some

fundamental concepts still need to be addressed to provide a full understanding of the effects of different features of the PWM supply and their impacts on machine insulation life expectancy. Furthermore, the soon-to-be-introduced fast power electronic switches that utilize wide band-gap (WBG) devices based on silicon carbide (SiC) and gallium nitride (GaN) semiconductors are making their way into medium voltage (MV) drives [5]. The use of these improved switches in MV drives will increase the efficiency of the drive; however, these switches are capable of generating higher switching frequencies with shorter rise times and higher dv/dt which will impose further stresses on the insulation of MV motors [5], [7]. Based on our current knowledge, these new devices will lead to additional stresses and faster ageing. Thus, it is very important to characterize these effects to gain a better comprehension of their impact on machine insulation life assessment. Hence, a brief introduction to the various insulation systems used in motors is given in the next few subsections. The emphasis of this research is on the turn-to-turn insulation of form-wound coils that are commonly used in the stator of MV and high voltage (HV) induction machines.

1.1 Motor Insulation System

Motor insulation systems differ widely based on ratings, application, and environmental and operating conditions. Also, different manufacturers will have their unique designs and structures which are most often based on the availability of materials and years of manufacturing experience. However, no matter what the differences are, typical HV machine insulation will consist of the following three parts which are shown in Figure 1.1:

- Main wall insulation
- Stress control system
- Turn and strand insulation

1.1.1 Main Wall Insulation

The purpose of main wall insulation, as the name suggests, is to provide enough insulation protection between the windings and coils of the stator and the grounded core. This type of insulation is mainly based on wraps of insulating mica-based tape which is dominant in form-wound motors [8]. While this is the main insulation that protects the motor HV coils from the grounded core, it is also the one that separates the HV coils from each other and provides phase-to-phase insulation protection. Accordingly, this insulation is made robust enough to withstand the normal operating and transient overvoltages expected during the typical lifecycle of a machine. Mica-based tapes are one of the most common types

of MV and HV motor main wall insulation due to their inherited PD and corona resistance. However, other types could be used as well with some restrictions regarding the voltage level or the mechanical strength such as varnish cambric or silicone rubber. For MV and HV inverter-fed motors, fibreglass-backed tape filled with mica particles and vacuum pressure impregnated (VPI) with epoxy resin is still the best performing insulation system and as such, has become the standard in the industry. This insulation is generally very robust as it is expected to withstand PD during the operation of the motor. Having said that, when it comes to the main wall insulation, the concern about thermal ageing is more prevalent than electrical ageing [1], [2], [6], [8].

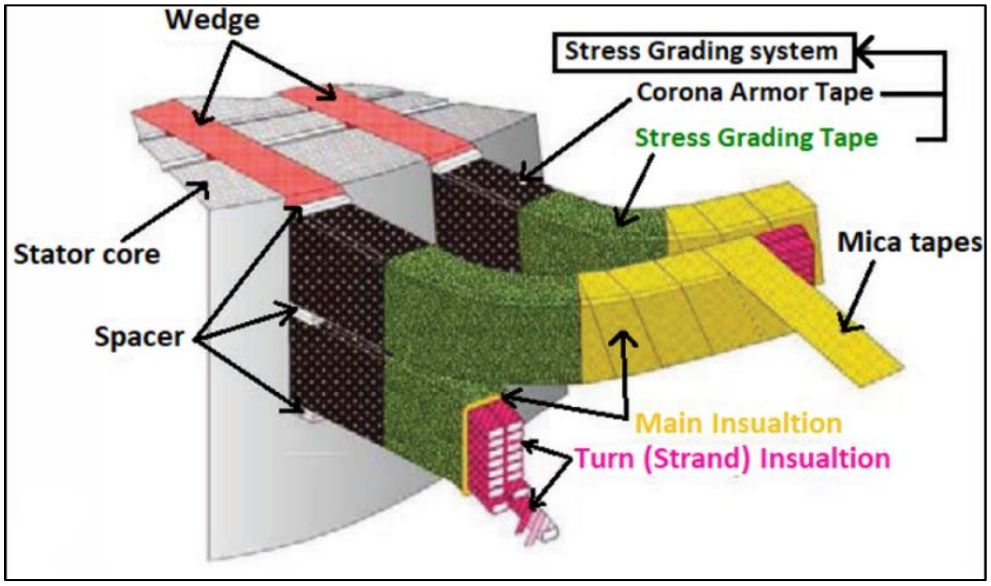

Figure 1.1 - Typical insulation system in an HV form-wound stator [9].

1.1.2 Stress Control System

A stress control system is usually required for MV and HV motors to reduce and smoothen the high electric field at the points where the coils exit the stator slot. A typical stress control system consists of both conductive slot coating and semiconductive stress control coating. A stress control system becomes essential on MV motors above 3 kV to prevent the high potential gradient at the slot exit which will cause PD and hence accelerate the coil insulation ageing. Normally, a conductive slot coating is sufficient for MV motors with a rated voltage of less than 6 kV; however, an additional stress control coating is required for machines with a rated voltage above 6 kV [8], [10]. The conductive slot

coating/tape, also known as conductive armour tape (CAT), is normally made from polyester glass fibre tape with carbon black filler and usually has a relatively high but constant conductivity in the range of 10^{-2} to 10^{-5} S/m, to ensure a more uniform electric field within the stator core. On the other hand, the stress grading coating is usually made from a field-dependent material where the conductivity increases as the stress increases. SiC-based tapes are popular for motors while micro-varistors-based materials such as zinc oxide (ZnO) are not yet commercially available for rotating machines [11]. These systems have shown accelerated degradation behaviour under high repetitive impulses produced by VFDs. The higher the switching frequency and the shorter the rise time of the generated impulses, the higher the frequency components penetrating into the insulation material. This has led to higher dielectric losses and hence a higher thermal effect. Research has tackled this issue to optimize the thermal and electrical performance of such systems under inverter use including those done at the University of Waterloo [11], [12], [13].

1.1.3 Turn and Strand Insulation

Turn and strand insulation vary significantly based on the voltage rating and thermal class of the machine. In Type II machines, rectangular shape conductors are used in the making of form-wound coils. Depending on the design and ratings, manufacturers can choose from different configurations. For higher voltages, the number of turns within a coil can be increased or the coils can be connected in series with a fewer number of turns. Additionally, turns in a coil can be made of a single strand or multistrand to increase the current capacity; otherwise, coils in the same phase can be connected in parallel for higher current ratings. When a turn consists of a single strand, the turn and the strand insulation are the same. However, in a multistrand turn, strand and turn insulations can be different. If the turns in a coil have dedicated insulation, then the strands will be enamel insulated and the turns will have separate resin-rich mica-wrapped tapes. Normally, for machines less than 3 kV, enamel insulation can be sufficient. However, fibreglass or mica-based tapes are recommended with inverter-fed machines for better insulation strength. For machines up to 6 kV, manufacturers can choose from either fibreglass or mica-based tapes for insulation. However, for higher voltages, mica-based tapes exhibit the best performance due to their superior PD resistance characteristics [2], [6], [10].

The main purpose of strand and turn insulation is to provide isolation between each strand/turn. The voltage difference between these turns in a standard AC machine is less than a 100 V under normal operating conditions. So, they are usually designed to only withstand an occasional overvoltage that

results from switching transients. However, this is not the case with the VSC supply where repetitive impulses with a high dv/dt are continuously applied resulting in significant terminal overshoot and non-uniform voltage distribution across the turns, and as such, causing additional continuous stresses and deteriorations to the turn insulation [14], [15], [16]. Although the main purpose of turn insulation is to prevent interturn faults, they are still part of the overall main wall and phase-to-phase insulations. Ground faults or short circuits can result in catastrophic damage to the motor. Most of these faults begin with a simple turn-to-turn fault that may lead to a complete breakdown.

One of the most challenging and hard-to-detect faults in induction motors is the stator winding interturn faults. Using a non-sinusoidal waveform supply which is produced by PWM-VSC makes it even harder to detect this type of fault. If not detected at an early stage, this type of fault begins at a low level and grows to a complete failure of the stator winding [17]. VSC supply imposes higher stresses on all parts of the machine insulation due to its switching characteristics and fast repetition as shown in Table 1.1 [4]. These additional stresses are causing accelerated ageing and early failures in the machine winding insulation. The next section will explain briefly the operation of a standard VSC and the features of the PWM supply that affect machine insulation.

Table 1.1 - Influence of features of the VSC supply on ageing of Type II insulation systems [4].

Insulation component	Fundamental frequency	Impulse voltage repetition rate f	Peak to peak voltage at the fundamental frequency $U_{pk/pk}$	Jump voltage U_j	Peak to peak impulse voltage at the impulse voltage repetition rate $U'_{pk/pk}$	Impulse voltage rise time t_r
Turn to turn insulation	○	●	○	●	○	●
Mainwall insulation	●	○*	●	○	○*	○*
Stress control system	○	●	●	●	●	●

○ Less significant

● More significant

NOTE 1 Testing of the phase to phase insulation is not necessary.

NOTE 2 If there are 2 levels in the converter voltage, these parameters (*) can become significant.

1.2 VSC and Features of the PWM Supply Affecting Machine Insulation

Advancement in power electronics has led to an increased use of VFDs in various machine applications and has allowed industries to move from low voltage to medium and high voltage applications [18], [19]. The main principle of such drives is converting the fixed AC supply to a variable frequency supply. This process is done namely in two stages: first, the input AC supply is rectified into DC and then the inverter converts the DC supply back into AC at different frequencies to be fed to the load. The input side converter can be as simple as a full-wave rectifier made up of 6 diodes or as it is commonly referred to, a 6-pulse rectifier. Alternatively, controllable switches can be implemented if an active-front-end option is required where the power can flow from either direction. Moreover, for smoother DC output and smaller harmonic contents, higher pulse topology can be implemented. Currently, up to 36-pulse rectifiers have been employed for MV drives [20]. Of course, that comes at an additional cost and space since additional pulses mean additional requirements for a phase shift transformer and more switching devices [21]. By comparison, controllable switches are a requirement at the inverter side to generate a variable frequency output through PWM. Depending on the application, torque, current, and voltage requirements, inverters can be either current source converters or voltage source converters. VSCs are dominant in MV and HV motor applications, and hence, reference will be made to this type of inverters throughout this research. Nevertheless, the effect of features of the PWM supply on motor insulation remains the same and can be deduced to other types of converters in the same way [4], [21].

Depending on the power requirement and the switching speed, different types of controllable switches can be used on the inverter side. The development of WBG devices has allowed for much higher switching speed, and it is just a matter of time till they make their way into medium- and high-power applications including MV and HV motors [5], [22]. Higher switching speed means higher efficiency and lower power losses but it also means higher stresses on the motor insulation [23]. The higher the speed of the switch, the closer the output shape is to the referenced sinusoidal voltage. However, higher speed also means more impulses delivered per second which can also necessitate shorter impulse rise times and higher voltage overshoots at the motor terminal [21]. Figure 1.2 defines the voltage impulse components associated with each of the square impulses [24]. Switching frequency, impulse rise time, and voltage overshoot are among the major components that greatly affect motor insulation [4]. Impulse rise time is defined as the time required for the voltage to rise from 10% to 90% of its final value. The final value in this context, also known as the step voltage, means the value of the flat portion of the square impulse without the overshoot component or in other words the DC bus voltage level in a two-level converter.

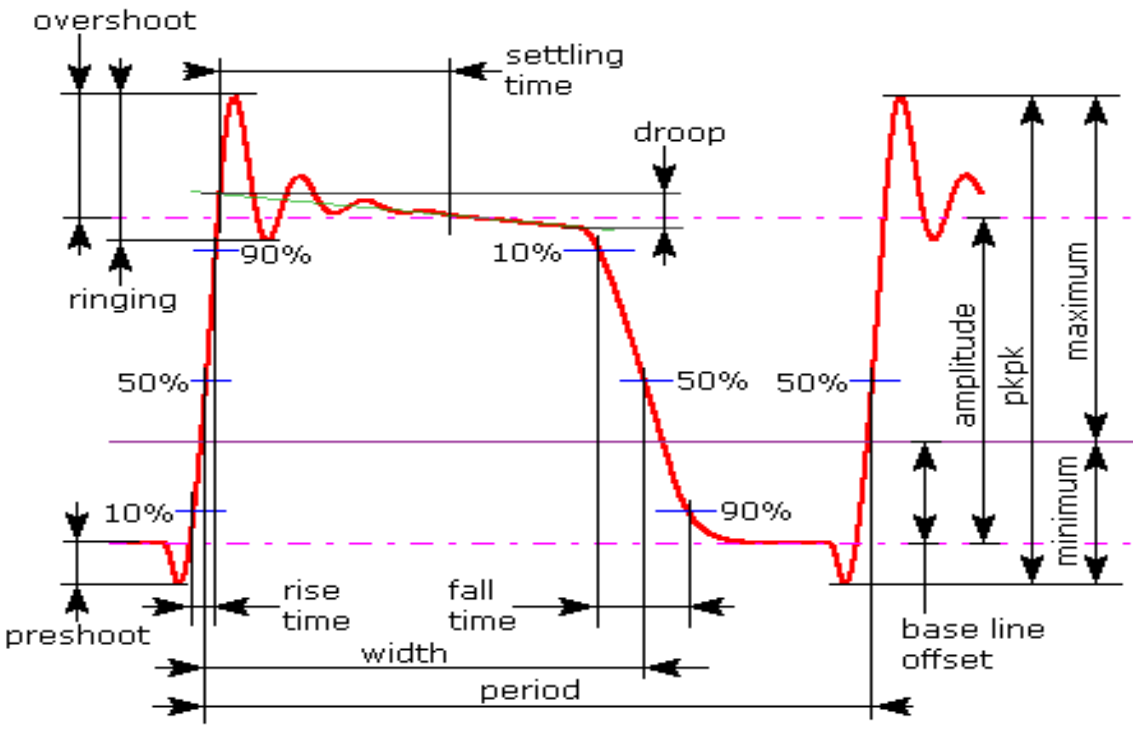

Figure 1.2 - Square waveform impulse components [24].

Impulse rise time reaching the motor terminal is a function of switching device speed, triggering circuit, various design aspects of the grounding system, and cable and motor surge impedances. The overshoot at the motor terminal is created by the reflected wave generated from the impedance mismatch between the cable and the machine impedance and hence it is a function of the drive impulse rise time, cable length, and machine impedance. The use of output filters such as sinusoidal and dv/dt filters can greatly affect the terminal voltage rise time and hence the terminal overvoltage; however, such filters can be extremely costly and bulky which might not be practical in many applications where space is a restriction [4], [21], [23]. The impulse jump voltage is defined according to [4] as the maximum voltage change at the impulse repetition rate, i.e. the step voltage plus any voltage overshoot. Figure 1.3 defines the jump voltage in a multi-level voltage inverter topology. Hence for a certain rated peak-to-peak voltage, the jump voltage is a function of the overshoot and the number of inverter output levels [4], [8], [25]. Although IEC recommends the use of a multi-level inverter to reduce the jump voltage and thus reduce the motor insulation stresses, two-level converters are still preferred and more common due to their reliability and relatively simple structure and control [8], [18], [21].

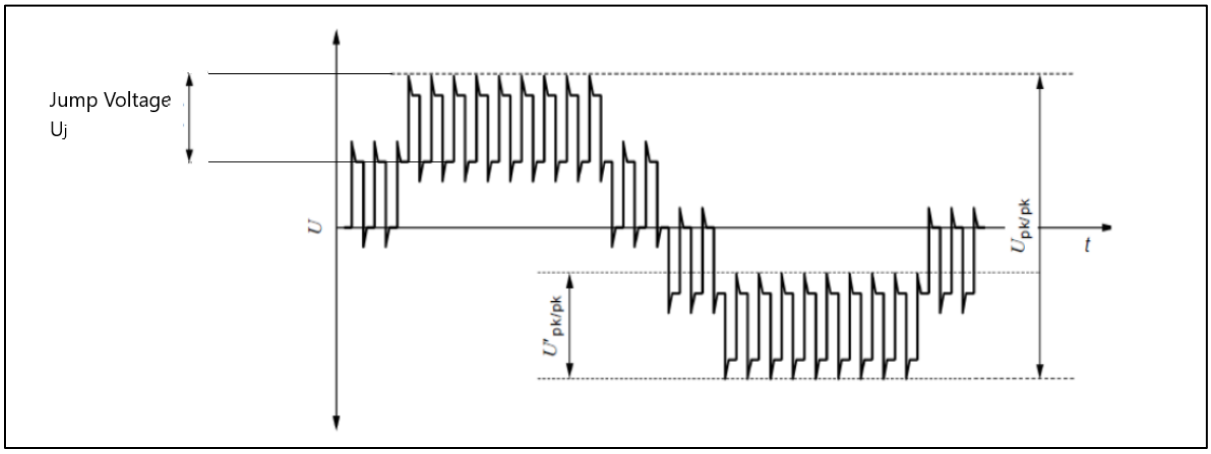

Figure 1.3 - Jump voltage in a multilevel converter [4].

Since the issuance of IEC 60034-18-42, the effect of features of PWM supply on the life of machine insulation has become an active area of research. Several researchers have investigated the effect of these features on different parts of the machine insulation system. Whether in support of or challenging the standard, one common stand among researchers in the field is that VSC-based supply causes additional stresses that AC-fed machines do not encounter. These additional stresses have already caused many premature machine insulation failures in the past, which made manufacturers increase the voltage insulation rating of their machines to withstand these additional stresses [2], [8], [10]. This solution might not continue to work with the continuous advancement of power semiconductor devices and their increased power and switching speed capabilities. Hence, a deeper understanding of these stresses is essential now more than ever to be able to maintain the reliability of rotating machines throughout their determined lifecycle. The following section will explore the literature on the research done in this area with a focus on the PWM components influencing the endurance of Type II turn-to-turn insulation.

Chapter 2
Literature Review

2.1 Literature Review

Two of the most important and perhaps most referenced documents for qualifying machines fed by VFDs are the IEC 60034-18-41 (IEC-41) and IEC 60034-18-42 (IEC-42) [3], [4]. IEC-41 was first issued in 2006 as a technical specification for qualifying Type I insulation for machines fed by voltage converters. The standard was subsequently updated in 2014 and amended in 2019. Type I insulation applies mainly for low voltage machines with a peak operating voltage of less than 1000 V. Typically, these machines are random-wound, and their insulation is organic in nature, and due to the low operating voltage, they do not experience PD caused by the repetitive impulse nature of the feeding voltage converter supply. The key factor for qualifying this type of insulation is to prove that the insulation will not experience any PD during its life term. In other words, manufacturers have to test their motors under fast-rising impulses and show that their PD inception voltage (PDIV) will be higher than a certain limit, which can be as high as six times the motor-rated voltage [3]. Of concern to this research is IEC-42, first published in August 2008 as a technical guideline for qualifying Type II insulation systems fed by voltage converters (hereinafter referred to as "the standard"). This standard was then updated in 2017 and amended in 2020 after receiving numerous comments from researchers in the field. Currently, an IEC committee consisting of researchers, manufacturers, and experts in the field is working on a new revision of the standard. Type II insulation systems are those which are made of PD resistance materials and hence are permitted to encounter PD during their life course, provided they pass the qualifying endurance test set by the standard. These Type II systems are usually used in machines with a rated peak voltage of more than 1000 V and their stators are often made of form-wound coils [4]. There are currently reports of installed form-wound motors with a capacity of up to 65 MW and a voltage rating of 13.8 kV operating under PWM-VSCs [10]. To qualify machines fed by VSC under the IEC-42 standard, manufacturers may have to qualify each part of their motor's insulation separately. The standard suggests the use of representing specimens of each of the main wall insulation, stress grading system, and turn-to-turn insulation of the candidate motor to undergo a voltage endurance test. Although the standard recommends the use of square impulses for the endurance test, it still allows both the main wall and turn-to-turn insulation to be tested under sinusoidal supply while adjusting the established life curve based on the used and targeted supply frequency. By doing so, the standard is simplifying the test but is also overlooking major PWM supply parameters that

may have a significant influence on the performance and life curve of such insulations. One of these ignored factors is the impulse rise time where a sinusoidal waveform would have a much larger rise time in comparison to a square one. The standard is also assuming a linear effect of the switching frequency on turn insulation ageing that can be accounted for by:

$$L_2 = \frac{L_1 f_1}{f_2} \tag{1}$$

where L_1 and L_2 are the lives of the insulation under frequencies f_1 and f_2 respectively and L is given by the commonly used life model given by [4]:

$$L = kU^{-n} \tag{2}$$

where k is a constant, U is the peak voltage applied, and n is the voltage endurance coefficient (VEC). In other words, it is suggested that the number of voltage cycles to failure is constant and the effect of changing the supply frequency can be simply adjusted by shifting the life curve up or down linearly by a factor of f_{new}/f_{old} as shown in Figure 2.1. Moreover, the suggested testing procedure overlooks the possible interaction between the impact of the other VSC parameters with that of the supply switching frequency and hence assumes an independent frequency effect and a fixed ageing mechanism. These assumptions mean disregarding the effect of the switching frequency and other features of the PWM supply on the resultant VEC and the slope of the life curve.

The standard recognizes the influence of features of the PWM supply on turn-to-turn insulation life assessment as per Table 1.1, however, it still assumes that their effects can be overlooked in some cases concerning long-term ageing and establishing a life curve. Another simplification that the standard has made is the effect of the impulse rise time on turn insulation ageing. The standard sees that while impulse rise time affects the voltage distribution within the coil, thereby affecting the voltage drop magnitude across the turns, its direct effect on turn-to-turn insulation ageing is negligible. Considerable research has been done to study the effect of the rise time on the voltage distribution of a form-wound coil [14], [15], nevertheless, a clear relationship has not yet been established, unlike what has been done with random-wound motors. In terms of the direct ageing effect of fast rise time on turn insulation, some researchers, [6], [26], [27], have supported the standard on the low significance of the waveform rise time on the ageing mechanism, while others, [28], [29], [30], have opposed this assumption. Besides its effect on voltage distribution, researchers have presented evidence of the effect of the rise time on the properties and occurrences of PD within machine turn insulation. Since PD is widely accepted by

researchers in this field to be the main ageing mechanism, ignoring the influence of the rise time might lead to an error in the insulation life expectancy.

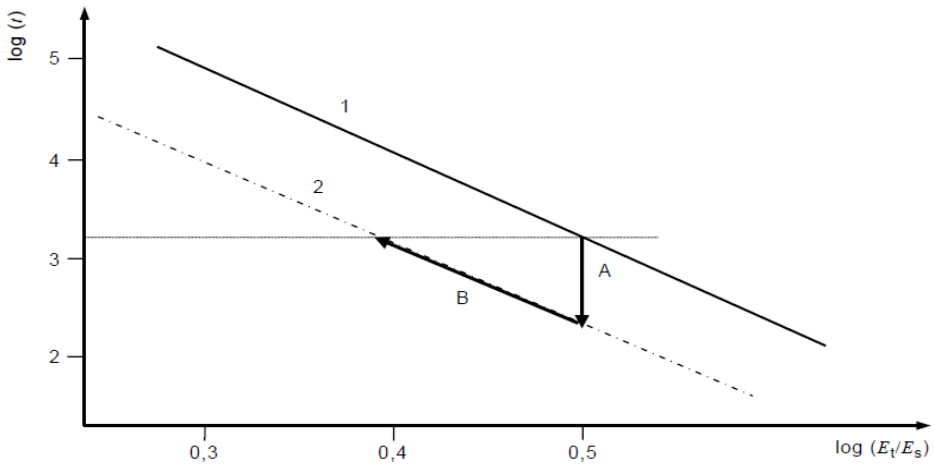

Key

E_t Electric stress at the peak to peak test voltage

E_s Electric stress at the peak to peak service voltage

t time to failure in hours

1 Life curve derived from power frequency endurance testing

2 Life curve predicted for the same insulation at x10 frequency

Figure 2.1 - Example of a life curve shifting based on frequency [4].

In [31], back-to-back turn samples were tested as per the IEC recommendation. To investigate the effect of the rise time, repetitive square waves were applied at different rise times, namely 270 ns and 4.5 µs, with two different impulse duty cycles, 15% and 50%. Moonesan et al. [31] found that the time-to-failure did not change between the two different rise times when the duty cycle was 50% while failures were slightly faster for a shorter rise time and a shorter duty cycle. Furthermore, fewer PDs occurred with higher magnitudes as the rise time was reduced, which the author attributed to the charge accumulation and distribution with different duty cycles and rise times. Nevertheless, when it comes to the rise time contribution to the time-to-failure, it was concluded that rise time has an insignificant effect on the turn-to-turn ageing within the studied range. The effect of switching frequency on the time-to-failure was also investigated in [32]. Switching frequency was found to have a linear effect on turn insulation ageing for the range between 500 to 750 Hz while the effect was non-linear for higher frequencies. Taking into

consideration the practical range of frequencies in modern MV drives, which is higher than 700 Hz, the results from [32] contradict the IEC-42 position on the linear effect of switching frequency.

Manns et al. [27] have investigated the effect of high-frequency supplies on Type II turn-to-turn insulation life assessment, using sinusoidal voltages of 60 Hz and 10 kHz. The study concluded a linear effect of the supply frequency, which supports the assumption made by the IEC standard and allows for a linear adjustment to the effect of frequency. The results also support the standard's position on the low significance of the rise time on the ageing process since changing the supply frequency from 60 Hz to 10 kHz has changed the waveform rise time from 4 ms to 25 µs with no apparent effect on the number of cycles to failure. Their findings are probably attributable to the use of sine waves instead of repetitive impulses, as it ignores the effect of other PWM components. Moreover, the effective rise times under sinusoidal supplies are much slower compared to the ones experienced under impulse-type supplies.

Alternatively, Florkowska et al. [30] have studied the effect of the switching frequency and rise time of unipolar impulses on the characteristics of PDs using a rod-plane setup. The authors provided evidence of higher PD magnitude and lower PDIV with faster rise time. The study also shows that a higher switching frequency results in a lower PDIV, meaning that PD would be created more quickly as the frequency increases. This finding suggests that the effect cannot be considered linear anymore, and a simple curve adjustment would result in a wrong life estimate. Similarly, using bipolar impulses on twisted enamelled wires, Lindell et al. [33] have presented results that show lower PD extinction voltages (PDEV) of up to 25% with a faster rise time. Thus, PD can be sustained longer under shorter rise time impulses, and hence the effect of the rise time on ageing cannot simply be ignored.

In [34], [35], Sahlén et al. investigated the effect of repetition frequency and impulse rise time on Type II turn insulation. The samples and test procedures were done in accordance with the standard recommendations. Their results are in line with those of [31], and so, support the standard position in regards to the low significance of the rise time on insulation ageing. On the other hand, their results on the effect of repetition frequency are opposite to those reported in [6]. Their findings, throughout the studied range of frequencies, are in line with the IEC standard position on a linear effect of the supply switching frequency. In [34], the authors reported a life curve for samples tested with a 50 Hz AC supply comparable to those tested under impulses of 1 kHz switching frequency. The results, which suggest a similar number of cycles to failure in both scenarios, indicate an independent effect of frequency and a similar ageing mechanism in both types of supplies. They also infer negligible

effects from the interaction between other factors and their contributions to the ageing process. When investigating the effect of the rise time, two impulse rise times were used to establish life curves for the turn insulation, namely 0.4 μs and 2 μs. Little difference was reported in the number of cycles to failure; however, a shorter rise time was found to cause higher magnitude PD within the samples, which suggests faster deterioration. In [35], the authors have compared the influence of switching frequency and impulse jump voltage on the life of Type II turn-to-turn samples to the influence of the peak-to-peak value and the fundamental frequency of the source supply. The supply used for the study was a 50 Hz AC supply superimposed with 1 kHz square impulses to simulate the shape of a multilevel converter supply as a sinusoidal waveform superimposed with voltage ripples. The frequency and the rise time of the superimposed impulses were fixed at 1 kHz and 1 μs respectively, while the jump voltage percentage to the peak-to-peak value of the AC supply varied from 0 to 43%. The reported results suggest that the switching frequency and the jump voltage do not affect the insulation health condition. Accordingly, the authors conclude that similar to AC supply, it is the peak-to-peak voltage of the supply and the fundamental frequency that affect the life of turn insulation rather than the factors specified in Table 1.1 as suggested by the IEC standard.

In [36], Montanari et al. investigated the effect of inverter levels and the impulse rise time on the characteristics of PDs and the life behaviour of Type I turn insulation. Using a PWM supply of a 50 Hz fundamental frequency, 1 kHz switching frequency, and 25 μs rise time, the effect of the number of levels of the inverter output and hence the jump voltage was demonstrated. It was found that as the number of inverter levels increases, PD patterns are getting closer to those generated by a 50 Hz sinusoidal supply. Since the jump voltage decreases with increasing the inverter levels, it was concluded that the main factor that affects the life of turn insulation is the inverter step voltage. It was also reported that PD magnitude and repetition rate were reduced as the number of levels increased. This, in one way, supports the life enhancement with increased inverter output levels as presented in [35], however, it completely opposes them with the role and effect of the jump voltage on the occurrence of PD and the insulation life expectancy. Using a PWM with 60 ns, 1 μs and 25 μs rise times, it was also found that the PD magnitude and repetition rate increased significantly when the rise time was reduced to 60ns, however, no difference was found between 1 μs and 25 μs rise times. Therefore, it was concluded that for machines fed by PWM, where the expected rise time is more than 1 μs, ageing can be done using a sinusoidal supply as proposed by the IEC standard. It also suggests that the effect of frequency can be estimated linearly based on the switching frequency for two-level converters while the fundamental

frequency should be used for multilevel converters. The same was concluded in [37], where the authors reported the fundamental frequency to be the main factor in multilevel converters, while a sinusoidal supply with a frequency equivalent to the switching frequency of a two-level converter exhibits the same life behaviour. On the other hand, when examining Type II insulation, the author in [38], has demonstrated results that support faster ageing with shorter rise time and higher frequency while different waveforms produce different PD patterns and characteristics. The author recommends the use of similar waveshapes when scaling life curves for the effect of frequency as using sinusoidal voltages instead of repetitive impulses may lead to a significant overestimation of the insulation life. This was also supported by [39], by providing evidence of different discharge patterns, numbers, and magnitudes when using a sinusoidal waveform as opposed to using square impulses. The authors also reported that the higher the frequency, the higher the concentration of PDs during the rise time. It was also reported that shorter rise times promote higher discharge energy and that was attributed to being the main reason for the significant life reduction of the specimens aged under repetitive impulses of a 150 ns rise time to those aged under sinusoidal supply.

In [40], Fabiani et al. investigated the effect of the switching frequency and waveform polarity on the PDIV in enamelled wires. It was concluded that the waveform polarity affects the space charge accumulation and hence the PDIV is much higher for unipolar waveforms as opposed to that of the bipolar ones. In regards to the switching frequency, the authors reported that the PDIV does not alter with increasing the switching frequency; however, it was found that the PD magnitude is higher. This suggests an accelerated rate of ageing, not only in terms of the number of cycles per second to failure but also in terms of the PD magnitude which supports the position on the non-linear effect of frequency. This was also demonstrated in [41], as the life of the twisted pair wires was reduced as the frequency of the supply, whether sinusoidal or square waves, increased even when there is no PD. The effect of the frequency was much higher when accompanied by PDs. That was demonstrated as a lower VEC in the established life curve which is different than what was suggested by IEC and demonstrated in Figure 2.1.

Studying the effect of square wave switching frequency and rise time on Type I and Type II insulation systems, a rather different conclusion was achieved by Wang et al. [29], [42], [43]. The authors reported lower PD magnitude and occurrence with higher frequency. This suggests a lower rate of ageing per impulse with increased switching frequency. In other words, the contribution of each impulse will be less than that of a lower switching frequency and the average number of cycles to failure will be more

for a higher switching frequency. Whereas when investigating the effect of the impulse rise time, it was concluded that a shorter rise time will lead to a lower PDIV and a higher PD magnitude. Thus, a shorter rise time results in a severe impact on the turn insulation, and as such, should not be ignored during ageing studies.

Different components of the PWM supply have also been investigated on twisted enamelled wires by Loucif et al. [44]. The authors studied the influence of the waveform duty cycle, switching frequency, rise time, overshoot and ringing on the PDIV. The switching frequency was varied from 100 to 1 kHz, while the rise time ranged from 70 to 250 ns. It was reported that a lower PDIV was achieved with a smaller duty cycle and slower ringing; however, neither the switching frequency nor the rise time had any effect on the PDIV. The lower PDIV as a result of the shorter rise time was attributed to the increased overshoot rather than the value of the rise time itself.

It is evident from the literature that a common outcome has not yet been deduced towards the effect of different features of the PWM supply. Some research results support the position assumed by the standard, while others have presented evidence to claim otherwise. Table 2.1 and Table 2.2 summarize the literature on the effect of the supply switching frequency and rise time on the endurance of machines turn insulation. The differences were not limited by whether the factors affect the insulation condition or not, but also extended to whether that effect is linear or not. Even when agreeing on a non-linear effect, reported results still vary on whether it is an increasing or a decreasing rate. Some differences could be related to the various voltage setups implemented and/or the different ranges of voltages, frequencies, and rise times considered; whereas, others are related to different samples and materials tested. Other variations may also arise from different factors and variables monitored and studied while using various approaches for conclusions.

One major aspect that is often overlooked is the interaction between different stressing factors. As stated before, a higher switching frequency may necessitate a shorter rise time, while a shorter rise time may cause a higher overshoot. Most of the studies reported have studied each of these factors independently without considering how they affect and interact with each other during the ageing process. For instance, most of the studies done on the effect of the rise time reported different ranges of rise times under study without recording the overshoot variations. The differences in the reported results of the effect of the rise time could be related to the overshoot caused by a shorter rise time.

Meanwhile, the overshoot is also a function of the cable capacitance and test object impedance; hence, similar rise times could create different overshoots in various setups.

Similarly, when comparing different switching frequencies, other parameters and factors should be recorded and a proper statistically designed experiment should be considered to understand the effect of each factor. Moreover, several conclusions on the endurance of turn insulation were made solely based on responses such as the PD magnitude, number, or inception voltage associated with varying a specific PWM component. Although PD is believed to be the main ageing mechanism, such conclusions should not be made on the endurance of an insulation material based purely on the measured PD value. There could be more than one factor affecting these responses, as well as different ageing mechanisms involved that might alter the process. Although it is a lengthy process, establishing a life curve might be essential for such comparisons and conclusions. Addressing the interactions and the combined effect of these factors is vital to avoid inaccurate conclusions made based on a single-factor experiment. The use of statistical models and confidence intervals in the analysis is also crucial to have more accurate and generalized conclusions. This can help in accounting for the random effect of the ageing process and aid in establishing more accurate and meaningful conclusions.

Table 2.1 - Summary of literature on the impact of the waveform applied rise time and switching frequency on machine turn insulation.

Impact on Life of Machine Turn-to-Turn Insulation*		
Reducing impulse rise time	Accelerate ageing	Has no significant effect
	[28], [29], [30], [33], [38], [39], [42], [43], [45], [46], [47], [48], [49], [50], [51], [52]	[2], [4], [6], [53], [26], [27], [34], [35], [36], [37], [41], [44], [54], [55]
Increasing switching frequency	Has a linear relation **	Accelerates ageing non-linearly***
	[4], [53], [26], [27], [34], [35], [36], [37], [38], [44], [48], [55]	[2], [6], [29], [30], [39], [40], [41], [42], [43], [47], [50], [52], [54]

** These conclusions are based on the ranges of the rise times and frequencies considered in the presented work. Some of the results are based on the data presented to support the derived conclusion such as the recorded PD statistics.*

*** Results include those supporting the significance of the fundamental frequency rather than the switching frequency and those showing no frequency dependence.*

**** Results include acceleration with increasing or decreasing rate and those showing different regions of action.*

Table 2.2 - Additional details on the summarized literature in Table 2.1 showing what has been studied, over what ranges, and what has been measured.

Ref.	Factors & ranges considered	Response measured	Study done on:
[28]	Slew rate: 5 to 75 kV/μs	Time-to-failure	Twisted pair of enamelled wires using 10 kHz bipolar square pluses.
[29]	Rise time: 50 ns, 200 ns, 1 μs, 16 μs Switching frequency: 1 kHz, 3 kHz, 5 kHz	Time-to-failure PD magnitude and repetition rate	Single contact point crossed enamelled wires using 50% duty bipolar square impulses and a fixed period unipolar impulse (different duty cycles).
[30]	Rise time: 0.8 to 3.5 μs Switching frequency: 0.1 Hz to 2 kHz	PDIV PD magnitude	Rod-plane setup and using unipolar square pluses.
[33]	Rise time: 2 to 100 μs	PDEV	Twisted pair samples using bipolar square impulses of 83 Hz switching frequency and 50% duty cycle.
[38] and [39]	Rise time: 150 & 2000 ns Switching frequency: 2, 20, 2000, 5000 Hz	Time-to-failure PD patterns & time behaviour	Type II samples using both sinusoidal and square waveforms. Rise time study is done using bipolar square impulses with a 5 kHz switching frequency and 50% duty cycle.
[42]	Switching frequency: 1 Hz to 5 kHz	PD magnitude and repetition rate	Type II samples using square impulses of 300 ns rise time.
[43]	Rise time (Type I): 50 ns, 200 ns, 1 μs, and 16 μs Rise time (Type II): 150 ns and 2 μs	Time-to-failure PD magnitude	Type I and Type II samples. For Type I, three switching frequencies were used (1, 3 & 5 kHz), whereas for Type II it was fixed at 5 kHz.
[45]	Rise time: 200 ns to 400 μs	PD magnitude and frequency spectrum	Type I samples using both sinusoidal waveforms and repetitive impulses.
[47]	Switching frequency: 60 Hz to 20 kHz Rise time: 0.04 to 0.1 μs	Time-to-failure	Type I twisted-pair samples. For the switching frequency study, the rise time was fixed at 0.025 μs whereas, for the rise time study, the switching frequency was fixed at 20 kHz.
[48]	Switching frequency: 15 to 40 kHz Rise time: 50 to 200 ns	Time-to-failure	Type I twisted-pair samples. For the switching frequency study, the rise time was fixed at 200 ns whereas, for

			the rise time study, the switching frequency was fixed at 15 kHz.
[49]	Rise time: 0.4 and 40 μs	PD magnitude, number and PDEV	Type I and Type II samples using multilevel PWM of 1.5 kHz switching frequency.
[50]	Rise time: 15 to 800 ns Switching frequency: 1.5, 4 and 600 kHz	PD magnitude, number and PDEV	Twisted-pair samples using PWM supply (Fixed duty was used for 600 kHz switching frequency).
[51]	Rise time: 70 to 250 ns	PD characteristics	Random wound motor using 10% duty cycle impulses with 40 kHz switching frequency.
[2] and [54]	AC frequency: 60 Hz to 4 kHz Switching frequency: up to 2000 Hz	Residual strength of the aged samples	Type II samples of different materials using AC and repetitive unipolar voltage impulses.
[6]	Rise time: 270 ns and 4.5 μs Switching frequency: 0.5, 1 and 3 kHz	Time-to-failure PD magnitude and repetition rate	Type II samples using unipolar and bipolar square impulses of different duty cycles. Rise time study is done using a 3 kHz switching frequency. The switching frequency study is done with a 300 ns rise time.
[53]	Rise time: 15 μs and 5 ms Switching frequency: 8.3 and 1000 Hz	Time-to-failure	Type II samples using both sinusoidal and repetitive impulses.
[26]	Rise time: 10 μs and 1.25 ms Switching frequency: 20 and 200 Hz	PD patterns	PE layers between two electrodes. The study also compares the differences between square and sinusoidal waveforms.
[34]	Rise time: 0.4 and 2 μs Frequency: 50 Hz (AC) and 1 kHz (impulse)	Life curve and time-to-failure	Type II samples using both sinusoidal and repetitive impulses. For the rise time study, the switching frequency was fixed at 1 kHz, whereas for the switching frequency study, the results are based on comparing a 50 Hz (AC) voltage to a 1 kHz impulse voltage.
[35]	Switching frequency: 1 kHz (superimposed on 50 Hz AC) Rise time: 1 μs	Life curve and time-to-failure	Type II samples using a 50 Hz (AC) voltage superimposed with impulse voltage. The results are based on comparing the effect of the

			superimposed impulse voltage ripple (up to 43%) on the insulation ageing rate.
[36]	Rise time: 60 ns, 1 μs, and 25 μs Frequency: 50 Hz (AC) and 1 kHz (both AC and impulse)	Time-to-failure PD magnitude and repetition rate	Twisted-pair samples using both sinusoidal and repetitive impulses. For the rise time study, the switching frequency was fixed at 1 kHz.
[27]	Frequency: 60 Hz, 418 Hz and 10 kHz	Life curve and time-to-failure	Type II samples using sinusoidal supply; corresponding rise times: 4.17 ms, 0.6 ms and 25 μs.
[37]	Frequency: 50 Hz (AC), 1 kHz (impulse) Rise time: 1 μs	Time-to-failure PDIV, PDEV and PD patterns	Twisted-pair samples using both sinusoidal and 2, 3 and 5-level inverter PWM supply.
[41]	Frequency: 50 Hz (AC) and 10 kHz (Both sinusoidal waveform and square impulse) Slew rate: ≤ 1 kV/μs	Life curve and time-to-failure	Twisted-pair samples of different materials using both sinusoidal and square impulses
[44]	Switching frequency: 100 Hz and 1 kHz Rise time: 70 and 150 ns	PDIV	Twisted-pair of enamelled wires using square impulses with different duty cycles. 70 ns rise time was used for the switching frequency study, whereas a 100 Hz switching frequency was used for the rise time study.
[52]	Rise time: 0.4, 20, 100, and 500 μs	PD patterns	Twisted-pair samples using 3- and 4-level PWM supply.
[55]	Frequency: 60 Hz (AC) and 14 kHz (impulse)	Time-to-failure	Type II samples using both AC and repetitive impulses of 0.1 to 0.3 μs rise time.
[40]	Switching frequency: 1 Hz to 10 kHz	PDIV and PD patterns	Different kinds of enamelled wire in twisted pair configuration using square impulses of 50% duty cycle and slew rate ranging from 1 to 3 kV/μs, while the repetition frequency varied.

2.2 Aim of Present Work and Thesis Organization

The main objective of this research is to study and verify the effects of medium voltage variable frequency drives on machine turn insulation. This research aims to provide a better understanding of

the effect of features of the PWM supply, in particular the switching frequency, rise time, jump voltage and overshoot components, on turn insulation life assessment. As demonstrated in the literature review, several shortcomings were identified that require further study and analysis. One major aspect is the IEC assumption on the linear effect of the supply switching frequency and the possibility of using a sinusoidal supply to create life curves for turn insulation instead of a repetitive square impulse or PWM supply. Accordingly, one of the main research objectives here is to create life curves for Type II turn insulation using repetitive impulses instead of a sinusoidal supply. This work will help not only in verifying and understanding the influence of switching frequency on turn insulation but also in providing the foundation on which to establish a standard reference lifeline for turn insulation under VSC supply. Moreover, the work can form the basis for machine turn insulation evaluation and possibly contribute to the next IEC standard update.

Another dispute that this research will attempt to address is the effect of impulse rise time. Substantial research has been done on the influence of the rise time on turn insulation ageing. Some researchers have presented results that support the IEC's position on the low significance of the waveform rise time towards the long-term ageing of turn insulation. In contrast, others have shown evidence of accelerated degradation accompanied by shorter rise times. This research will tackle this issue by using an approach that is new and distinct in this field utilizing the design of experiment (DoE) principles [56]. The goal is to provide a better and more thorough understanding of the direct effect of rise time on the ageing process. It is identified that reducing rise time can affect the stress on turn insulation by one or both of the following; increasing the high-frequency contents penetrating the insulation due to the increased dv/dt, and/or increasing the voltage drop across turn insulation within a coil. Moreover, depending on the cable and load impedances, increasing the slew rate may generate a higher overshoot, causing additional voltage stresses on turn insulation. However, very limited research has been done to distinguish the effect of the rise time from the overshoot. By means of varying the rise time, researchers are also, unintentionally, varying the overshoot ratio. Broadly speaking, most of the studies done to address the effect of the rise time reports none or just limited information on the overshoot ratio and hence overlooking a potential variable that might have a distinct impact on the ageing mechanism. As per the current procedures given in the IEC standard, researchers are generally concerned with maintaining a similar peak voltage throughout the voltage endurance test without much focus on the variation of the waveform shape or maintaining a similar overshoot ratio. Moreover, different research studies would have different experimental setups and hence different overshoots for

a similar range of rise times. Thus, considering the variation in the overshoot ratios while studying the effect of the impulse rise time is essential. In fact, this embedded effect between the rise time and the overshoot could be one of the reasons for the variation in the conclusions made and the outcomes reported in different studies. This research will address the effect of both the waveform's rise time and overshoot while investigating their interactions and how they contribute to the ageing process. Therefore, the objectives of this research are threefold:

1) Investigate the effects and interactions between the impulse rise time and overshoot components, characterize their influence, and determine their role in the ageing process.
2) Provide a thorough understanding of the effect of the supply switching frequency on the life of turn insulation by establishing reference life curves for Type II turn-to-turn insulation based on a repetitive impulse supply.
3) Study, compare and analyze the influence of switching frequency, rise time, and overshoot component on the characteristics of PDs during the ageing process while relating their effect on the ageing mechanism and life of turn insulation.

The thesis is organized as follows:

Chapter 3 presents the materials and methods used in this research. This includes a detailed description of the experimental setup and diagnostic tools used in the ageing experiments, the PD detection system implemented and how it correlates to a standard PD detection system, the preparation of the back-to-back turn insulation samples, as well as the use of the single cavity model, and finally an illustration of the statistical methods and simulation tools used to analyze and explain the experimental findings.

In Chapter 4, the results of the time-to-failure and voltage endurance tests are detailed for different features of the repetitive impulse supply. Life curves for Type II turn insulation are established under repetitive square impulse voltage stresses. Moreover, the effect of switching frequency, rise time, jump voltage, and overshoot on PDs within Type II turn-to-turn insulation is reported for both the back-to-back turn insulation sample and the single cavity layered insulation.

Chapter 5 discusses the results reported in the previous chapter. The influence of varying the switching frequency, rise time, and overshoot ratio on the characteristics of the PDs during ageing are discussed and compared to the results from the time-to-failure experiments in order to explore how these factors interact with each other and contribute to the ageing mechanism and life of machines'

turn-to-turn insulation. Finite element method (FEM) simulation is also used to explain and support the experimental findings and to suggest and describe the ageing and failure mechanism associated with the test samples.

Chapter 6 provides a summary and conclusion of the thesis along with a highlight of the main research outcomes and potential contributions as well as recommendations and suggestions for future work.

Chapter 3
Research Methodology

The focus of this research is to provide a comprehensive understanding of the degradation and ageing processes of turn insulation in form-wound coils under repetitive impulses. This is done by performing voltage endurance tests, obtaining time-to-failure data and establishing life curves that are relevant and representative of turn insulation in actual form-wound coils. It is also important to monitor and compare the changes in PD as a response to changes in the impulse waveform features to evaluate the importance and the role of the studied factors of ageing, their relationship to the ageing factors, and how they affect the life of turn insulation using time-to-failure measurements and statistical methods. This chapter describes the procedures followed to achieve the research objectives, from sample preparation and experimental setup to the statistical and simulation tools used. The block diagram in Figure 3.1 illustrates the research methodology.

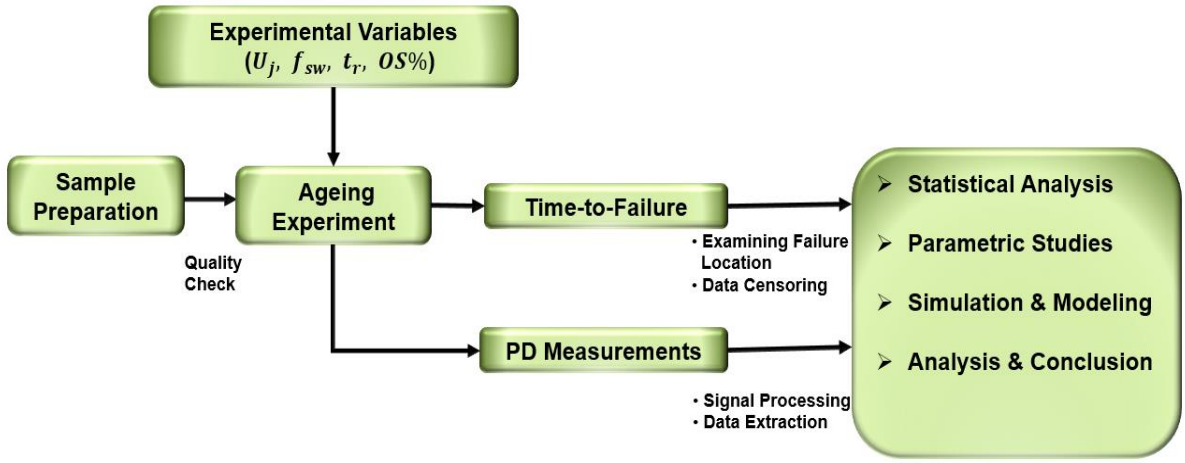

Figure 3.1 - Block diagram of the research methodology.

3.1 Sample Preparation

3.1.1 Back-to-Back Turn Insulation

The back-to-back turn insulation samples used in this research are prepared by Motion Electric, a company that specializes in the manufacturing, rewinding, and overhauling of motors and generators HV coils, following the guidelines and recommendations given in the IEC-42 standard. The prepared

turn-to-turn sample consists of two rectangular copper strands identical to the ones used in actual form-wound coils [57]. Each of the strands is coated with enamel insulation and wrapped with Conductofol® 2371 mica tape, one of the commercial mica tapes used for Type II turn insulation. The wrapping profile is a 50% overlap (half-lap) and the edges of the strands are bent smoothly at a 135º angle. Due to the enhanced electric field caused by the bend, an extra layer of Kapton® is added to provide additional dielectric strength to avoid unwanted failures at the crotch area. Figure 3.2 shows the dimensions and construction of a sample [58].

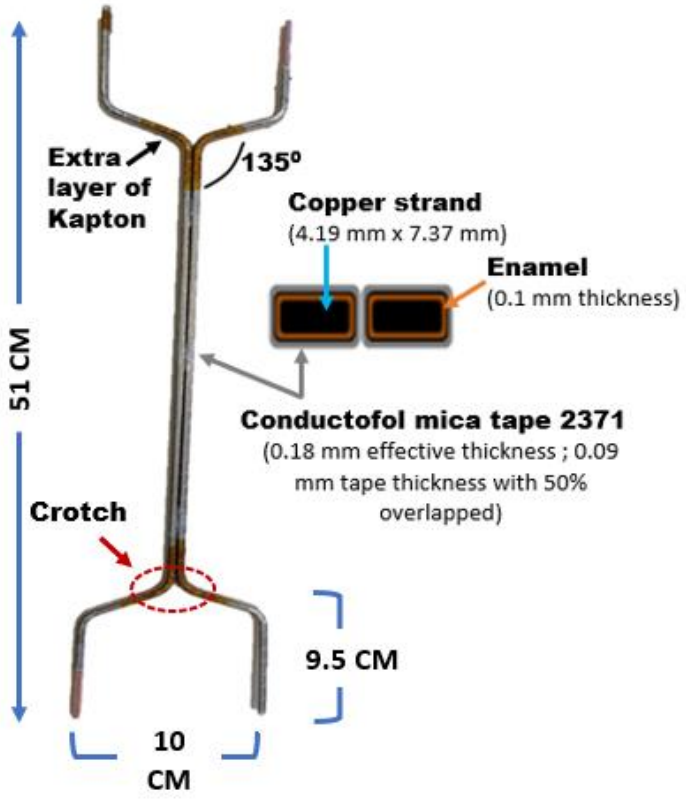

Figure 3.2 - Prepared Type II turn-to-turn sample showing the general construction layout and a cross-sectional view of the insulation layers, prior to the application of the outer polyester tape and the final VPI process.

In practice, the crotch area is unaltered as the electric stress is sufficiently low that failures do not occur quickly; however, for accelerated ageing studies of the flat portion of the samples the stress level must be increased, so the crotch area must be over insulated to prevent failures in this region. The mica wrap twists slightly but does not significantly compromise the dielectric strength. However, for

insulation ageing studies, this twisting might be a concern. Adding another layer of insulation at the crotch area will increase the dielectric strength and leave the straight area with just one layer. Consequently, the strands are expected to fail along the straight portion as opposed to the crotch area. The two strands are held together with polyester tape in a back-to-back construction. The final samples are then fixed on a wooden frame and baked in a VPI oven while impregnated with epoxy resin to fill voids and gaps that are inevitable in sample construction [59]. Figure 3.3 shows the prepared samples before and after the VPI process.

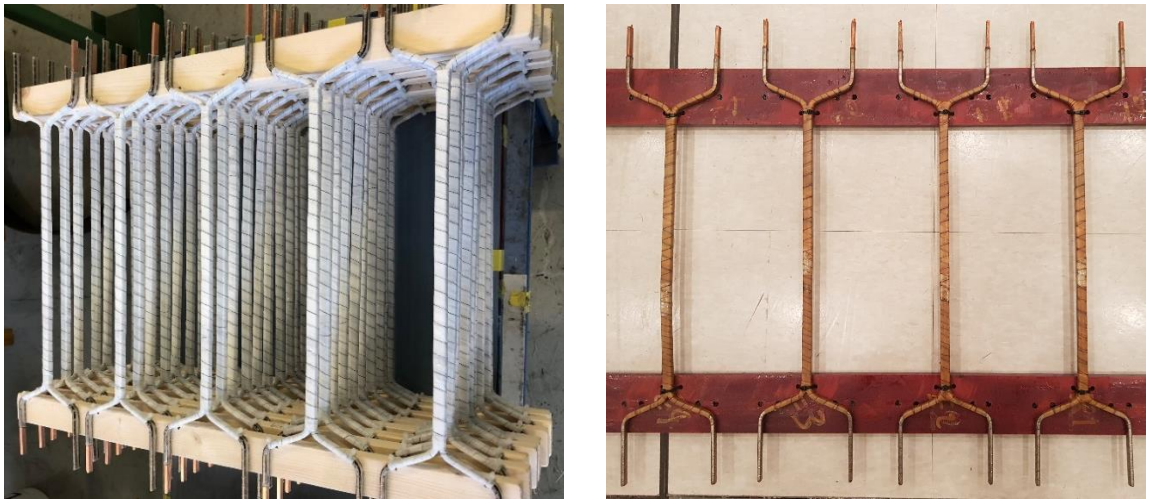

(a) Samples before VPI (b) Samples after VPI

Figure 3.3 - Prepared turn-to-turn samples; (a) before VPI, (b) after VPI.

As part of the initial quality control test on samples to confirm uniformity and equivalency, PDIV, PDEV, and capacitance measurements, at power frequency were done on each sample. A standard PD measurement system utilizing a coupling capacitor is used to record the PDIV and PDEV in accordance with the IEC 60034-27-1 procedures [60]; whereas, a high-precision inductance, capacitance, and resistance (LCR) meter is used as an insulation diagnostic analyzer for the capacitance measurement. Respectively, Table 3.1 and Table 3.2 detail the two measurement system specifications. The AC breakdown strength was randomly tested on a few of the prepared samples to confirm their equivalent strength. Table 3.3 demonstrates the initial quality control test results performed on the prepared samples prior to the endurance tests.

Table 3.1 - Partial discharge measurement system specifications.

Designation	Value
AC test set	Hipotronics, 7150-20AM-AX-G
PD detector	Hipotronics, DDX 9101
Transformer Input	600 Vac, 60 Hz, 33 A
High Voltage Output	0-150 kVac, 20 kVA
Duty Cycle	20 kVA at 1 hr, 15 kVA continuous
Partial Discharge	< 2 pC @ 150 kV
Distortion	< 5 %

Table 3.2 - Precision LCR meter specifications.

Designation	Value
Model	E4980A Precision LCR Meter + E4980A-001
Test Frequency	20 Hz-2 MHz
Test Voltage	0-20 V_{rms}
Accuracy	0.05%

Table 3.3 - Initial quality control tests on prepared samples.

Test	Value
PDIV	$2.1 - 2.2\ kV_{rms}$
PD magnitude at inception	$60 - 80\ pC$
PDEV	$1.6 - 1.8\ kV_{rms}$
AC breakdown strength	$15.8 - 16.2\ kV_{rms}$
Capacitance	$147 - 165\ pF$

Samples that failed in the crotch area were progressively censored and excluded from the analysis following the statistical procedures given by the IEC 62539/ IEEE 930 guide [61]. It is worth noting that the failure location was not always visible during the ageing experiment. In such cases, an HV-DC source was connected to the failed sample, and the failure location was thermally detected using an infrared (IR) camera as shown in Figure 3.4 [58], [59].

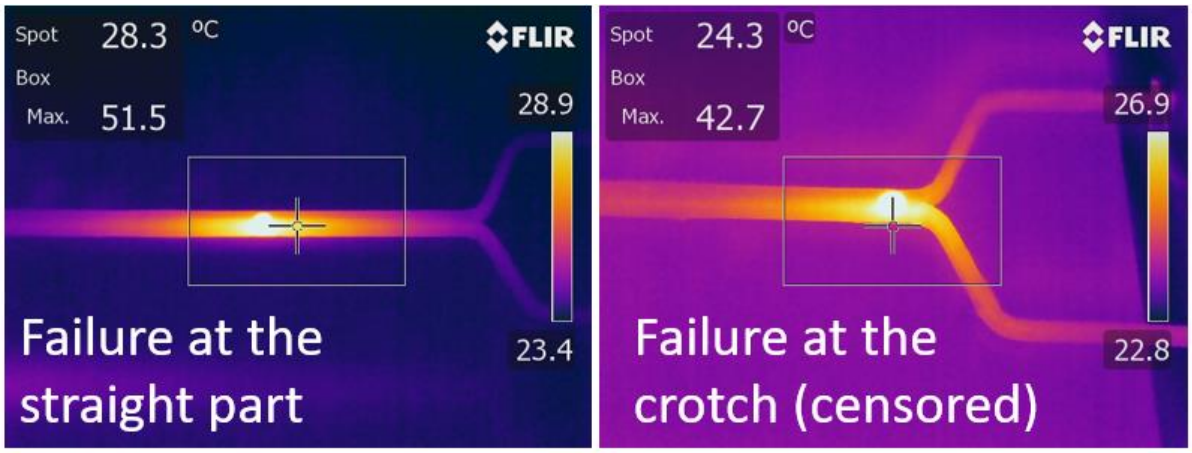

Figure 3.4 - Detection of the failure location using thermal imaging.

3.1.2 Single Cavity Layered Insulation

The back-to-back samples inevitably contain multiple voids of various shapes and sizes. As such, samples prepared with a single cavity of a known size and shape in a layered structure, are introduced and investigated in this work. Having control over the size, shape, and number of voids within a sample allows for ease of modelling and additional investigations of their influence on PD. The prepared single cavity specimen consists of three mica-tape layers, each of 0.09 mm thickness, held between two electrodes. A 0.78 mm diameter hole is made through the middle sheet to represent the embedded cavity between the insulation layers. The ground electrode is equipped with a micrometer caliper to control and maintain the same position and pressure applied to each test sample for measurements. Figure 3.5 shows a photograph of the single cavity sample with a sketch of the mica-tape sample with dimensions along with microscopic images of dissected sections from the back-to-back sample that is used to estimate the dimensions of the embedded cavity [62].

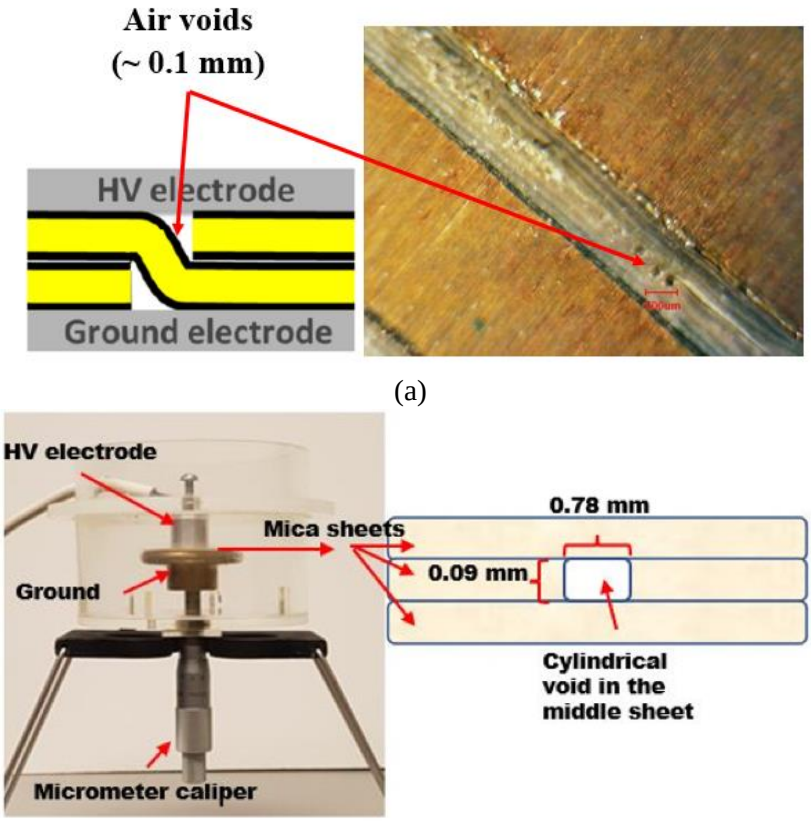

Figure 3.5 - (a) Microscopic views and a sketch of a back-to-back specimen used to estimate the dimensions of the single cavity specimen, (b) a view of the prepared single cavity specimen showing its various components along with a sketch of the mica sheets arrangements.

3.2 HV Impulse Generator

The HV impulse generator used in this research for the ageing studies was previously developed at the University of Waterloo [63]. It is built using insulated gate bipolar transistors (IGBT) and is based on a design inspired by the Marx principle. Ten switching stages are cascaded together to generate a voltage up to a 20 kV peak. Each of the generator stage capacitors is charged in parallel and discharged in series. Figure 3.6 displays both the actual generator and a schematic of its configuration topology. The generator is capable of producing both PWM and square impulses with switching frequency up to 4 kHz and a rise time as low as 170 ns. Table 3.4 describes the generator specifications.

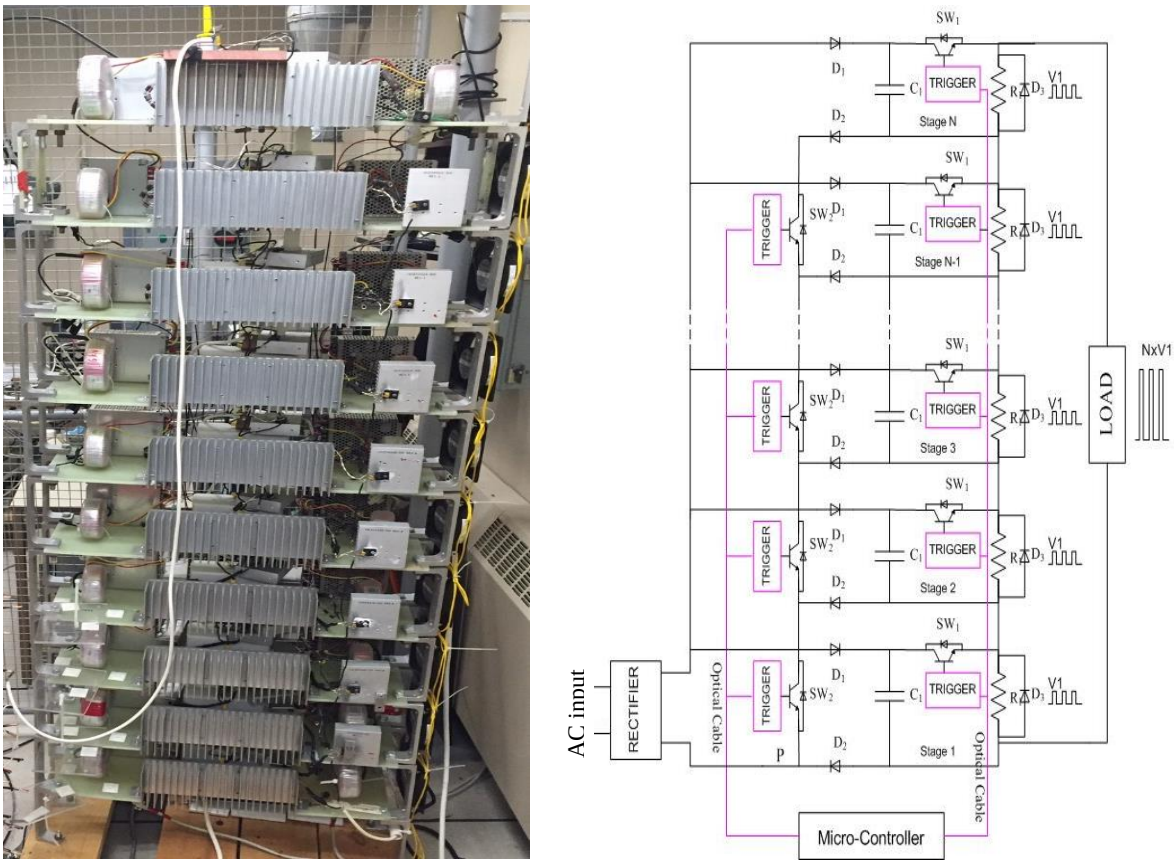

(a) (b)

Figure 3.6 - HV impulse generator; (a) actual generator, (b) schematic diagram [63].

Table 3.4 - HV impulse generator specifications.

Parameter	Value
Input	600 V_{AC}, 4 kVA
Duty	Continuous
Impulse type	Square, PWM
Impulse amplitude (peak)	0 - 20 kV
PWM fundamental	20 - 200 Hz
Switching frequency	500 - 4000 Hz
Rise time	>170 ns

The ten-stage generator is used in the ageing studies to obtain the time-to-failure of the prepared specimens and to produce a reference life curve. A low inductance HV series resistance is used to control the applied slew rate and to modify the waveform rise time. To alter the waveform overshoot, a shunt capacitance is used at the terminal of the load. The effect of the shunt capacitance on the rise time can be tuned back by adjusting the value of the HV resistor. Through different combinations of the series resistance and shunt capacitance, the waveform rise time is changed while maintaining a similar overshoot and vice versa. It is important to note that in order to sustain a relatively similar wave shape without generating extra oscillations while adjusting the rise time and overshoot ratio, the HV series resistors and shunt capacitors must be of very low inductance. Figure 3.7 shows a schematic of the test setup [58].

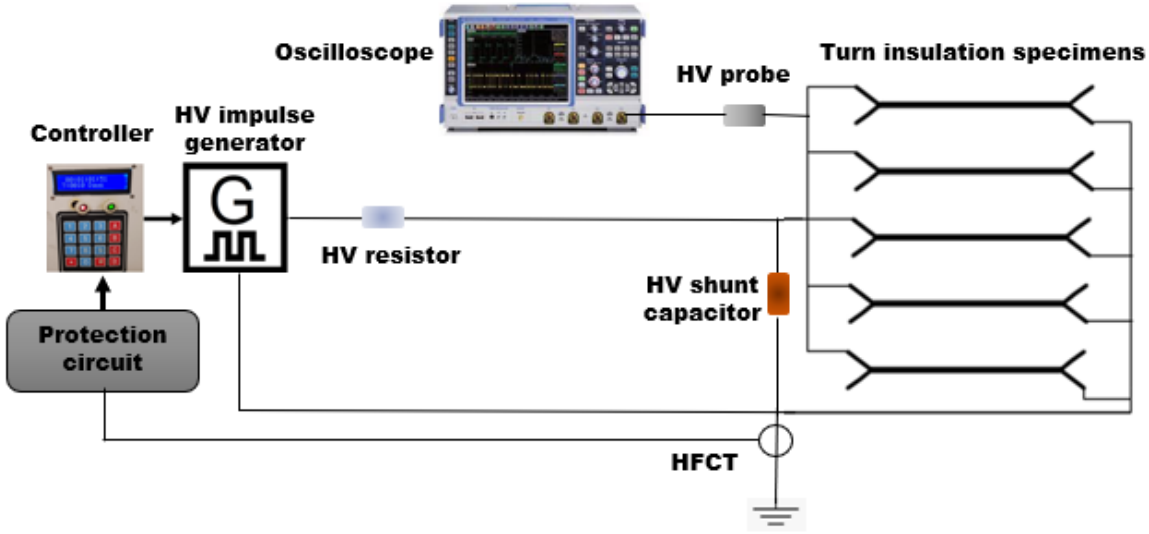

Figure 3.7 - Schematic of the circuit used for the voltage endurance studies.

For PD measurements, a two-stage modified version of the impulse generator with adjustable IGBT gate driver resistances is also utilized to vary and control the rise time of the voltage waveform. The two-stage generator is used to generate both unipolar and bipolar impulses for voltages up to 4.5 kV peak-to-peak with an option to vary the rise and fall times of the generated impulses through the gate driver circuit. Figure 3.8 demonstrates the generator schematic and specifications [6]. The generator is equipped with adjustable gate driver resistances, through which the rise and fall times of the generated impulses are altered as required. The overshoot component is boosted by terminating the cable with an additional low inductance capacitor load. The influence of the additional capacitance on the rise time

is adjusted back through the gate resistances. In doing so, the effect of the rise time is separated from the overshoot, and it would be possible to generate different overshoots with the same rise time as well as different rise times with the same overshoot [62].

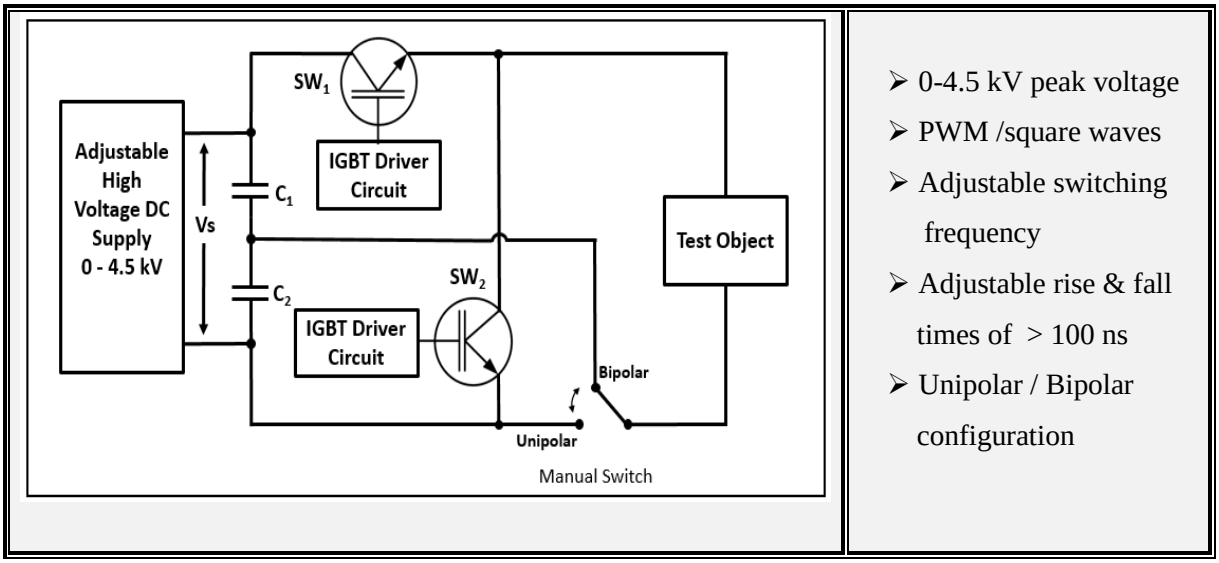

Figure 3.8 - Schematic and specification of the two-stage impulse generator [6].

3.3 PD Measurement

During each study, PD from the samples under different voltage waveform settings is captured using an A-INFO octave horn antenna (Model: LB-OH-650-15-C-NF) as a part of the PD detection system. The antenna has a 1-2 GHz bandwidth with a corresponding gain of 14-17 dB within a one-metre distance from the sample. This choice of antenna arose after several trials with other antennas of different bandwidths. Using time-frequency analysis, it was found that PD from the samples under the impulse energization has significant energy, in the range of 1-1.8 GHz, and hence, the selected antenna bandwidth is suitable for the detection. In order to verify that all the captured signals are related to internal discharges from the samples, the antenna detection system is tested with different types of controlled samples to generate different types of discharges. Signals emitted due to surface discharges and corona discharges have a much lower frequency content compared to the actual PD from a cavity [64], and thus are attenuated and any traces detected are further filtered during the post-processing stage. Electromagnetic waves from the impulse generator contain frequencies of up to 250 MHz which are well below the antenna bandwidth and do not interfere with PD detection. Moreover, the horn antenna has the advantage of directionality which reduces the switching supply interference. Prior to

each measurement, the antenna detection system is tested to ensure a high signal-to-noise ratio measurement and to verify minimum interference from other sources of PDs. The antenna is connected to a Rohde and Schwarz (R&S) oscilloscope with a 2 GHz bandwidth and a sampling rate of 10 GS/s to capture and store PD data for analysis and post-processing. The connection is done via a flexible RG-142 double shielded coaxial cable of a 50 Ω characteristic impedance and the input to the oscilloscope is terminated with a shielded connection of a matching impedance. In this work, PD that is produced during the waveform rise time and overshoot is of interest. Therefore, the oscilloscope detection window is set to 4.5 µs from the start of the applied voltage waveform (voltage triggered) which covers the region of interest. This also aids in utilizing the full resolution of the oscilloscope thereby capturing many signals while minimizing the size of the collected data. Moreover, PDs during the off-period between the impulses are also collected in order to study the impact of the waveform parameters on the accumulated charges. For each measurement set, PD signals from 100 consecutive applied voltage impulses are captured and stored. The recorded PD signals are then transferred to a computer for additional processing and analysis where the extracted PD signals are further segmented, and an envelope detection algorithm with a 30% threshold is used to record the amplitude of the PD signal in each segment referencing the position to the applied impulse. Figure 3.9 displays the general schematic of the PD detection setup and Figure 3.10 shows a screenshot of the applied voltage waveform (yellow trace) along with the captured PD signal (green trace) [62].

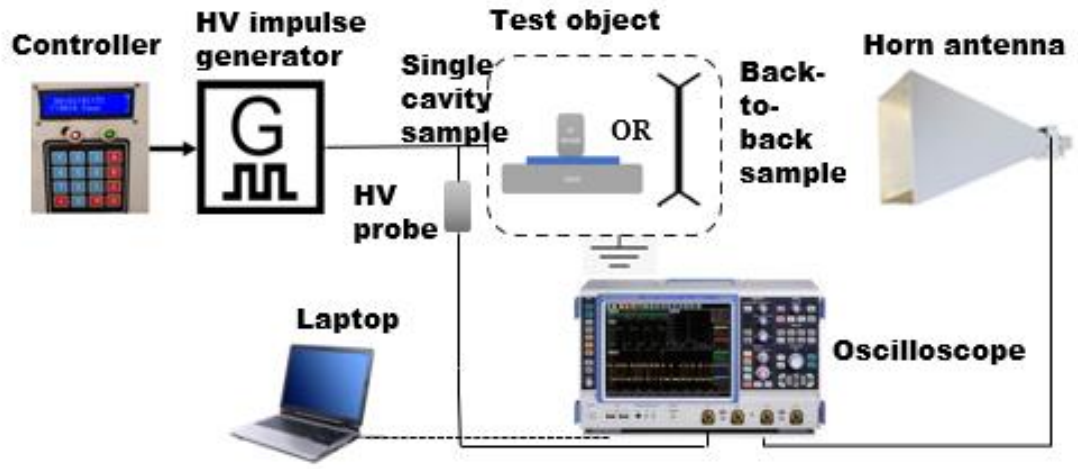

Figure 3.9 - Schematic of the experimental setup used for PD detection under impulse energization.

To confirm the validity of the PD detection system, the magnitude of the captured PD signal, in mV, using the antenna detection system, is compared to the apparent charge, in pC, using Hipotronics, DDX 9101, a standard PD detector which utilizes a coupling capacitor in its detection circuit, in accordance to IEC 60270 [65]. Table 3.5 summarizes the values of the measured apparent charge in pC to the measured electromagnetic wave in mV captured using the horn antenna placed at 1.2 meters from the test specimen. As can be seen from Figure 3.11 and Figure 3.12, a power model can be used to fit a relationship between the measured PD in pC and the detected electromagnetic wave signal associated with each discharge and captured using the horn antenna in accordance with:

$$P = \frac{V^2}{R} \tag{3}$$

where V is the peak of the captured PD signal in mV and R is the termination impedance which is equal to 50 Ω.

In order to distinguish PD signals detected using an antenna, which is measured in mV, from those measured in pC using a standard PD detector, the PD signals detected using an antenna are referred to, hereinafter, as PD_A to denote the detected electromagnetic wave associated with each PD.

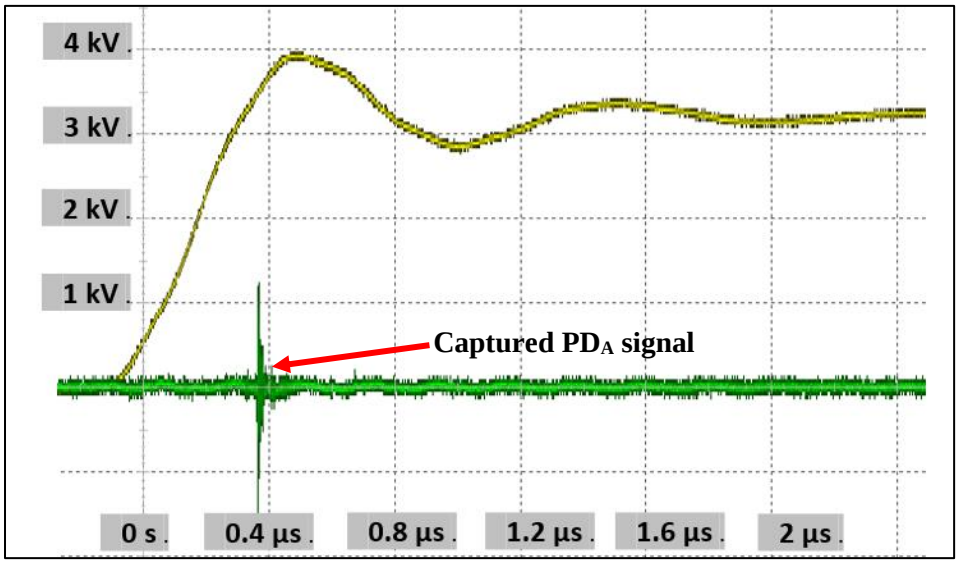

Figure 3.10 - Screenshot of the captured PD_A signal (green trace) during the rise time of an applied impulse waveform (yellow trace).

Table 3.5 - Relationship of the average magnitude of the apparent charge measured using a standard PD detector to the strength of the electromagnetic wave captured using the horn antenna.

Avg. PD magnitude (pC)	Avg. PD_A magnitude (mV)	Avg. Power (µW)
107	8	1.28
190	11	2.42
410	13.5	3.65
590	14.7	4.32
780	16.3	5.31
950	18	6.48
1210	19.3	7.45
1480	21	8.82
4450	34	23.12

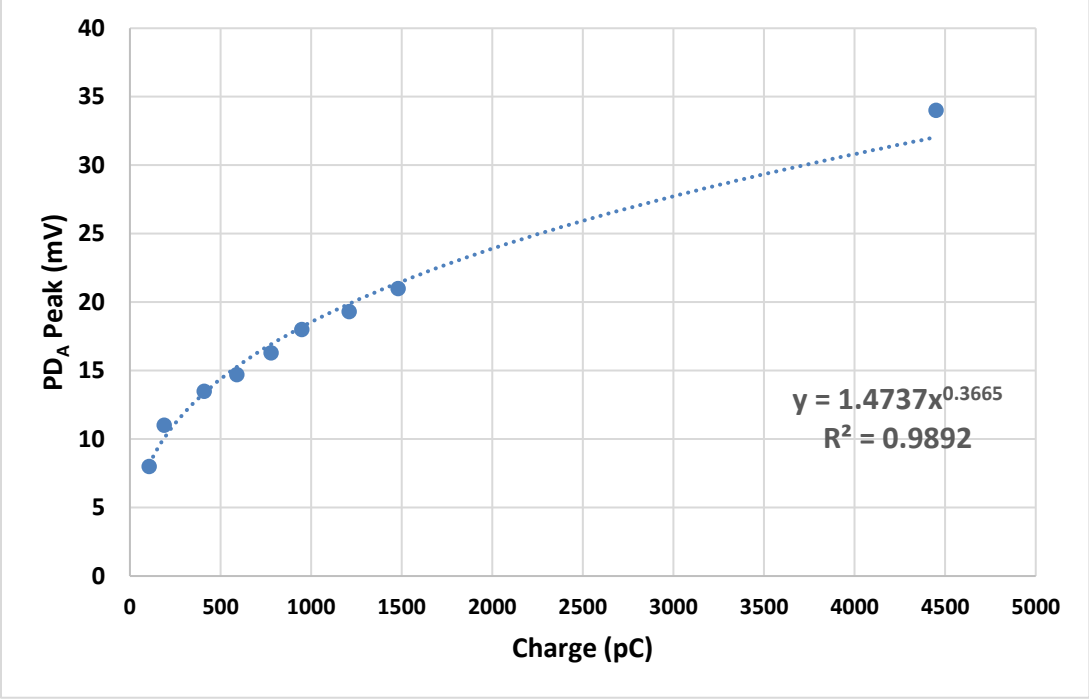

Figure 3.11 - Power model for the charge in pC vs the measured PD_A using antenna on a single back-to-back specimen.

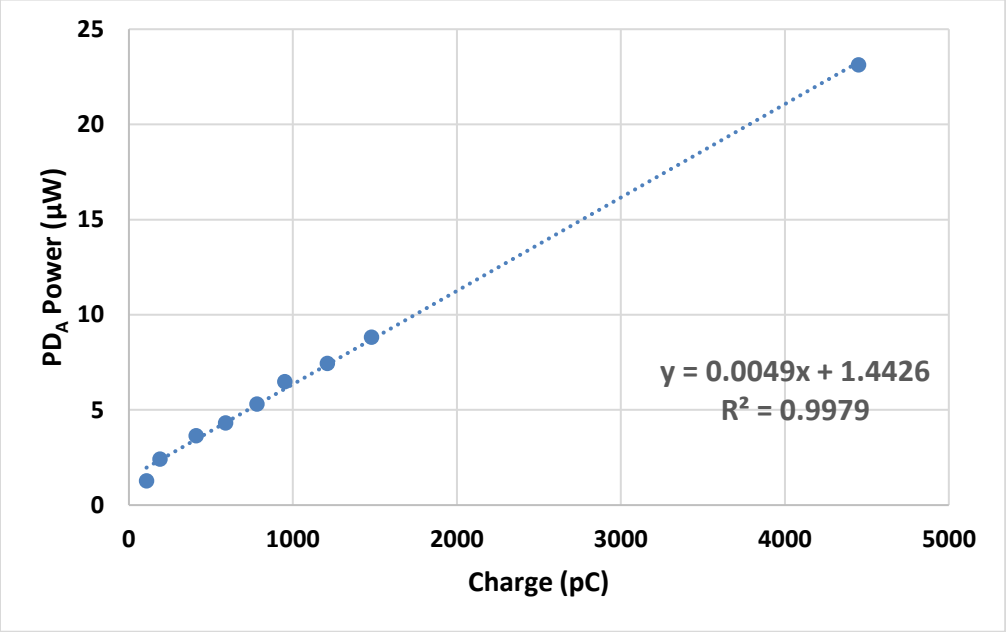

Figure 3.12 - Relationship between the measured charge and the antenna calculated power.

It is important to note that the antenna detection system is a non-standardized method for measurement of PD signals and it is generally used as a non-quantitative method to detect or locate the source of PD. Moreover, any change in the measurement environment such as changing the location of the antenna or changing the test object requires recalibration of the derived relationship. Therefore, for the purpose of this work, the horn antenna detection system is utilized to obtain trends of the strength and number of detected PD_A pulses as a response to changes in the supply factors rather than a quantitative method of measuring the discharge magnitude. Of particular interest is the average discharge rate, calculated as per Equation (4) and defined as the average PD magnitude per unit time normalized over the number of waveforms captured.

$$Avg.\,Discharge\ Rate = \frac{\sum_1^{N_w} \frac{\sum_1^{N_{PD}} PD_{magnitude}}{N_{PD}}}{N_w} \,.\, R \tag{4}$$

- where N_w and N_{PD} are the total number of waveforms captured and the total number of PD per impulse, respectively. R is the repetition rate adjustment factor and is equal to the applied waveform switching frequency in kHz.

As the average discharge rate considers the total number of PD detected and their magnitudes while accounting for the repetition rate, it can be considered analogous to the rate of energy delivered by PDs; thus the rate of damage that PDs may cause.

3.4 Statistical Analysis

Endurance studies of electrical insulation can be performed by either applying a constant stress voltage and measuring the time-to-breakdown or by applying progressive voltage stress in which the breakdown voltage is recorded. In either case and no matter how often the test is repeated, the probability of breakdown plays a major role. When using constant stress testing on a number of specimens, the time-to-breakdown of the last failed sample can be more than two orders of magnitude above the time needed for the first sample to fail [61]. This scatter in life data is typical and expected in ageing studies and insulation life assessments. Therefore, time-to-failure and life data must always be represented using statistical techniques. Some of the most common distributions used to represent insulation life data include the log-normal, Gumbel, and Weibull distributions. The latter, being an extreme value distribution, is most applied in solid insulation failure analysis where specimens fail where the insulation is the weakest. Gumbel distribution might be more applicable when percolation is involved or when prior information of exponentially distributed defects exists. Using the log-normal distribution may be an advantage when representing failures caused by reasons beyond the applied test. Since this research is concerned with solid insulation, the Weibull distribution is used to analyze the time-to-failure data, in accordance with the statistical guide in IEEE-930/IEC-62539 standard [61].

3.4.1 Weibull Distribution

Similar to the normal distribution where the distribution can be represented by the mean and the standard deviation of the data, the Weibull distribution can be represented by two parameters that define the scale and shape of the distribution, namely, α and β. Equation (5) defines the general form of a two-parameter Weibull cumulative distribution function.

$$F(t) = 1 - e^{\left(-\frac{t}{\alpha}\right)^{\beta}} \tag{5}$$

where;

- t represents the measured variable. In this work, this is the time-to-failure of the specimens.

- $F(t)$ is the probability of a sample failure at a time equal to or less than t. Hence, at $t = 0$, the probability of failure is 0, whereas, at $t = \infty$, failure is certain.

α and β are essentially positive. The scale parameter (α) has the same units as t and it represents the time required for a failure probability of 63.2% of the samples under test or in other words, the characteristic time-to-failure. This α is, in a way, equivalent to the mean in a normal distribution. On the other hand, β, known as the shape parameter, represents how widely the data is spread. The larger the shape parameter, the narrower the spread of the breakdown times and vice versa, a parameter analogous to the inverse of the standard deviation in a normal distribution. A more general form of the Weibull cumulative distribution function is demonstrated by Equation (6). This general form can be obtained by introducing the location parameter (γ), which defines a zero-failure probability for $t \leq \gamma$.

$$F(t) = 1 - e^{\left(-\frac{t-\gamma}{\alpha}\right)^{\beta}} \tag{6}$$

For meaningful statistics, the standard recommends that a minimum of 5 specimens should be used to collect time-to-failure data at each stress level. However, if feasible, a sample size of more than 10 specimens provides more accurate results. To check the adequacy of a Weibull distribution fit, the data must produce a reasonably straight line on a Weibull probability paper. Moreover, several computer packages provide a goodness-of-a-fit test, including the "lillietest" function by MATLAB®. Alternatively, simple mathematical models and techniques are available and can be used as well. To use probability papers or mathematical models; first, the failure data is ranked from lowest to highest and given a rank i , where $1 \leq i \leq sample\ size\ (n)$. The probability of a sample failure $F(I)$ is then approximated by Equation (7), where *I* is the modified rank and is equal to i for non-censored data; that is, a complete failure data set where all the samples have failed without any suspension or disqualification of any of the test data.

$$F(I) = \frac{I - 0.44}{n + 0.25}\ x\ 100\% \tag{7}$$

As explained earlier, the failure location of the samples is examined after each test. If the specimen has failed in the crotch area, the data is progressively censored and that sample should be tagged as suspended. The modified rank, I, is given then by Equation (8), where C_i is the total number of samples, including the suspended ones at the time the i^{th} failure happens.

$$I(i) = I(i-1) + \frac{n + 1 - I(i-1)}{n + 2 + C_i} \tag{8}$$

The failure probability $F(I)$ can then be plotted on a Weibull probability plot where the goodness-of-a-fit can be checked, and an estimation of the shape and scale parameters can be obtained. Alternatively, the correlation coefficient using the least-squares regression method can be used on the variable Y_i and X_i given in Equations (9) and (10) respectively to determine the goodness-of-fit [61], [66].

$$Y_i = \ln(t_i) \tag{9}$$

$$X_i = \ln\left(-ln\left(1 - \frac{F(I)}{100}\right)\right) \tag{10}$$

For a large set of data, both the scale and shape parameters can be estimated from the data calculated using Equations (8) and (9) and utilizing the slope and intercept of the calculated variables. However, for a smaller dataset (typically less than 15 samples), a weighted average of X & Y, is used for a more accurate estimate of the Weibull's shape and scale parameters, as shown in Equations (11) and (12), respectively.

$$\beta = \frac{\sum_{i=1}^{r} w_i \left(X_i - X_{avg}\right)^2}{\sum_{i=1}^{r} w_i \left(X_i - X_{avg}\right)\left(Y_i - Y_{avg}\right)} \tag{11}$$

$$\alpha = e^{Y_{avg} - \frac{X_{avg}}{\beta}} \tag{12}$$

where;

- X_{avg} and Y_{avg} are the weighted averages of X_i and Y_i and calculated as per Equations (13) and (14), respectively.

$$X_{avg} = \frac{\sum_{i=1}^{r} w_i X_i}{\sum_{i=1}^{r} w_i} \tag{13}$$

$$Y_{avg} = \frac{\sum_{i=1}^{r} w_i Y_i}{\sum_{i=1}^{r} w_i} \tag{14}$$

and

- r is the rank of the last broken sample, ($r < n$ for censored data).

- w_i is the i^{th} data weighting factor, which varies based on the total number of broken samples, and the complete sample size. A complete list of the weighting factors based on the values of n & r can be found in [61].

It is very common to represent electrical insulation failure data with a Weibull probability plot as opposed to a Weibull cumulative distribution function plot. The measured variable (x_i), the time-to-failure in this research, can be plotted on the X-axis, which is logarithmically scaled. The failure probability is drawn on the Y-axis, which is scaled non-linearly such as $Y_{axis(i)} = \log(-\ln(1 - F(x_i))$. Confidence intervals for the failure probability can also be estimated and drawn on the same plot. Furthermore, confidence intervals can be calculated for the estimates of the Weibull parameters, α and β, as well. It is worth mentioning that less confidence can be given to censored data than to complete data. The higher the confidence percentage for a given sample size, the wider the interval would be. On the other hand, increasing the sample size helps in narrowing the bounds of a certain confidence interval. A complete list of the parameters and weighting factors to be used in the calculation and establishment of the lower and upper bounds of the confidence interval based on, r, and the selected confidence percentage are available in the IEC/IEEE statistical guide [61].

3.4.2 Design of Experiments

A well-designed experiment helps in determining the important factors that impact the process and assists in identifying possible interactions between the studied factors. Moreover, a properly-designed experiment is vital in modelling the behaviour of the system as results and conclusions depend largely on the way the experiment is set and how the data is collected and interpreted. One of the most commonly used methods is the one-factor-at-a-time approach where the response of a system is measured by varying one factor at a time while holding all other factors constant. Although this is extensively used in practice, it is an inefficient way of scanning the impacting factors as it fails to determine the interaction effect between the factors and can lead to seriously inaccurate conclusions [56]. An interaction between the studied factors is common in engineering and it is defined as the inability of a certain factor to reproduce the same influence on the measured response at different levels of the other factors. The proper way to approach an experiment with several factors is by conducting a statistically designed experiment utilizing a factorial design approach where factors are allowed to change together systematically to determine the main effect of each factor and the important interactions between them. Of interest is the 2^k factorial design where each factor (k) has two levels,

namely the low and high settings, generally denoted by "-1" and "+1" respectively [67]. In this particular design, each of the studied factors would have two responses at each level of the other factors, and therefore, in a way, replicas of the factor response are provided without the need for a second observation at each level. The main effect of the factor is then calculated by averaging the responses of the factors at different levels of the other factors and hence obtaining results that are valid over a various range of experimental conditions [68]. To better illustrate the advantages of a factorial design and how it is conducted, consider the following data displayed in Table 3.6 for an ageing experiment with only two stress factors considered; factor A representing the supply switching frequency (f_{sw}) and factor B representing the jump voltage (U_j).

Table 3.6 - Factor settings and their responses based on a factorial design.

Factor A: f_{sw} (kHz)	**Factor B: U_j (kV)**	**A**	**B**	**AB (Interaction)**	**Response: Characteristic-Time-to-Failure (Hrs)**
1	**6**	-1	-1	+1	362.96
1	**10**	-1	+1	-1	15.58
4	**6**	+1	-1	-1	34.74
4	**10**	+1	+1	+1	4.11

- Where +1 represents the high setting of the factor/ interaction while -1 represents the low setting accordingly.

The main effect of a factor or an interaction is calculated by subtracting the average value of the responses at the low setting for the factor/interaction under study from the average value of its responses at the high setting as follows:

$$Main\ effect\ or\ interaction = AVG\ of\ responses\ at\ high\ (+1)\ setting - AVG\ of\ responses\ at\ low\ (-1)\ setting$$

For example, the main effect of the switching frequency is calculated accordingly as follows:

$$Main\ effect\ of\ f_{sw} = AVG\ of\ responses\ when\ f_{sw}\ is\ 4kHz - AVG\ of\ Responses\ when\ f_{sw}\ is\ 1kHz$$

That is:

$$Main\ effect\ of\ f_{sw}\ (Factor\ A) = \frac{34.74 + 4.11}{2} - \frac{362.96 + 15.58}{2}$$

Similarly, for the interaction effect, it is found by subtracting the average of the responses when one of the factors is low and the other is high (AB= -1) from the average of the responses when both are high or low at the same time (AB= +1). Another way to visualize the impact of the interaction between the factors is shown in Figure 3.13 where the response to a change in one factor is clearly not the same at different settings of the other factor. This type of interaction sometimes can mask the importance of the main factor effect whereas in many cases where the interaction effect is not recognized, misleading conclusions are likely to be made [56].

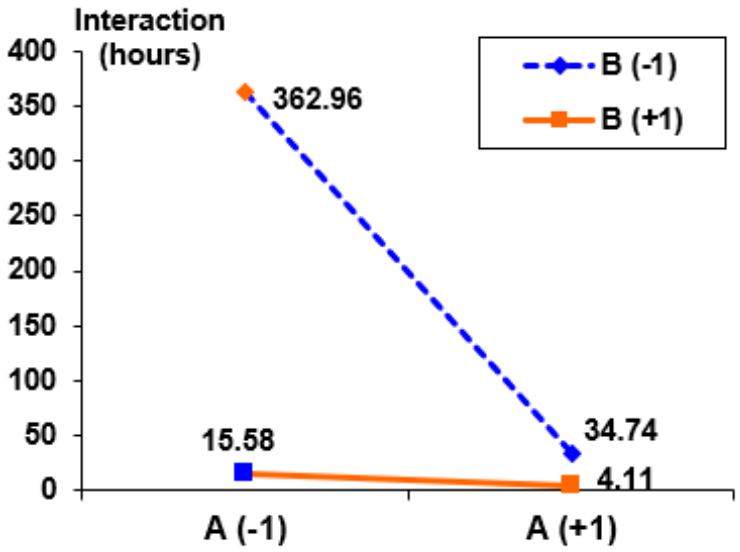

Figure 3.13 - Interaction between A and B factors.

In comparison, suppose a single factor experiment is to be made instead of the factorial approach to identify the effect of factors A and B. Information on the influence of each factor can be obtained by changing the levels of each factor one at a time in accordance to Figure 3.14. Therefore, three experimental combinations are needed to study the effect of factors A and B. To avoid error, it is strongly recommended to have at least one more observation at each of the experimental combinations making the total number of the required experimental runs six for a two-factor experiment. The same precision can be obtained using a factorial design with just one treatment added at the high level of both factors A and B without the need of repeating any of the observations making the total number of experimental runs required as four. Not only does the efficiency increase by a factor of 1.5 using a factorial design, but also, the primary effect of each factor is distinguished from the interaction effect

rendering the validity of the results over a wider range of experimental conditions and preventing a possibly serious error in the interpretation of the results. The efficiency of factorial design becomes even much higher as the number of factors considered increases and therefore it is a superior approach in dealing with multifactor experiments [56].

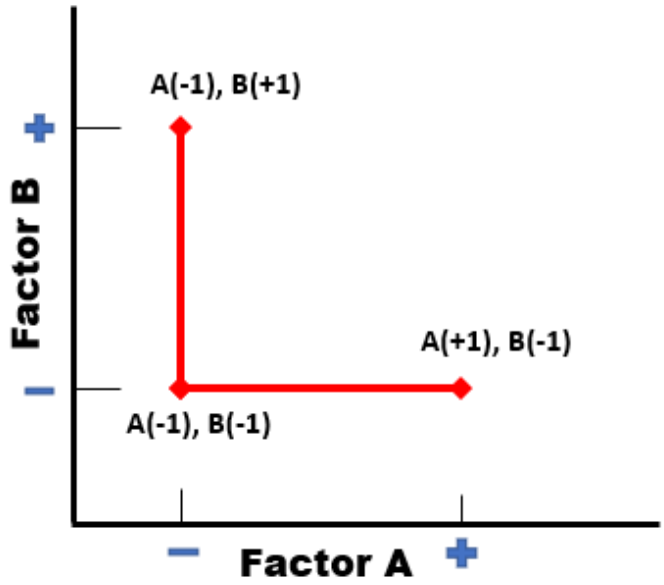

Figure 3.14 - Experimental runs for a one-factor-at-a-time experiment approach.

3.5 Modelling and Simulation

The electric stress within the turn insulation is not only determined by the instantaneous applied voltage itself but also by the waveform and voltages that have been previously applied and stressing the insulation. This is due to the space, interfacial, and surface charge accumulations within the insulation layers. Direct measurement of the electric stress under impulse conditions is a challenge; therefore, simulation studies are performed to help in understanding and investigating the effect of features of the PWM supply on the electric stress and space charge limited field within turn insulation. COMSOL Multiphysics® is used as a tool to perform numerical simulations to solve partial differential equations based on Maxwell's unified electromagnetic theory in discretized domains. The tool is used to simulate the effect of varying the switching frequency, rise time, and impulse overshoot on the electric field distribution within the turn insulation taking into account the effect of charge accumulation and surface charge decay. The results of the simulation work can be utilized to obtain a better understanding of the

behaviour of PD obtained in the experimental work. By understanding the significance of the charge accumulation and the variation of the space charge limited field on PD, one can further relate the results obtained from the time-to-failure studies and determine the significant factors in the ageing mechanism and how they affect the insulation lifespan.

3.5.1 Governing Field Equations

The electric current module in COMSOL combines Gauss's law and Ohm's law with the current continuity equation to solve for the electric field and the potential distributions in dielectrics. The basic field equations are given by [69]:

$$\nabla . D = \rho \qquad (Gauss's\ law) \tag{15}$$

$$J = \sigma E \qquad (Ohm's\ law) \tag{16}$$

$$\nabla . J + \frac{\partial \rho}{\partial t} = 0 \quad (Current\ continuity\ equation) \tag{17}$$

- where D is the electric displacement field, ρ is the charge density, J is the electric current density, σ is the material conductivity, E is the electric field intensity and;

$$E = -\nabla V \tag{18}$$

$$D = \varepsilon E \tag{19}$$

- where V is the electric potential and ε is the material permittivity.

Therefore, by combining Equations (15) and (16) with Equations (18) and (19), Equation (17) can be rewritten as:

$$\nabla . (-\sigma \nabla V) - \nabla . \varepsilon \nabla \left(\frac{\partial V}{\partial t}\right) = 0 \tag{20}$$

COMSOL electric current interface utilizes FEM to solve Equation (20) and obtain the local electric potentials within the material over a set of explicit boundary conditions given that the permittivity and conductivity of the material are defined [69].

3.5.2 Geometry, Materials, and Boundary Conditions

The simulation model geometry and materials are based on the single cavity sample introduced earlier in Figure 3.5, and the dimensions and thickness of each layer are set therefore accordingly. Other dimensions and material properties are adjusted whenever possible based on actual measurements or

according to the insulation material data sheets [70]. The model includes a dedicated layer of 1 µm thickness to represent the cavity surface and the interface boundaries between the insulation layers which allows for the modelling of the charge mobility and decay through surface conductance [71]. It is important to note that this model deals only with the macroscopic aspect of the field simulation within the cavity which depends on the permittivity and the conductivity of the material as the main governing properties. Microscopic aspects of the PD and charge mechanisms such as electron attachment and detachment process, drift-diffusion, avalanche propagation, and so on are not modelled or considered in this simulation. Figure 3.15 shows the sample geometry along with the modelled void to simulate a defect or an imperfection, as multiples of those are expected to occur within an actual coil during the manufacturing process. Table 3.7 defines the geometry and material settings used in the simulation model.

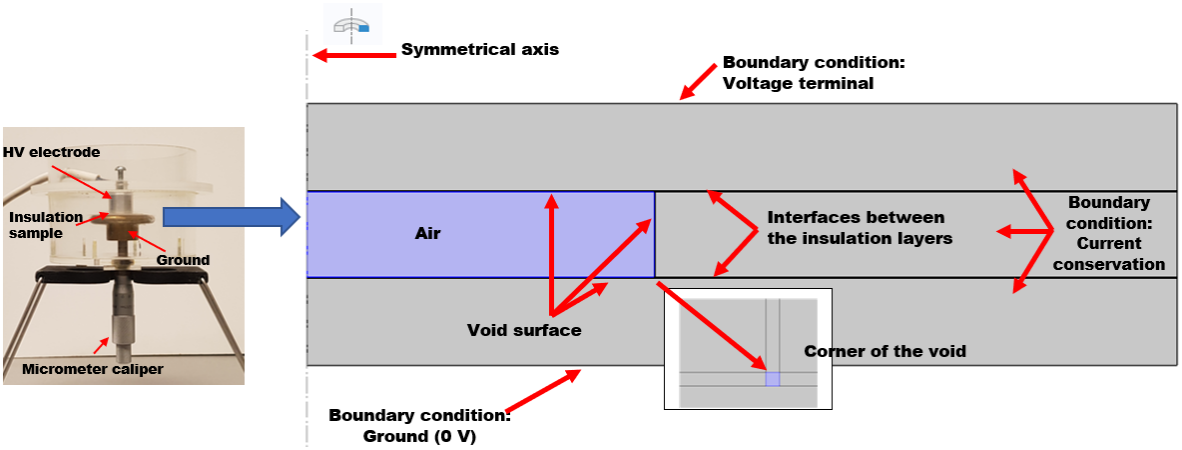

Figure 3.15 - Geometry, boundary, and layer descriptions of the single cavity simulation model.

In this model, charge simulated surface conductivity plays an important role in controlling the rate at which the resultant field at the center of the void increases/decreases through surface conduction which simulates the effect of surface charge mobility and decay time. The impact of the accumulated charges from previous PDs on the electric field within an embedded cavity through cavity surface conduction is first modelled in [72] and verified numerically by [71] and [73]. This is simulated through the impact of charge deposition on the cavity surface conductivity (σ_s). The decay rate of the accumulated charges on the surface of the void is controlled through the surface conduction by the cavity surface time constant (τ_s), where $\tau_s = \frac{\sigma_s}{\varepsilon_s}$. The cavity surface conductivity affects the decay rate and therefore faster surface charge decay is induced by greater σ_s, which causes the electric field in the

cavity to decrease. This is modeled through a field-dependent surface conductivity which simulates the free charge movement through the cavity surface and depends on the magnitude of the electric field at the center of the cavity (E_{cav}):

$$\sigma_s = \sigma_{s_0} \exp(\alpha |E_{cav}|) \tag{21}$$

Table 3.7 - Geometry and material settings used in the simulation model.

Parameter	Symbol	Value
Cavity height	h_c	0.09 mm
Cavity radius	r_c	0.39 mm
Cavity relative permittivity	$\varepsilon_{r.c}$	1
Cavity conductivity	σ_c	$1x10^{-18}\ S/m$
Cavity surface thickness	Th_c	1 μm
Cavity surface relative permittivity	$\varepsilon_{r.s}$	6
Cavity surface initial conductivity	σ_{s_0}	$2.01x10^{-15}\ S/m$ (unaged), $1x10^{-11} S/m$ (aged)
Cavity surface maximum conductivity	$\sigma_{s_{max}}$	$1x10^{-9}\ S/m$ (unaged), $1x10^{-5} S/m$ (aged)
Insulation layers height	h_i	0.09 mm
Insulation layers relative permittivity	$\varepsilon_{r.i}$	6
Insulation layers conductivity	σ_i	$2.01x10^{-15}\ S/m$
Interfaces thickness	Th_{int}	1 μm
Interfaces relative permittivity	$\varepsilon_{r.int}$	1
Interfaces initial conductivity	σ_{int_0}	$2.01x10^{-15}\ S/m$
Interfaces maximum conductivity	$\sigma_{int_{max}}$	$1x10^{-9}\ S/m$
Coefficient for the surface and interface conductivity	α	10 mm/kV

Similarly, the interface layer surface conductivity is modelled through field-dependent conductivity that depends on the electric field at the corner of the void (E_{cor}):

$$\sigma_{int} = \sigma_{int_0} \exp(\alpha |E_{cor}|) \quad (22)$$

The field-dependent coefficient (α) is set to control the rate of change in the surface and interface conductivities following the applied field. Therefore, if α is set too small, σ_s and σ_{int} will increase too slowly towards the maximum limit causing insufficient decrement of the resultant field. However, if α is set too large, the increment of the field-dependent conductivity will be too fast, resulting in too fast reduction in the resultant field. This simulates the effect of charge mobility and accumulation during the applied waveform on-time and the charge decay and relaxation during the off-time. For the purpose of simplifying the model, the strand tape is assumed to be homogenous, isotropic, and non-dispersive and therefore its relative permittivity is assumed to be fixed and not influenced by the applied frequency. Material properties including those of the conductivity and relative permittivity of air and strand tape (mica paper based on calcined muscovite impregnated with resin) are set following the values provided in [6], [74] and as per the default material properties defined in COMSOL at room temperature [69]. The relative permittivity and the initial value for the unaged cavity surface as well as the interface layers are adopted from the default insulation material properties. In order to maintain numerical stability and control the rate at which the field is decaying, a maximum value for the surface and interface conductivity should be set. For this model, this value was found to be in the range of 10^{-7} to 10^{-11} S/m which agrees with the values given in the literature [71], [73]. These values are applicable for an unaged cavity. For an aged cavity, the surface conductivity is determined by the ageing state of the stressed surface. Heat and ionization by-products generated from the discharge activities on the surface of the void can cause physical and chemical deterioration to the surface of the void. Continuous PD can lead to corrosion and the initiation of surface tracking. Therefore, to simulate the deterioration and surface tracking effect, a higher surface conductivity limit is applied. From the literature [72], the initial surface conductivity for an aged void is estimated as 1×10^{-11} S/m while the maximum surface conductivity is set as 1×10^{-5} S/m.

Chapter 4
Results

4.1 Turn Insulation Ageing Tests and Time-to-Failure Analysis

In this section, the impact of the waveform switching frequency, overshoot, and rise time on the time-to-failure and the endurance of Type II back-to-back turn insulation, described in Subsection 3.1.1, is reported. Unipolar square repetitive impulses of 50% duty cycle are used in all of the ageing experiments. Reference life curves at 1 kHz and 4 kHz switching frequencies are derived utilizing repetitive impulse energization. The effects of the impulse overshoot and rise time on the endurance of turn insulation are also investigated in the ranges of 0% to 30% and 400 ns to 600 ns, respectively. Factors selection and limits are set based on current practical considerations, and recent concerns and research studies presented in Chapter 2. The experimental setup used for the endurance test is in accordance with the schematic described in Figure 3.7. Test voltages, sample size selection and other experimental procedures are performed following the standard guidelines as described in Chapter 3.

4.1.1 Life Curve and the Impact of Switching Frequency

In order to investigate the influence of the supply switching frequency on the endurance of turn insulation and establish a reference life curve, accelerated ageing using repetitive impulse energization is done on the prepared specimens. Unipolar square repetitive impulses of 50% duty cycle are used in the ageing experiment and the establishment of the life curves for both 1 kHz and 4 kHz switching frequencies. The overshoot percentage and the rise time of the impulse supply are respectively retained at 15% and 300 ns. To maintain the same overshoot and rise time throughout the ageing experiment (within 10% variation), failed samples are replaced with equivalent low inductance capacitance, while the time-to-failure data are recorded at each voltage level and analyzed using Weibull statistics.

The IEC standard recommends that the time-to-failure data for the turn insulation endurance testing be recorded for at least 3 different test voltages while a minimum of five specimens are to be tested at each voltage level. The standard requires a voltage endurance test to qualify turn insulation only if PD is detected at a peak voltage below 1.5 of the nominal turn insulation voltage (U_{turn}), otherwise, a qualification test is not required [4]. According to the measured values reported in Table 3.3, the PDIV for the prepared specimens is in the range of 2.1 to 2.2 kV_{rms}. This is approximately equal to a peak voltage of 3 kV; therefore, U_{turn} for the prepared specimens is considered as 2 kVp. The test voltages,

as recommended in [4], are to be chosen between 3 to 5 of U_{turn}; thus, peak voltages in the range of 6 kV to 10 kV are selected to establish the reference life curves in this work. This allows for the test voltages to be well above the inception voltage of the samples while allowing enough margin from their breakdown strength. Only failures that take place in the straight portion of the specimens are considered valid; consequently, specimens which happen to fail in the crotch area are censored following the procedures described in Section 3.4. Less confidence can be placed on the analysis of censored data as opposed to a complete data set; therefore, a larger sample size is selected in the very first few experiments to ensure enough valid data are collected from the endurance test and to gain more trust in the proper construction of the test specimens to serve the intended purpose. As all of the specimens used in the development of the life curve failed in the straight part, moving forward, the sample size is set to 6 specimens per test voltage. Figure 4.1 and Figure 4.2 display the Weibull probability plots with their relevant 90% confidence interval for each of the voltage endurance tests at switching frequencies of 1 kHz and 4 kHz, respectively; whereas, Table 4.1 summarizes the relevant statistical results in which Vp is the peak voltage applied (in this case it is the same as the jump voltage U_j), N_s is the sample size, and r is the correlation coefficient. The subscripts (l and u) represent the 90% confidence interval (lower and upper bounds limits, respectively.) Since the coefficient of determination (R-squared) for the 1 kHz data (considering the initially selected test voltages at 10 kV, 8 kV and 7 kV) is below the 95% passing criteria, an additional point at 6 kV is obtained following the standard guidelines resulting in four test voltages used per life curve.

Table 4.1 - Summary of the Weibull statistical parameters for the 1 kHz and 4 kHz endurance tests.

f_{sw}	Vp	N_s	r	β		α	
1 kHz	10 kV	9	94.5%	2.68		15.58	
				β_l = 1.74	β_u= 4.56	α_l = 12.37	α_u= 19.14
	8 kV	7	94.6%	1.74		87.7	
				β_l = 1.13	β_u= 2.96	α_l = 61.43	α_u= 120.26
	7 kV	6	97.6%	2.68		71	
				β_l = 1.74	β_u= 4.56	α_l = 56.36	α_u= 87.14
	6 kV	6	96.4%	1.33		362.96	
				β_l = 0.74	β_u= 1.93	α_l = 210.07	α_u= 589.57

4 kHz	**10 kV**	**7**	**73.8%**	3.33		4.11	
				β_l = 2.16	β_u= 5.66	α_l = 3.41	α_u= 4.84
	8 kV	**7**	**97.5%**	2.65		13.24	
				β_l = 1.72	β_u= 4.51	α_l = 10.48	α_u= 16.3
	7 kV	**6**	**92.8%**	4.3		17.19	
				β_l = 2.79	β_u= 7.31	α_l = 18.88	α_u= 19.54
	6 kV	**6**	**98%**	3.02		34.74	
				β_l = 1.96	β_u= 5.13	α_l = 28.29	α_u= 41.69

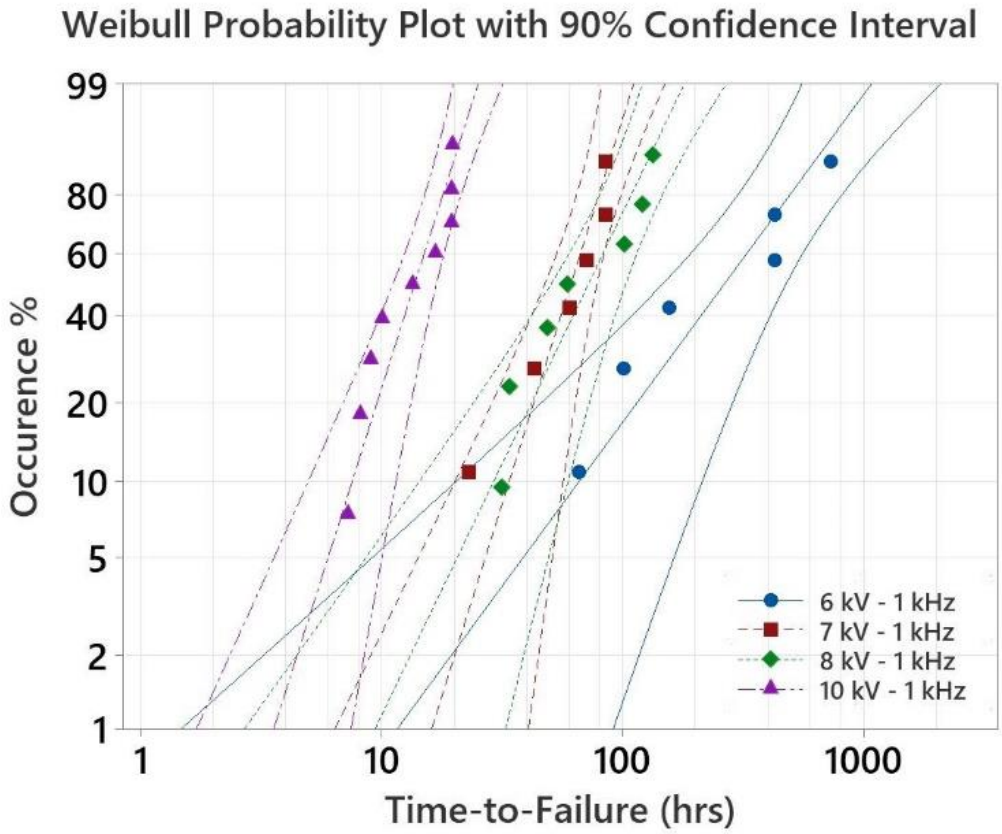

Figure 4.1 - Weibull probability plots with 90% confidence intervals for the 6, 7, 8, and 10 kV repetitive impulse ageing experiments at 1 kHz switching frequency, 0.3 µs rise time and 15% overshoot.

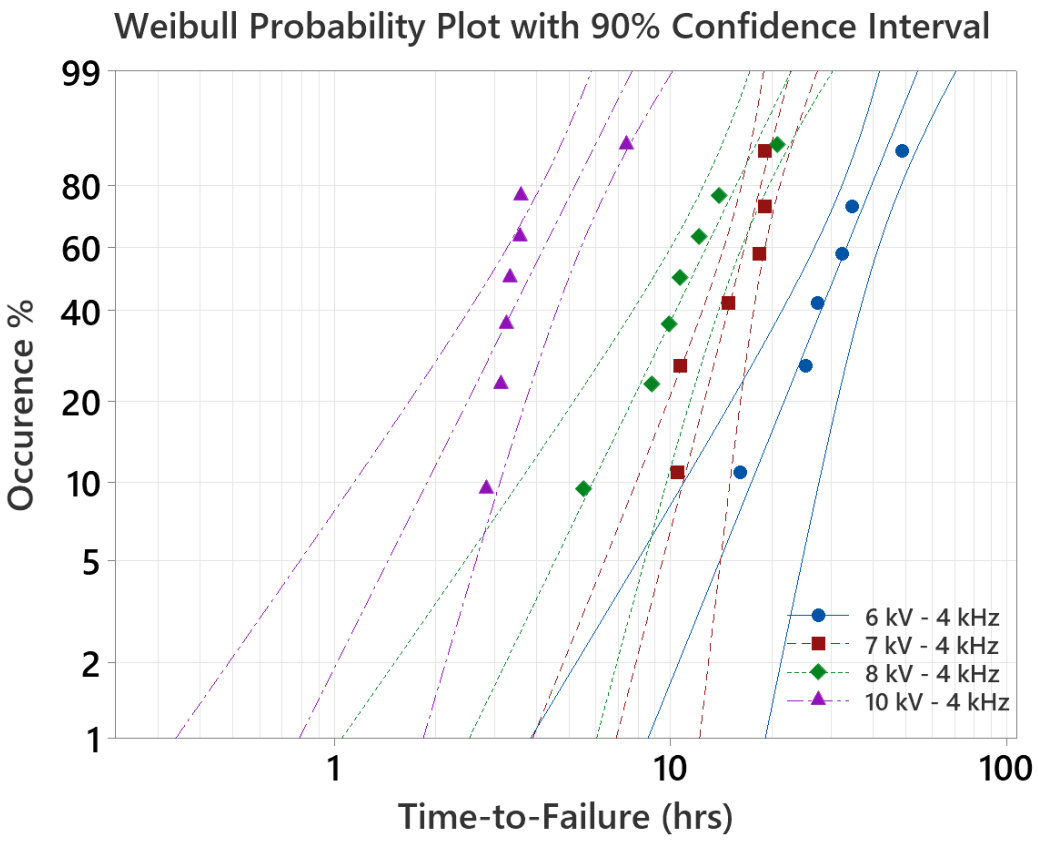

Figure 4.2 - Weibull probability plots with 90% confidence intervals for the 6, 7, 8, and 10 kV repetitive impulse ageing experiments at 4 kHz switching frequency, 0.3 µs rise time and 15% overshoot.

As can be seen from Table 4.1, the shape parameters in both experimental data sets are close. Looking at their confidence interval overlap, one cannot conclude whether they are different, meaning that the spread of failure data in both experiments is equivalent. Moreover, the goodness-of-fit test and the correlation coefficient in both experiments confirm that the data has a good fit and can be represented by a Weibull distribution. As seen from both Figure 4.1 and Figure 4.2, there is a slight change in the Weibull probability slope as the stress level increases in both 1 kHz and 4 kHz ageing experiments. This could indicate a change in the ageing mechanism, or possibly an interaction between the stressing factors. This might also imply that the resultant VEC is stress-dependent contrary to what is assumed in the standard. Using the characteristic time-to-failures derived from the respective Weibull plots at each of the test voltages, reference life curves for both 1 kHz and 4 kHz switching frequencies are established and shown in Figure 4.3.

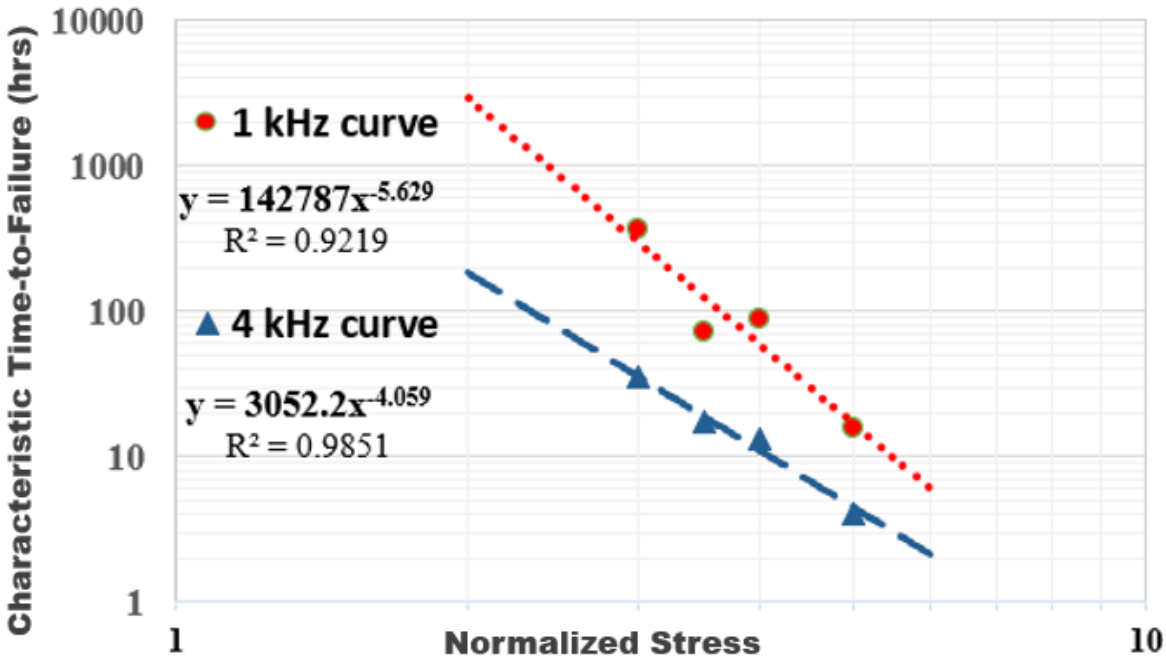

Figure 4.3 - Experimentally established life curves for 1 kHz and 4 kHz ageing experiments under repetitive impulse supply of 0.3 µs rise time and 15% overshoot.

As can be seen in Figure 4.3, the derived VEC under impulse energization for Type II insulation varies between 4 and 6, which is roughly half of what has been specified by IEC 60034-18-42 for a VEC established under a sinusoidal supply. This suggests that the turn insulation encounters a much higher ageing rate under impulse energization than it does under sinusoidal stress. Moreover, the VEC for the 4 kHz life curve is almost 30% lower than that of the 1 kHz curve. The change in the life curve slopes, defined by the VEC, at different frequencies indicates that the proportion of the additional stress caused by increasing the supply switching frequency is not consistent at different voltage stresses.

4.1.2 Impact of the Waveform Rise Time

To study the direct impact of the waveform rise time on the life endurance of turn insulation, time-to-failure data are collected from accelerated ageing experiments under repetitive impulse energization utilizing a sample size of 6 specimens per test. The applied waveform switching frequency is fixed to 1 kHz in all of the endurance tests in order to reflect the result on the established reference life curve. As changing the impulse rise time may affect the waveform overshoot, the impact of the waveform rise time is often inseparable from that of the overshoot. Therefore, in this work, both the rise time and the

overshoot are varied independently using two different levels per factor. This not only helps in isolating the impact of the rise time at different overshoot levels but also assists in pointing out possible interactions between both factors in terms of their direct impact on ageing if any. Table 4.2 summarizes the Weibull statistical parameters for the voltage endurance tests at each of the waveform settings; whereas, Figure 4.4 displays their resultant probability plots accordingly. Note that the displayed points in Figure 4.4 refer to specimens that failed on the straight part of the coil; therefore, only 4 points are shown for the "5.4 kVp - 0% OS - 0.4 µs t_r" plot since 2 out of the 6 specimens tested are censored.

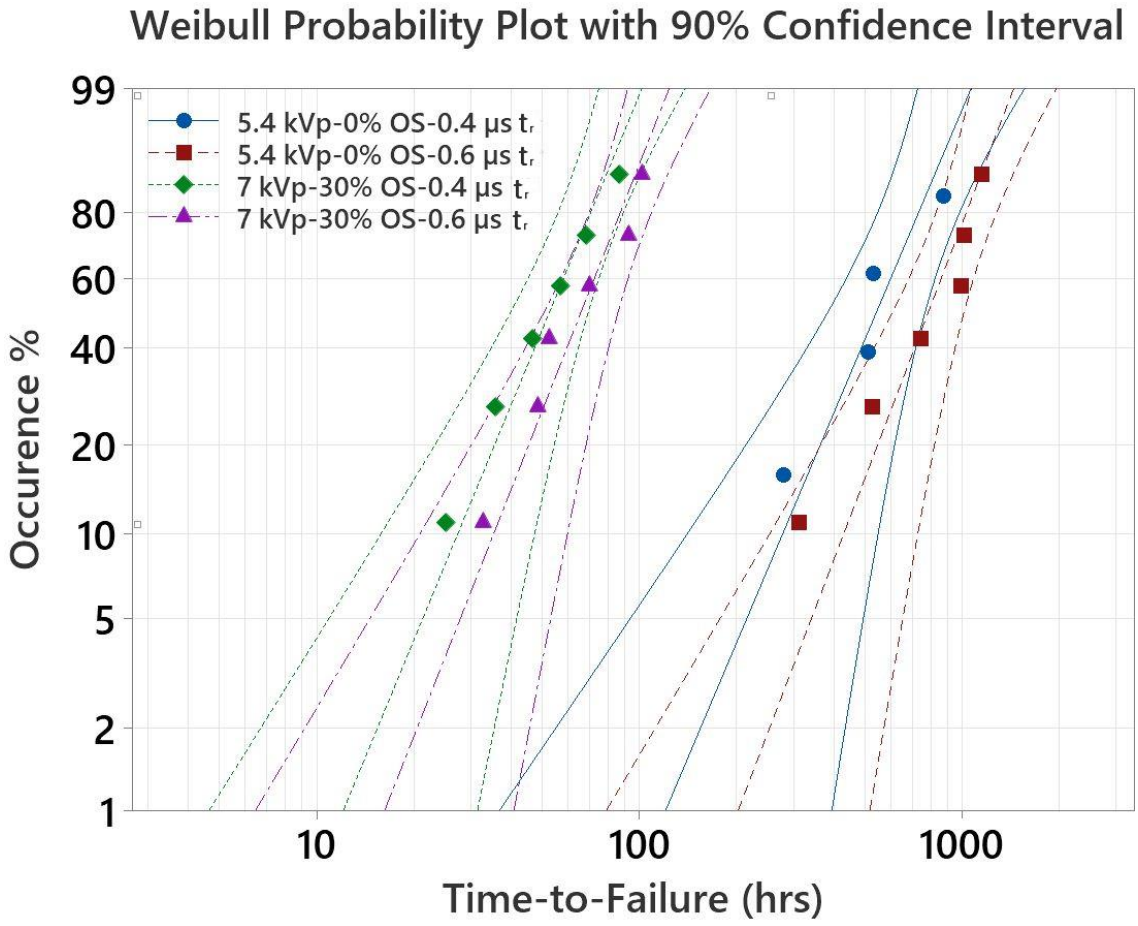

Figure 4.4 - Weibull probability curves with a 90% confidence interval for the repetitive impulse ageing experiments at 0.4 µs and 0.6 µs rise times for waveforms with and without overshoots.

Table 4.2 - Summary of Weibull statistical parameters for the impact of the waveform rise time and overshoot at equal step voltage (V_{DC}).

OS	N_s	Vp	V_{DC}	t_r	β		α	
0%	**6 (censored)**	**5.4 kV**	**5.4 kV**	**0.4 µs**	2.07		764.95	
					β_l = 1.34	β_u= 3.52	α_l = 566.82	α_u= 997.97
0%	**6 (complete)**	**5.4 kV**	**5.4 kV**	**0.6 µs**	2.61		920.99	
					β_l = 1.70	β_u= 4.44	α_l = 726.56	α_u= 1136.6
30%	**6 (complete)**	**7 kV**	**5.4 kV**	**0.4 µs**	2.42		61.60	
					β_l = 1.57	β_u= 4.11	α_l = 47.67	α_u= 77.34
30%	**6 (complete)**	**7 kV**	**5.4 kV**	**0.6 µs**	2.52		76.48	
					β_l = 1.64	β_u= 4.29	α_l = 59.81	α_u= 95.12

As can be seen from Figure 4.4, a shorter rise time results in a shorter time-to-failure for both types of applied waveforms, with and without overshoot. Although this slight reduction of the time-to-failure in both scenarios seems consistent, statistically speaking, it still falls within the 90% confidence interval of the distribution, and hence, a definite conclusion on the impact of the rise time cannot be made. This minor impact of the rise time could be, on the other hand, attributed to the limited range of rise times considered in this study due to experimental limitations. Moreover, it appears that the interaction between the rise time and the overshoot factors is insignificant, given the relatively similar impact of the rise time on the time-to-failure at different overshoot settings. This implies the possibility of generalizing the impact of either factor at different settings of the other factor allowing single-factor experiment designs. To further validate the impact of the rise time and investigate whether this minor impact is proportional to the limited range of the rise time settings considered, an endurance test on a sample size of 3 is performed under repetitive impulse voltage of 5.4 kV peak, 1 kHz switching frequency, 0% overshoot, and 1 µs rise time and compared to those of 0.4 µs and 0.6 µs rise times with similar supply configurations, Table 4.3.

Table 4.3 - Impact of the waveform rise time on the times-to-failure (in hours) for turn insulation specimens subjected to unipolar impulses of 5.4 kV peak voltage, 1 kHz switching frequency, 0% overshoot.

Sample rank #	$t_r = 0.4\ \mu s$	$t_r = 0.6\ \mu s$	$t_r = 1\ \mu s$
1	241.17	312.53	401.58
2	281.20	529.30	617.75
3	513.50	748.45	986.73
4	530.77	993.65	---
5	880.83	1015.22	---
6	1077.90	1150.92	---

The highlighted times-to-failure in Table 4.3 are those which considered invalid due to the location of the failure and are therefore disregarded from the analysis. Unfortunately, there is not enough valid failure data for the 1 µs endurance test to form a meaningful statistical analysis. Nevertheless, it is evident that the time-to-failure increases with longer rise times. This increase is seen between the 0.4 µs and 0.6 µs endurance tests despite the small difference in their rise time settings. On the other hand, there is no apparent difference between the test done at 0.6 µs and 1 µs rise times despite the larger difference in their settings. There appears to be a range beyond which a shorter rise time might become significant and could have a direct impact on the ageing and the endurance of turn insulation. In addition, waveforms with rise times more than 1 µs do not cause as much voltage drop across the turn insulation compared to waveforms with shorter rise time, and thus, are not a concern in practice.

4.1.3 Impact of the Waveform Overshoot

In Subsection 4.1.2, the impact of the rise time, although slight, was highlighted at different overshoot levels emphasizing the direct influence of the waveform rise time on the time-to-failure detached from the overshoot impact. Comparably, Figure 4.4 and Table 4.2 also demonstrate a clear impact of the overshoot factor at different rise times for the case where the applied waveforms would have equal step voltages. In this situation, waveforms with a higher overshoot ratio result in a higher jump/peak voltage

(7 kVp for the waveform with overshoot compared to 5.4 kVp for the one without overshoot) as can be seen in Figure 4.5.

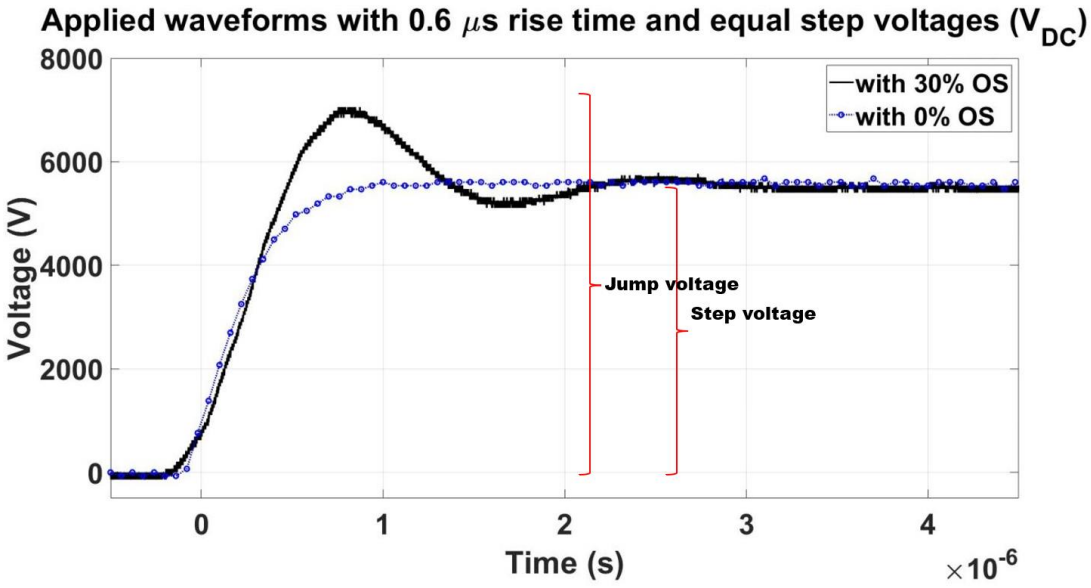

Figure 4.5 - Example of the applied voltage waveforms at 0.6 µs rise time, with and without overshoot, measured at the terminal of the test objects when the applied step voltages are the same.

The difference in the peak voltage as a result of the overshoot may appear as an unfair comparison, however, it is more of a realistic application scenario, where the step voltage is determined based on the machine operating voltage and the overshoot appears as an additional component at the terminal of the load due to the mismatch impedance between the cable and the running load. Therefore, the impact of the additional overshoot component on the time-to-failure may be attributed to the jump voltage effect where in fact it includes the effect of two factors at the same time; a higher peak/jump voltage and a higher overshoot percentage. Therefore, in order to determine the unique impact of the overshoot and distinguish its influence from the jump voltage, time-to-failure data are collected and examined when the applied peak voltage is the same with and without overshoot. For the analysis, 0% and 30% overshoot settings are considered while the applied waveform switching frequency and rise time are fixed at 1 kHz and 0.4 µs, respectively. Figure 4.6 demonstrates examples of the applied waveforms, measured at the terminal of the test object, at equal jump voltages with and without overshoot.

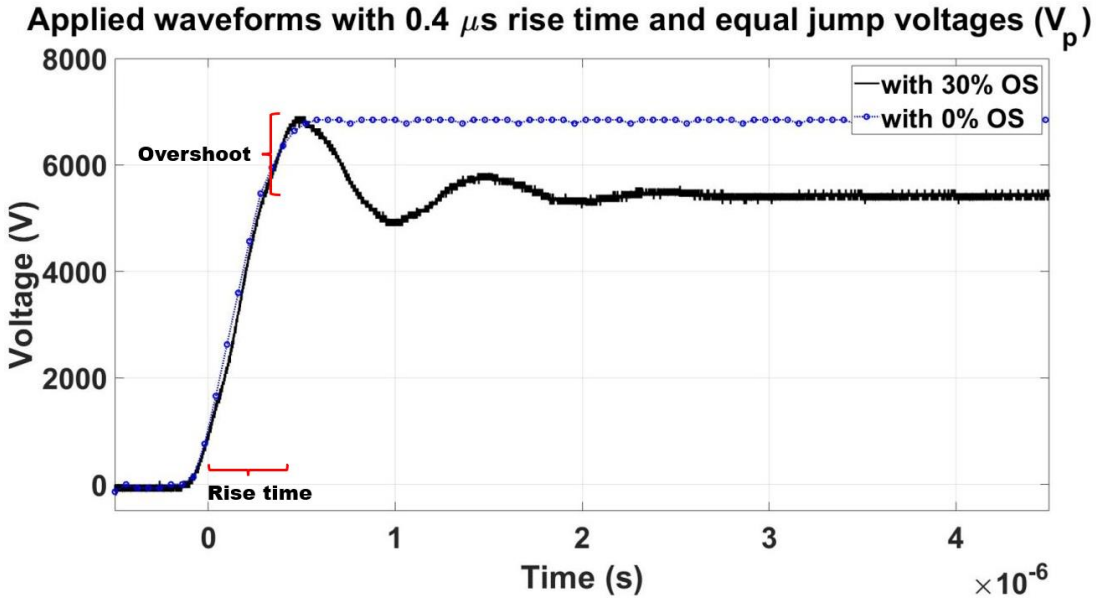

Figure 4.6 - Example of the applied voltage waveforms at 0.4 μs rise time, with and without overshoot, measured at the terminal of the test objects when the applied jump voltages are the same.

As previously indicated, highlighting the influence of the overshoot, as a separate factor from the jump voltage, is a special case in which the impact is a result of a combined two-factor action. Table 4.4 depicts the Weibull parameters for the voltage endurance tests at each of the waveform settings; whereas, Figure 4.7 displays the corresponding resultant probability plots. Note that 2 out of the 6 specimens tested during the "7 kVp - 0% OS" voltage endurance test failed close to the crotch area (censored) and therefore are not shown in Figure 4.7.

Table 4.4 - Summary of the Weibull statistical parameters for the impact of the waveform overshoot at equal jump/peak voltages.

OS	N_s	Vp	V_{DC}	β		α	
0%	6 (Censored)	7 kV	7 kV	2.22		132.04	
				β_l = 1.44	β_u= 3.78	α_l = 47.67	α_u= 77.34
30%	6 (Complete)	7 kV	5.4 kV	2.42		61.60	
				β_l = 1.57	β_u= 4.11	α_l = 99.89	α_u= 168.13

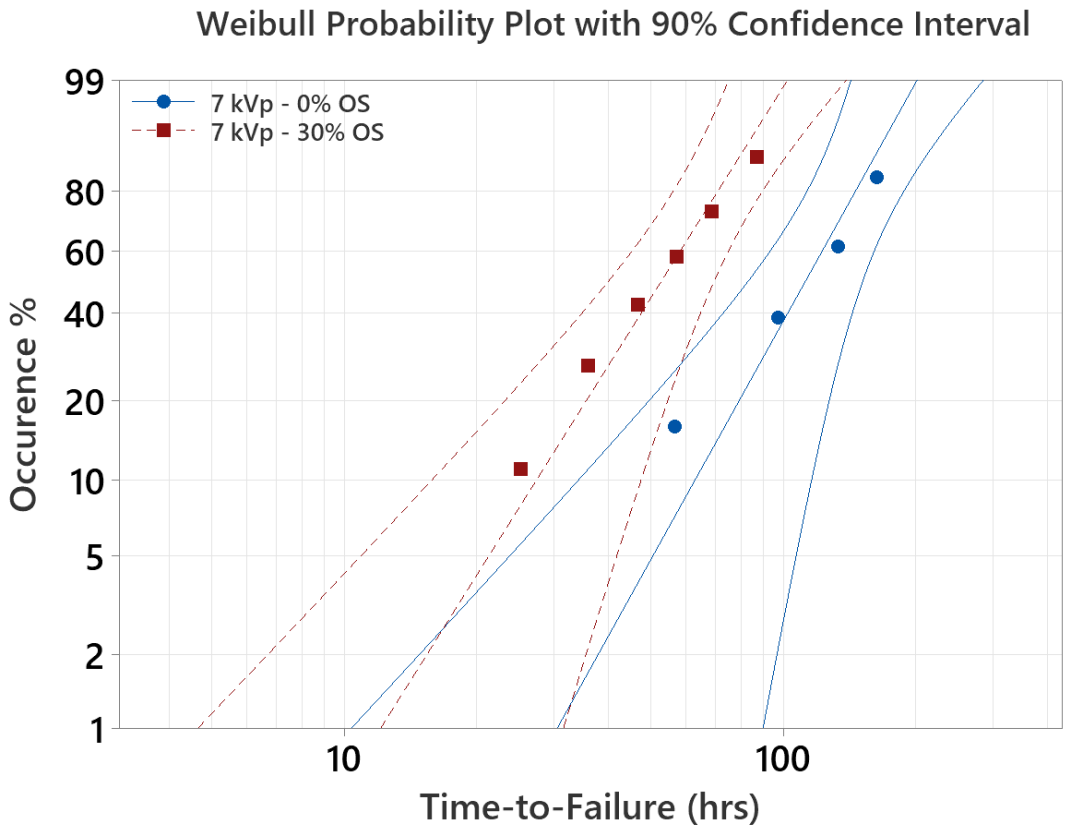

Figure 4.7 - Weibull probability curves with a 90% confidence interval for the impact of the overshoot at equal peak/jump voltages with and without overshoot.

As can be seen from Figure 4.7, the 90% confidence intervals from the Weibull probability plot for both waveform types (with and without overshoot) are barely overlapping indicating a distinct impact of the overshoot component. Even at an equal jump voltage, there is about a 50% reduction in the characteristic time-to-failure resulting from applying waveforms with 30% overshoot compared to those with no overshoot. This is a clear indication that the overshoot component of the waveform has its discrete influence on the endurance of machine turn insulation where a higher overshoot ratio would exert higher stress on the insulation resulting in a shorter time-to-failure [58].

4.2 PD Measurements

To study the influence of the repetitive impulse supply features on the occurrence of PD from turn insulation, two different types of test objects are used in this work. The first type consists of back-to-back samples made in accordance with the standard specifications to represent the insulation system

used in turn-to-turn insulation of a typical form-wound coil and the second type consists of samples prepared with a single cavity of a known size and shape in a layered insulation structure. This is done to distinguish PD from multiple voids in a practical situation from PD from a single void. A detailed description of the test objects and their preparation are given in Section 3.1. The experimental setup used in this work consists mainly of a test object, a high voltage impulse generator, and a PD_A detection system utilizing a horn antenna as detailed in Section 3.3. The test voltage waveform used to stress the samples and initiate PDs consists of unipolar square repetitive impulses of a 50% duty cycle. The applied switching frequency, rise time and overshoot are varied according to the low and high settings provided in Table 4.5 to investigate the influence of varying these factors on the detected PD_A signals.

Table 4.5 - The high and low settings of the factors considered in the PD analysis.

Factor	Identification	Low Setting	High Setting
Switching frequency (kHz)	A	1.0	4.0
Rise time (μs)	B	0.3	0.5
Overshoot (%)	C	0	30

Three cases are considered to characterize the influence of each of the factors under study. Cases I and II aim to highlight the role of the overshoot as an independent factor from the step and jump voltages and to investigate the effect and interaction with switching frequency and rise time. Case III covers the step voltage effect without the influence of the overshoot. PD_A signals from 100 consecutive applied voltage impulses are captured and recorded for each combination of the waveform settings presented in Table 4.5 for both the single cavity and back-to-back samples. With three factors considered, eight combination runs are performed following full-factorial two-level DOE principles for each study. It is important to note that other factors, such as the impulse polarity, duty cycle, or the number of inverter output levels are fixed and treated as constants throughout the measurements and, hence, their effects and interactions with other factors are not considered. Figure 4.8 (a) and (b) depict examples of the applied voltage waveforms with two different rise times (with and without overshoot) when the step voltage is the same or when the jump voltage is the same, respectively.

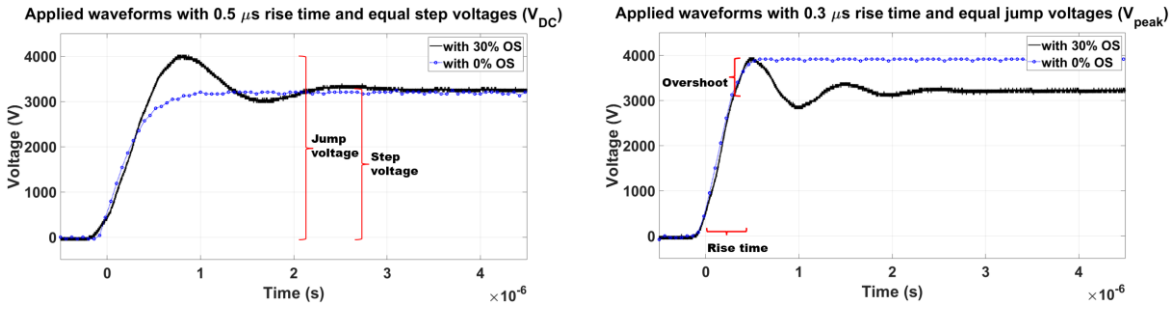

(a) (b)

Figure 4.8 - Examples of the applied waveforms with and without overshoot; (a) at equal step voltages and rise time of 0.5 µs, (b) at equal jump voltages and rise time of 0.3 µs.

4.2.1 Case I: Similar Step Voltage (V_{DC}) With and Without Overshoot

In this case, the comparison is based on equal V_{DC}, that is the final step voltage after the overshoot, as shown in Figure 4.8 (a). Accordingly, the waveforms with overshoot exhibit a higher peak voltage than those without overshoot. Table 4.6 depicts the settings of the waveform parameters and factors used; whereas, Table 4.7 and Table 4.8 summarize the corresponding PD_A statistics for the single cavity and back-to-back samples, respectively. Figure 4.9 and Figure 4.10 depict the analysis of the effect and interaction of the considered factors for the single cavity and the back-to-back samples, respectively.

Table 4.6 - Description of the applied waveform settings for Case I.

Waveform Setting	f_{sw} (kHz)	t_r (µs)	OS%	V_{peak} (kV)	V_{DC} (kV)
S1	1	0.3	0	3.1	3.1
S2	1	0.3	30	4.0	3.1
S3	1	0.5	0	3.1	3.1
S4	1	0.5	30	4.0	3.1
S5	4	0.3	0	3.1	3.1
S6	4	0.3	30	4.0	3.1
S7	4	0.5	0	3.1	3.1
S8	4	0.5	30	4.0	3.1

Table 4.7 - Summary of PD_A statistics for the single cavity specimen (Case I).

Setting	PD_A Num.	Max PD_A Mag. (mV)	Total PD_A Mag. Sum (mV)	Avg. Discharge Rate (mV/s)
S1	26	2.93	49.14	1.89
S2	76	7.52	315.96	4.16
S3	44	2.15	71.28	1.62
S4	105	5.69	416.59	3.97
S5	18	1.68	17.64	3.92
S6	53	4.48	111.61	8.44
S7	31	1.37	25.11	3.24
S8	74	3.79	141.14	7.64

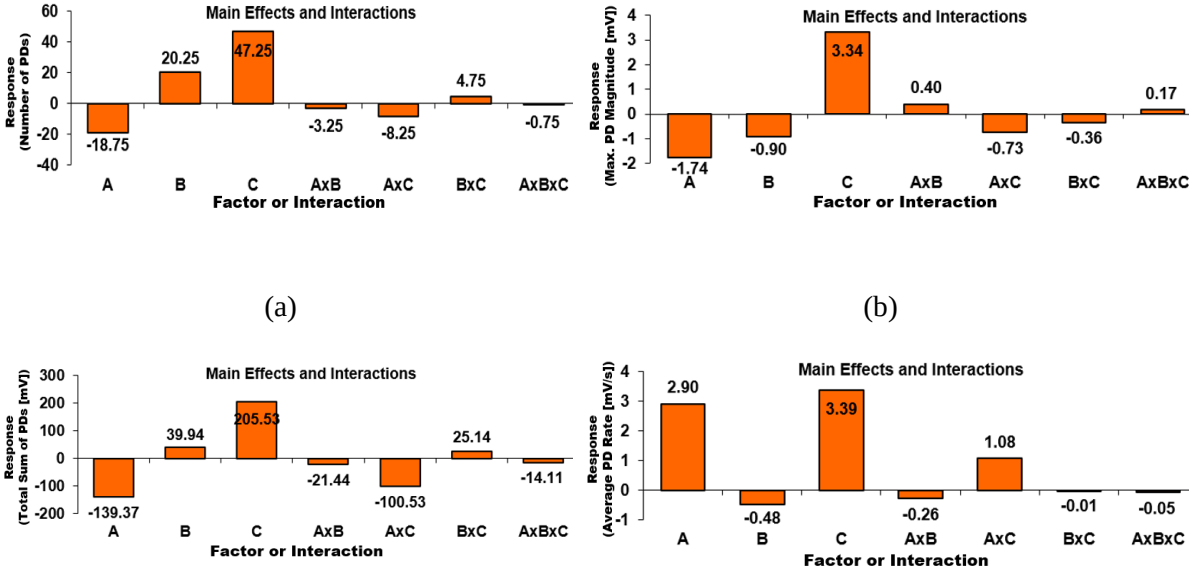

Figure 4.9 - Main effects and interactions for the single cavity specimen considering: (a) the number of detected PD_A signals as a response, (b) the maximum PD_A magnitude as a response, (c) the total sum of PD_A magnitudes as a response, and (d) the average discharge rate as a response.

Table 4.8 - Summary of PD_A statistics for the back-to-back specimen (Case I).

Setting	PD_A Num.	Max PD_A Mag. (mV)	Total PD_A Mag. Sum (mV)	Avg. Discharge Rate (mV/s)
S1	82	7.96	229.96	2.8
S2	311	20.42	2132.64	6.86
S3	149	5.97	339.67	2.28
S4	362	17.89	2341.24	6.47
S5	50	4.94	82.42	6.59
S6	192	12.48	788.31	16.42
S7	83	4.01	103.17	4.97
S8	226	10.79	880.79	15.59

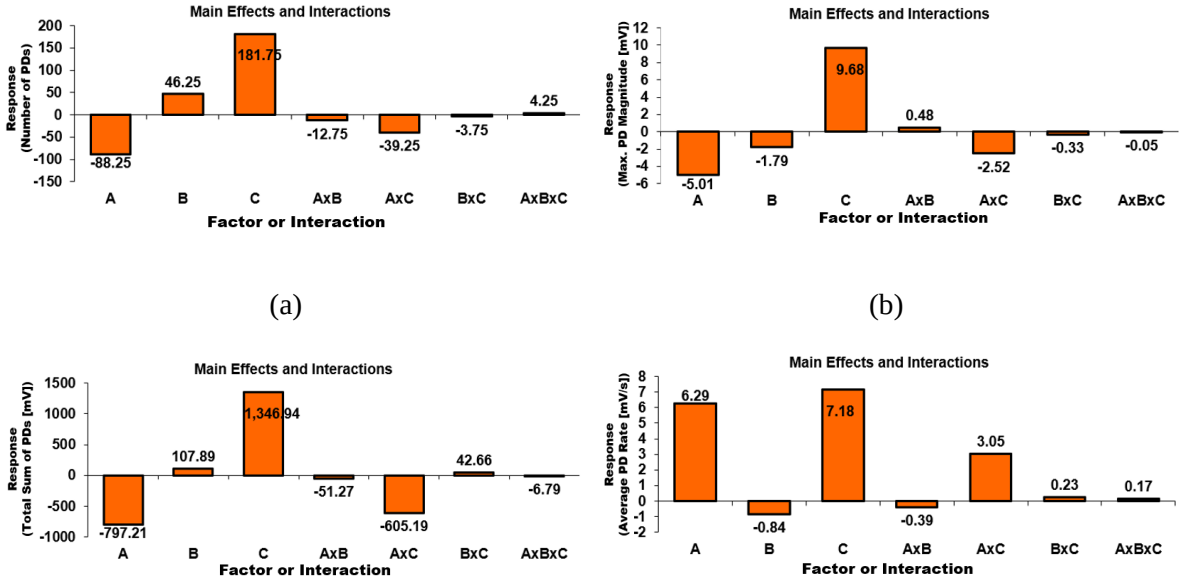

Figure 4.10 - Main effects and interactions for the back-to-back specimen considering: (a) the number of detected PD_A signals as a response, (b) the maximum PD_A magnitude as a response, (c) the total sum of PD_A magnitudes as a response, and (d) the average discharge rate as a response.

As can be seen from Table 4.7 and Table 4.8 as well as Figure 4.9 and Figure 4.10, a large number of PDs with lower magnitudes are associated with longer rise times. The average PD magnitude slightly reduces with longer rise times; whereas, the total sum of the PD magnitudes increases.

Alternatively, the effect of switching frequency is negative in regard to the number of PDs, the maximum PD magnitude, and the total sum of PD magnitudes per impulse. This suggests a lower rate of ageing per voltage impulse with increased switching frequency. In other words, the impact of each impulse is less than that of a lower switching frequency which could mean a higher number of cycles to failure with a higher switching frequency setting.

On the other hand, higher PD magnitudes and numbers are linked to waveforms with higher overshoots. According to Figure 4.9 (d) and Figure 4.10 (d), the overshoot factor has the most dominant effect followed by the switching frequency factor. The dominant effect of the overshoot might seem to be caused by the higher peak voltage exhibited by the voltage waveforms with the additional overshoot and, hence, the insulation is under higher stress. This is true to some extent; however, to isolate the impact of the overshoot from the peak voltage, the next case analysis considers two waveforms with and without overshoot, with the same peak voltage applied. The effect of the rise time is negligible in comparison to the switching frequency and the overshoot impacts. Whereas this might be due to the small range, 0.3-0.5 μs, considered in this analysis, it still aligns with the position adopted by the standard and agrees with the findings reported from the time-to-failure analysis in Section 4.1.

According to Figure 4.9 and Figure 4.10, the interaction between the rise time and the other factors is minimum and therefore, can be ignored. In other words, the influence of the rise time can be generalized with different switching frequency and overshoot settings. That is, the switching frequency or the overshoot factor would have the same trend at different rise times. This does not imply that the rise time might be changed freely while studying the impact of the other factors, but rather indicates that it is not required to investigate how these factors would impact the ageing mechanism at various rise times or how the rise time would influence the response of these factors. On the other hand, when studying the impact of switching frequency, the overshoot setting should be specified and vice versa. The interaction between the overshoot and the switching frequency factors is significant; thus, it should not be overlooked. The impact of the overshoot factor is higher at a higher switching frequency setting which means that the overshoot is causing a higher discharge rate at a higher frequency setting.

4.2.2 Case II: Similar Peak Voltage (V_{peak}) With and Without Overshoot

In the previous case, the overshoot factor was treated as an additional component above the specified V_{DC}. In other words, its effect was combined with that of the jump voltage. As indicated in Section 4.1, this is more of a practical scenario as the operating voltage of a machine is based on the step voltage of the drive; whereas, the percentage of the additional overshoot experienced at the motor terminal is created by the reflected wave generated from the impedance mismatch between the cable and the machine impedance. In this case, rather than the step voltage, the impact of the applied waveforms (with or without overshoot) is investigated at a similar jump/peak voltage, as shown in Figure 4.8 (b). Table 4.9 depicts the description of the waveform settings used and Table 4.10 and Table 4.11 show the relevant measured PD_A for the single cavity and the back-to-back samples, respectively. This is a more evident case compared to the previous one to highlight the primary effect of the waveform overshoot when the applied peak/jump voltage is the same.

Table 4.9 - Description of the applied waveform settings for Case II.

Waveform	f_{sw} (kHz)	t_r (µs)	OS%	V_{peak} (kV)	V_{DC} (kV)
S1	1	0.3	0	4.0	4.0
S2	1	0.3	30	4.0	3.1
S3	1	0.5	0	4.0	4.0
S4	1	0.5	30	4.0	3.1
S5	4	0.3	0	4.0	4.0
S6	4	0.3	30	4.0	3.1
S7	4	0.5	0	4.0	4.0
S8	4	0.5	30	4.0	3.1

Table 4.10 - Summary of the PD_A statistics for the single cavity specimen (Case II).

Setting	PD_A Num.	Max PD_A Mag.	Total PD_A Mag. Sum	Avg. Discharge Rate
S1	56	4.26	117.39	2.10
S2	76	7.52	315.96	4.16
S3	73	3.21	141.40	1.94
S4	105	5.69	416.59	3.97
S5	41	2.32	66.28	6.48
S6	53	4.48	111.61	8.44
S7	54	1.87	85.87	6.36
S8	74	3.79	141.14	7.64

Table 4.11 - Summary of the PD_A statistics for the back-to-back specimen (Case II).

Setting	PD_A Num.	Max PD_A Mag.	Total PD_A Mag. Sum	Avg. Discharge Rate
S1	178	11.57	549.34	3.09
S2	311	20.42	2132.64	6.86
S3	248	8.91	673.81	2.72
S4	362	17.89	2341.24	6.47
S5	114	6.82	309.70	10.87
S6	192	12.48	788.31	16.42
S7	144	5.47	352.82	9.80
S8	226	10.79	880.79	15.59

Similar to Case I, the effect of switching frequency is negative with regard to the number of PDs, the maximum PD magnitude, and the total sum of PDs from both samples. Fewer PDs with higher magnitudes are associated with shorter rise times. A higher number of PDs with larger magnitudes still accompany waveforms with overshoot even when the same peak voltage is applied. Figure 4.11 (a) and (b) depict the analysis of the effect and interaction of the considered factors for the single cavity and the back-to-back sample, respectively while considering the average PD rate as a response. At a similar peak/jump voltage applied, the supply switching frequency becomes the dominant factor followed by the overshoot ratio. The rise time effect is still minor and almost similar to the previous case. It is worth noting that the main effect of the overshoot on the average discharge rate in both samples is almost equal to half the effect of increasing the switching frequency from 1 to 4 kHz. Demonstrated results

suggest that higher PD magnitudes and discharge rates are in favour of waveforms with higher overshoot ratios. Therefore, a higher overshoot ratio imposes additional stresses on machines' insulation which necessitates treating the overshoot component as a separate factor from the jump voltage when evaluating the life performance of turn insulation.

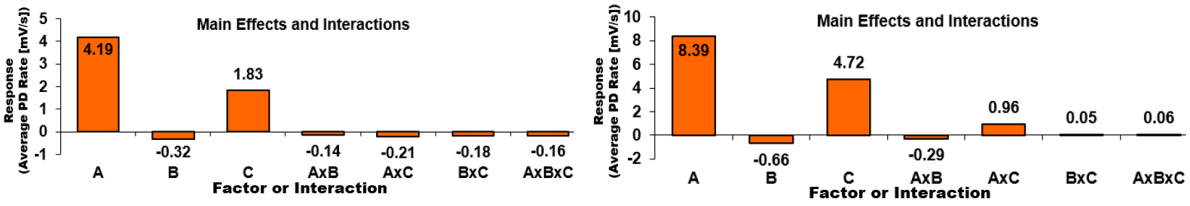

(a) (b)

Figure 4.11 - Main effects and interactions analysis for Case II considering the average discharge rate as a response; (a) single cavity specimen, (b) back-to-back specimen.

4.2.3 Case III: Impact of the Step Voltage Without Overshoot

In Case II, the impact of the overshoot is isolated from the jump voltage and its primary effect is highlighted for the first time as a main and distinct factor influencing the characteristics of PDs initiated from the stressed samples. In this case, the impact of the step voltage is investigated in order to observe the effect of the jump voltage without the influence of the overshoot. Table 4.12 shows the settings of the waveform factors considered; whereas, Figure 4.12 depicts the analysis of the main effects and interactions considering the average PD rate as a response. The details of the PD measurements are as per the values given in S1, S3, S5 and S7 entries from Table 4.7 and Table 4.10 (for the single cavity specimen) and Table 4.8 and Table 4.11 (for the back-to-back specimen) presented in Case I and Case II, respectively.

Table 4.12 - The high and low settings of the factors considered in Case III.

Factor	Identification	Low Setting	High Setting
Switching frequency (kHz)	A	1.0	4.0
Rise time (µs)	B	0.3	0.5
Step voltage (kV) [OS% = 0]	C	3.1	4.0

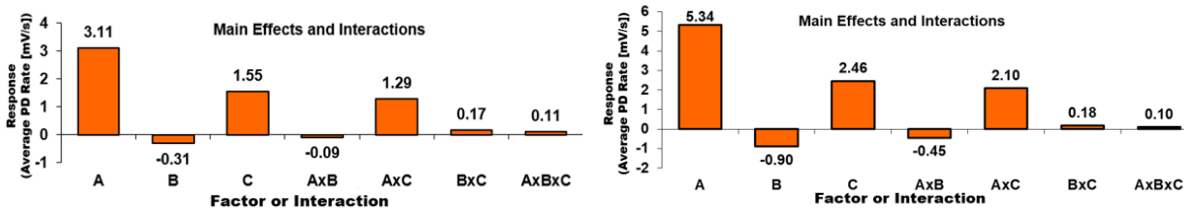

(a) (b)

Figure 4.12 - Main effects and interactions analysis for Case III considering the average discharge rate as a response; (a) single cavity specimen, (b) back-to-back specimen.

The influence of switching frequency and rise time on PDs, in this case, are in agreement with those presented in Case I and Case II. Unlike the results from Case I — where a higher peak voltage caused by the addition of the waveform overshoot made the effect of the peak voltage higher than the effect of the switching frequency — in this case, the switching frequency is the dominant factor. The increase in the level of the jump/peak voltage in both Case I and Case III is the same, about 1 kV; however, the additional influence of the overshoot has made the impact of the peak voltage higher in Case I. This additional impact is shown clearly in Case II where similar peak voltages are applied with and without overshoot. The interaction between the voltage level and the switching frequency factors is clearer in this case compared to the previous cases. The effect of a higher step voltage is more severe at a higher switching frequency setting than at a lower frequency setting as can be perceived from Figure 4.13. Fewer PDs occur due to the elimination of the overshoot component which likely results in higher accumulated charges. Accordingly, part of the higher rate of PDs caused by the higher step voltage at higher switching frequency settings is not a result of the switching frequency or the step voltage increase alone but rather the interaction of these two factors. A higher interaction between these two factors would result in a larger difference between the lines' slopes; whereas, a negligible interaction would make the two lines parallel [62].

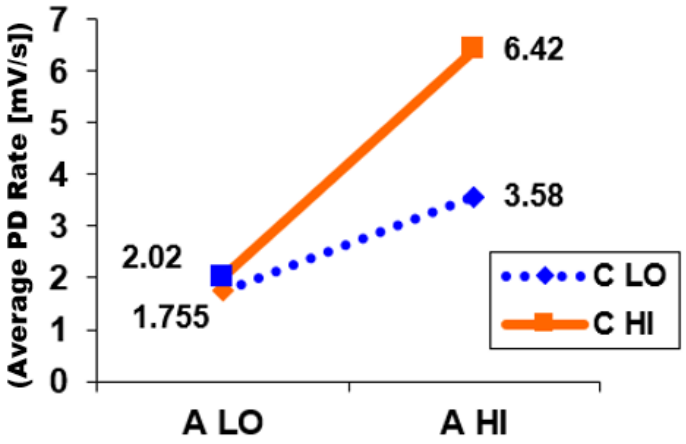

Figure 4.13 - Interaction plot between the switching frequency and the step voltage for the single cavity specimen considering the average discharge rate as a response.

4.3 Examination of the Failed Samples

To examine the ageing effect within the insulation layers, failed back-to-back turn insulation samples from the endurance tests were dissected, and the insulation layers were separated and examined under a digital microscope. Figure 4.14 shows microscopic images of some of the failure locations along with traces of electrical tracking at various sites along the failed samples. Electrical tracking is most often observed in the failed specimens and the tracks can be traced back to, or very close to, an insulation layer overlap where an air pocket is likely trapped. This is seen not only at the failure sites but also almost at each layer overlap within aged samples. The surface conductivity of these tracks is examined based on the resistivity measurement using an insulation diagnostic analyzer. Due to the small surface area of the tracks and the nature of the insulation layers, accurate surface conductivity measurements could not be made. This is due to the nature of the insulation and the fact that many of these electrical tracks are buried between the layers of the insulation and attempts to separate the insulation layer has led to the destruction of these tracks. Nevertheless, several of the tracks show increased surface conductivity of at least 3 orders of magnitude. This confirms that the electrical surface properties of the resin-impregnated mica-based layers surrounding the voids are significantly affected by the continuous PD during the ageing study. No evidence of significant thermal ageing at sites away from the failure site could be found. It is speculated that electrical and mechanical stress from the continuous PD results

in the expansion of these tracks and the development of micro-cracks between the electrode and/or the insulation layers by the separation of the epoxy bonding material.

(a) Tracking at failure sites

(b) Tracking at sites away from the failure

Figure 4.14 - Electrical tracking in failed samples; (a) at failure sites, (b) away from the failure.

The slow erosion of mica flakes and the development of tracking on the epoxy resin between the flakes and between the insulation layers continue until a full conductive path between the electrode is formed, or the localized stress is high enough, to puncture the insulation and bridge the conductors. Figure 4.15 shows various stages of tracking and the expansion of the micro-cracks through the ageing process. To capture the growth stages of tracking between two voids in layered insulation without the need to dissect the specimen, a simplified test specimen of two resin-impregnated mica sheets held between two electrodes is utilized. Each of the mica sheets contains a single hole of 0.39 mm radius. The specimen is meant to be analogous to two voids in a back-to-back turn insulation specimen that can exist between two insulation overlapped layers.

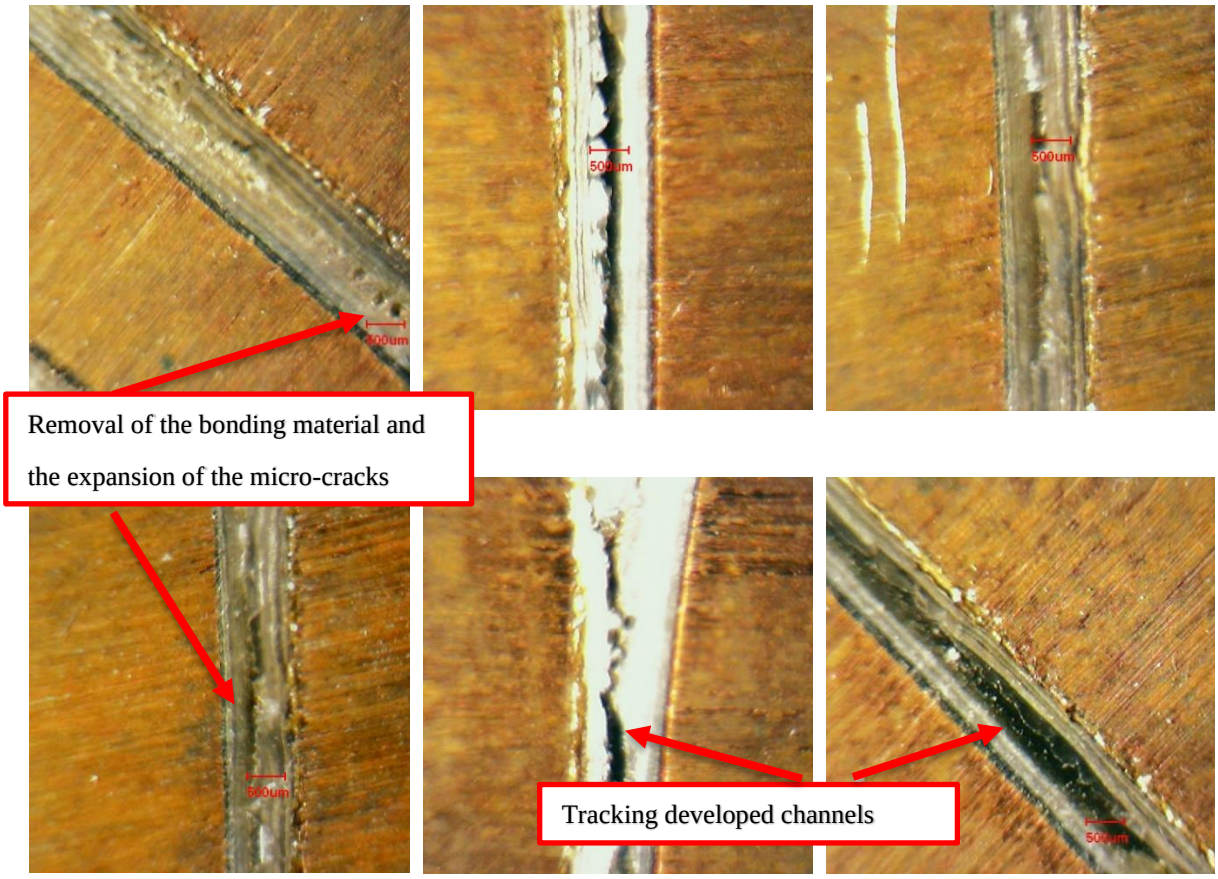

Figure 4.15 - Different stages of the tracking developed channels and the expansion of micro-cracks through the ageing process.

Figure 4.16 shows a sketch of the test object along with a top view of the actual mica sheets displaying the location of the voids. Test samples are stressed approximately for a total of 22 hours until failure using a sinusoidal waveform of 4.5 kV_{rms}. Microscopic images of the aged insulation sheets are taken every 4 to 8 hours to capture the progressive tracking on the surface of the insulation between the two cavities until failure, Figure 4.17.

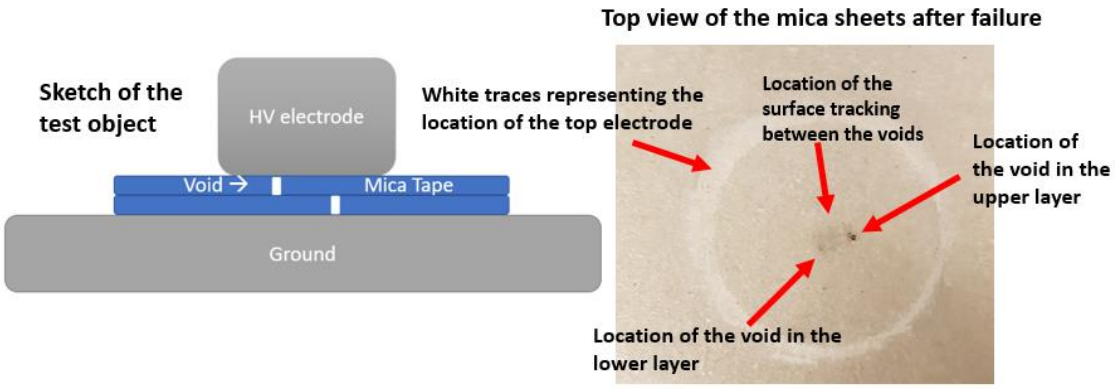

Figure 4.16 - Left – a sketch of the test object used to investigate the tracking growth between two cavities. Right – a top view of the mica sheets after failure.

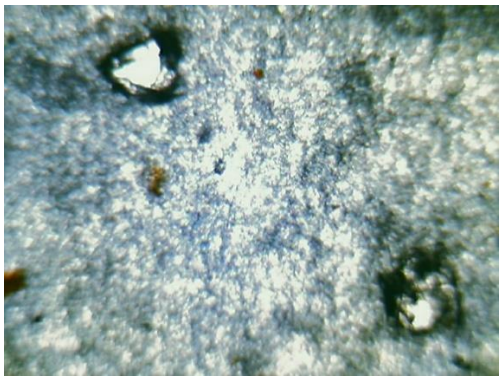

(a) after 4 hours

(b) after 8 hours

(c) after 16 hours

(d) after failure (~22 hours)

Figure 4.17 - Microscopic images of the tracking development between two cavities; (a) after 4 hours, (b) after 8 hours, (c) after 16 hours, (d) after failure (~22 hours).

To confirm the initial stage of tracking, another two-cavity specimen is stressed for just 4 hours before the specimen is separated and inspected. Figure 4.18 shows microscopic images of the primary stages of the tracking path initiation.

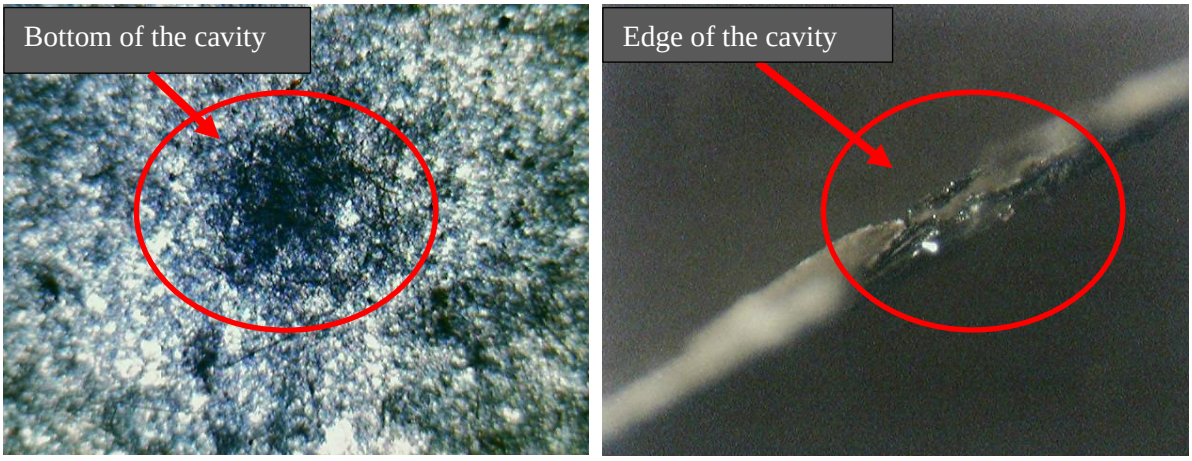

(a) Tracking at the bottom of the cavity (b) Tracking at the edge of the cavity

Figure 4.18 - Microscopic images of the tracking around the cavities after 4 hours of stress; (a) at the bottom of the cavity, (b) at the edge of the cavity.

As evident from Figure 4.17 and Figure 4.18, PD creates localized tracking around each of the cavities including the edges as the initial stage of tracking. It is surmised that with continued PDs, the conductivity of the localized tracking increases. Each cavity, therefore, develops discharges that cause tracking to propagate along the insulator surface until bridging both sides of the electrodes.

Chapter 5
Discussion

5.1 Life Curves and the Endurance of Turn Insulation

Based on the Weibull probability plots of the time-to-failure data for both the 1 kHz and 4 kHz voltage endurance studies presented in Figure 4.1 and Figure 4.2 of Section 4.1, it is clear that the ageing process is influenced by an interaction between the stressing factors [59]. The change in the derived endurance coefficient as the stress level is increased demonstrates this interaction as depicted in Figure 4.3. To examine this further, an analysis of the main effect and interaction between the stressing factors, in this case, the switching frequency and the peak voltage, is demonstrated in Figure 5.1.

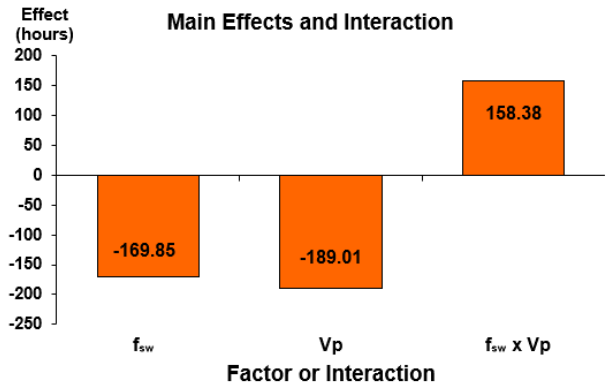

Figure 5.1 - Analysis of the main effect and interaction between the switching frequency and the test voltage considering the characteristic time-to-failure from the 6 kV and 10 kV ageing experiments as a response.

While these factors adversely impact the lifespan of the insulation, their interaction reduces their total influence. This is better visualized through the interaction plot between the switching frequency and the testing voltage as illustrated previously in Figure 3.13. According to the switching frequency and testing voltage interaction plot, it is clear that the influence of raising the voltage level is more noticeable at a lower switching frequency than its influence at a higher switching frequency. Similarly, the consequence of increasing the supply switching frequency at a lower voltage level would have a higher impact than that at a higher voltage stress level. This is in line with the analysis of the PD results in response to different waveform settings reported in Section 4.2, where the main effect of the switching frequency was found to be highly influenced by the applied voltage and the overshoot ratio.

According to [32], [42], and the results presented in Section 4.2, a higher switching frequency setting promotes fewer PDs with smaller magnitudes per impulse. This is explained through the impact of the accumulated charges deposited on the surface of the voids from the previous discharge. The remanent field applied from these charges opposes the direction of the applied field from the voltage impulse and hence the resultant field within the void is reduced [71]. As the switching frequency increases, the duration of the applied impulse reduces and hence there is less time for the surface charges to decay limiting the impact of the applied field. To further analyze the effect of the switching frequency on the accumulated charge and the total number and magnitude of PDs, the impact of increasing the switching frequency on the average PD magnitudes per impulse is compared with the average discharge rate during the off period between the impulses. Figure 5.2 demonstrates the captured PDs during the off period; whereas, Figure 5.3 shows the obtained trends based on a total of 100 waveforms captured from the back-to-back sample. To distinguish PDs during the fall time from those caused by the residual field from the accumulated charges, only PDs after 1 µs from the zero-crossing are considered [75], [76]. It can be seen that the average magnitude of PD decreases with higher switching frequency and at the same time, the average discharge rate due to the residual space/surface charges increases. The rate of change in the PD magnitudes for the switching frequency between 600 Hz and 4 kHz follows a non-linear behaviour. Since PD is widely accepted to be the main ageing mechanism [28], [38], [77] this would also point toward a non-linear relation of the supply switching frequency on the life of Type II turn insulation.

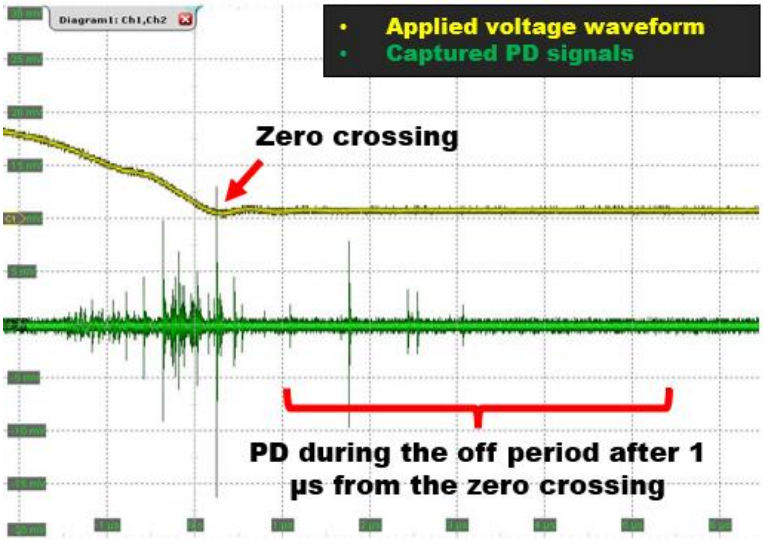

Figure 5.2 - Captured PDs during the off period from back-to-back turn insulation sample.

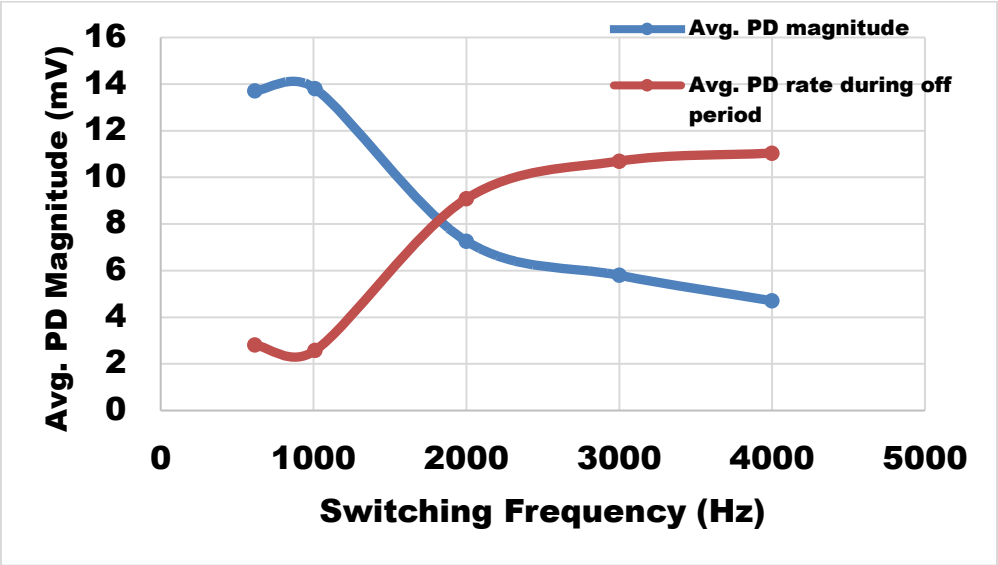

Figure 5.3 - Effect of increasing the supply switching frequency on the accumulated charges within a back-to-back sample and the average PD magnitude per impulse.

This explains the variation in the VEC for various stressing factors and levels as each factor may influence the ageing mechanism in a distinct way, yet, the interaction between the stressing factors may in fact boost or limit the primary impact of the main factor. Furthermore, the highest survival rate of the accelerated ageing tests did not exceed 1000 hours with a characteristic time-to-failure of less than 400 hours for the lowermost stress level although the stress levels used to establish the life curves were based on the recommended levels in IEC 60034-18-42 [4]. This may be a sign of extreme stressing factors which could be the reason for the obtained low VEC values under impulse energization. Similar findings have been reported in [41], where the VEC for twisted pair samples made from Type II materials, was found to be in the range of 5 to 6. These low VEC values, compared to the ones normally derived from a life curve generated under sinusoidal supply stress (10 to 12), may be due to the additional stress imposed by the supply's switching nature when an impulse energization is used [78]. Therefore, lowering the stress levels when testing under impulse may be required to control this accelerated ageing impact to obtain more reliable data.

As the case with the switching frequency impact, to examine the effect of the waveform rise time and overshoot on the lifespan of machine turn insulation, the characteristic time-to-failures for the ageing experiments reported in Table 4.2 and Table 4.4 are reflected in the derived 1 kHz reference life plot, Figure 5.4.

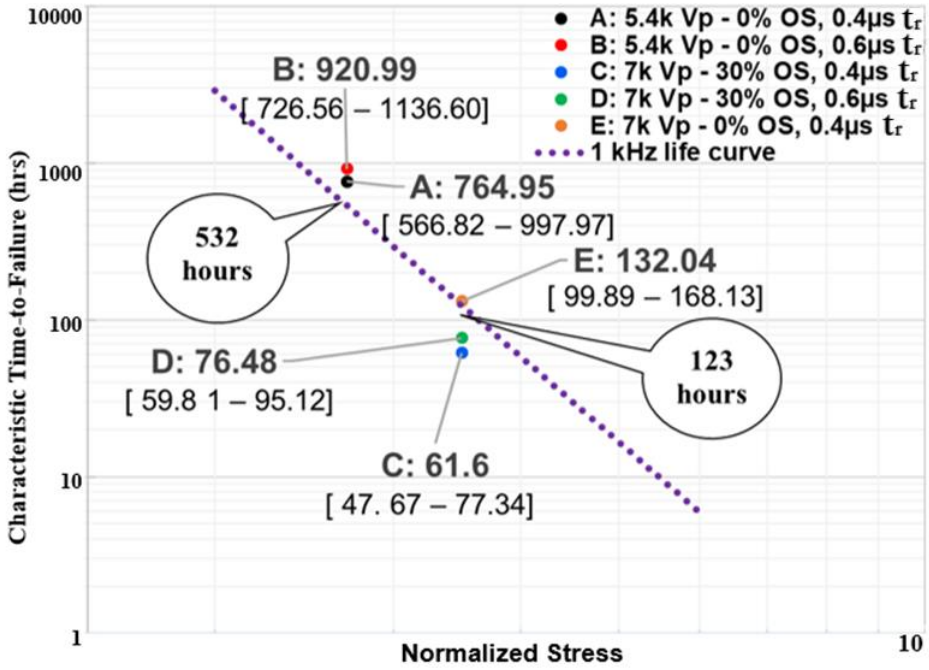

Figure 5.4 - Impact of the waveform overshoot (0% - 30%) and rise time (0.4 µs - 0.6 µs) reflected on the established reference life curve of 1 kHz switching frequency, 15% overshoot and 0.3 µs rise time.

In terms of the rise time, the reported results, within the considered range, support the IEC assumption and other research findings [31], [34], on the low significance of the rise time on the life of turn insulation. As can be seen from Figure 5.4, the slight change in the time-to-failure between points A and B or C and D falls within their corresponding confidence intervals which makes the impact statistically insignificant. A similar outcome is also reported in Section 4.2, where although a shorter rise time leads to fewer PDs with larger magnitudes, the increase in the rate of the average discharge magnitude per unit time is found to be negligible in comparison to the impact of the other factors. Nonetheless, this effect, although minor, seems to be consistent at different stress levels. This may be a concern if a shorter rise time (in the range of nanoseconds), made possible through the use of wide-bandgap switches, stresses the insulation [5], [50].

On the other hand, in terms of the overshoot impact, the lower bounds of the characteristic time-to-failure for waveforms without overshoot (represented by points A and B) do not overlap with the reference life curve established with repetitive impulses of 15% overshoot. Likewise, for waveforms with 30% overshoot designated by points C and D, the upper bounds do not overlap with the established

life curve at 15% overshoot. This signifies the impact of the overshoot even at a ±15% difference. The impact of the waveform overshoot as an additional component, as represented in Table 4.2, is also clear when comparing the reduction of the resultant time-to-failure between points A and C. The impact of the overshoot, in this case, represents a combined action of the jump voltage and the overshoot ratio. This combined action can be divided as follows; first, a change in the life endurance between points A and E which represents the impact of the jump voltage at 0% overshoot and second, the impact of the overshoot ratio at similar jump voltages represented by the reduction in the time-to-failure between points E and C. Accordingly, increasing the jump voltage without overshoot causes the reduction of the time-to-failure parallel to the established life curve indicating an independent stressing factor and a comparable endurance coefficient [58]. Therefore, applied waveforms of similar shapes can be considered to have an equivalent ageing rate and a direct relation of their impact on the endurance of turn insulation can be derived. This supports the conclusion in [38] where different PD patterns are observed with waveforms of different shapes, and thus, suggests that the life of turn insulation may be estimated from reference life curves only if they are generated under a similar type of waveform.

Accordingly, when it comes to the overshoot effect, maintaining the same peak voltage level (defined by the jump voltage) without considering the variation in the overshoot ratios significantly affects the resultant life curve. This is clearly shown through the downward shift in the time-to-failure from point E to C. Waveforms with higher overshoot ratios exhibit higher stresses on turn insulation specimens which leads to a significant reduction in their endurance, albeit equal jump voltages applied. In this particular case, assuming a comparable VEC between waveforms of different overshoot settings, a 30% increase in the overshoot ratio shifts the resultant life curve downward by nearly a factor of 2. This would be equivalent to the impact of doubling the supply switching frequency if there is a linear relationship between the switching frequency and the life of turn insulation. This effect is also shown and highlighted in Section 4.2 where higher PD magnitudes and numbers are associated with waveforms of higher overshoot even at similar peak voltages. Similar observations are also reported in [50], where waveforms with overshoots result in a larger number of PDs than those with higher voltage levels without overshoot. This unique impact of the overshoot on PDs along with its impact on the endurance of turn insulation signifies the role of the overshoot not only as an independent factor from the jump voltage but as a major one affecting the life of turn insulation.

5.2 Partial Discharge Mechanism under Impulse Energization

For PD to occur within a cavity, two conditions must be satisfied; first, there must be a free electron to initiate the electron avalanche and second, the electric field must exceed the inception value for a duration enough to form a discharge. The electric field within a cavity is not only determined by the instantaneous applied voltage but also significantly influenced by the previously applied waveform and the space and surface charge accumulation from the previous discharges [72], [79]. Therefore, to understand the behaviour of PD in response to features of the impulse supply, the space charge limited field is investigated utilizing the model described in Section 3.5 for an unaged void. To get the best match between the simulation results and the PD measurements, the model-free parameters, namely, the field-dependent coefficient and the maximum surface and interface conductivity of the cavity and the interface layers, are adjusted accordingly based on the trends obtained from the maximum PD magnitudes as reported in Section 4.2. These parameters help in controlling the maximum electric field within the cavity and the rate at which the resultant electric field is increasing/decreasing in response to charge accumulation and decay [71], [80]. Figure 5.5 shows the effects and interaction comparison between the simulation results of the maximum electric field value in the center of the cavity and the maximum PD magnitude using the results obtained from Table 4.7 after adjusting for the number of cycles per seconds to account for the repetition rate effect per unit time.

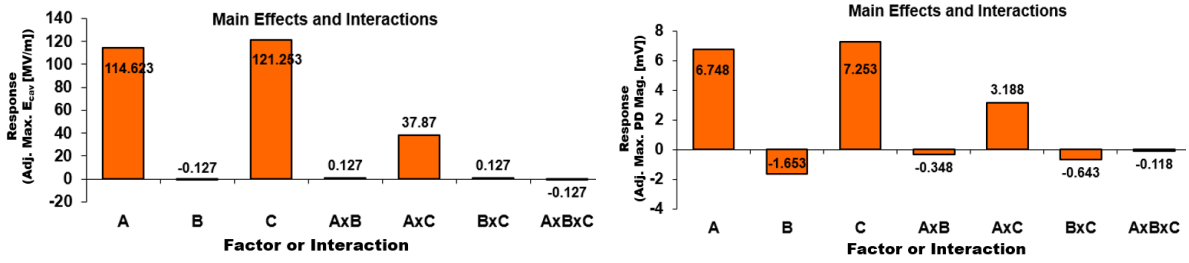

(a) (b)

Figure 5.5 - Main effects and interactions after accounting for the number of cycles per second for the switching frequency (A), rise time (B) and overshoot (C) factors considering; (a) the simulated maximum electric field as a response, (b) the measured maximum PD magnitudes as a response.

Similar behaviour can be seen in Figure 5.5 when comparing the effect of the waveform factors on the maximum electric field at the center of the cavity to their effect on the maximum PD magnitude. Except for the effect of the rise time, as this is associated with the statistical time delay and the instant when the PD occurs, which will be discussed further in Subsection 5.2.2.

As in Section 3.5, the surface conductivity of the cavity plays an important role in the rate at which the resultant electric field at the center of the cavity increases or decreases through surface conduction which simulates the effect of surface charge mobility and decay time. This effect can be divided into four regions:

A- During the waveform rise time,

B- During the DC part of the waveform,

C- During the fall time, and

D- During the off period between the impulses.

Figure 5.6 shows the simulation result of the magnitude of the electric field at the center of the void when stressed by repetitive impulses of 1 kHz switching frequency.

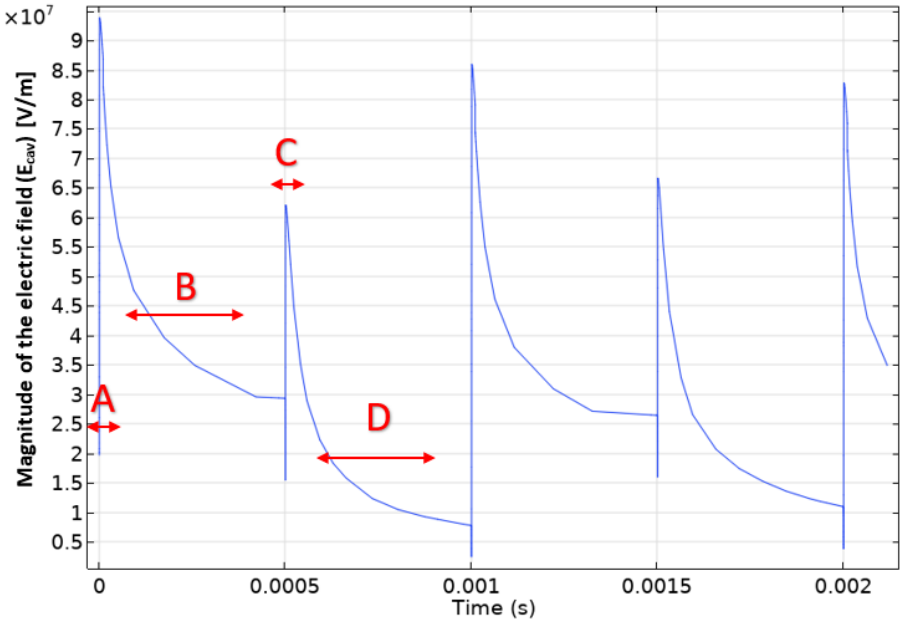

Figure 5.6 - Simulation results for the magnitude of the electric field at the center of the cavity when stressed by repetitive impulses of 1 kHz switching frequency, 0.3 µs rise time and 30% overshoot.

As evident from Figure 5.6, during the waveform rise time (region A), the applied voltage across the cavity increases rapidly at a higher rate than the increase in the surface conductivity resulting in a higher electric field at the center of the cavity given by $E_{cav}(t) = \gamma E_{app}(t) - E_s(t)$ where E_{cav} is the resultant electric field at the center of the cavity, E_{app} is the applied electric field (in the absence of the surface charge field), γ is the field enhancement factor in the cavity, and E_s is the cavity surface charge induced field [81]. This results in high values of the electric field during the rise time which produces higher discharge levels during the rise time. In region B, since the surface conductivity is field-dependent, a higher field leads to faster charge mobility implemented through the increase in the surface conductivity. This leads to an increase in the surface-induced field, which opposes the applied field, resulting in the reduction of the resultant field at the center of the cavity until it falls below the PD extinction field. During the waveform fall time (region C), the applied voltage is decrementing at a higher rate than the decay of E_s resulting in a high E_{cav} in the reverse direction. During the off period (region D), the total field at the center of the void is limited to the residual field from the surface charges as the applied voltage is zero during this period. In this case, the field-dependent surface conductivity of the void simulates the surface charge decay action through surface conduction. Figure 5.7 summarizes these actions following the voltage waveform.

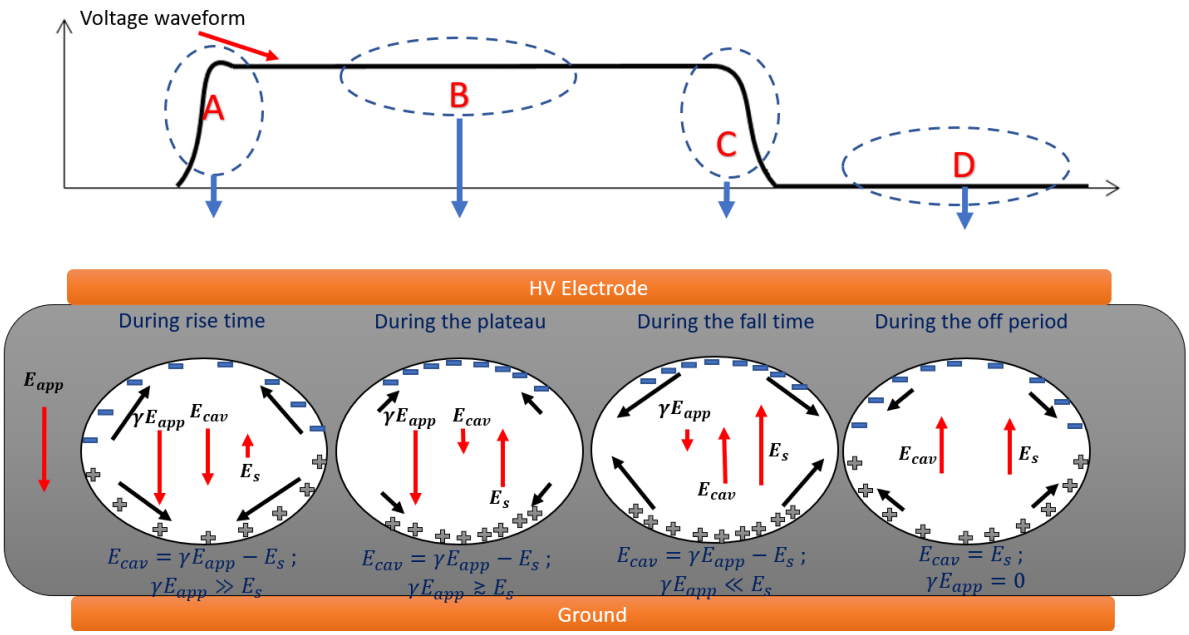

Figure 5.7 - Schematic of the resultant electric field stress at the center of the void due to charge movement and deployment at different parts of the waveform.

5.2.1 Effect of Switching Frequency

From the analysis of the effects and interactions between the supply factors in the initiation of PD, it is observed that a higher switching frequency triggers fewer PDs with lower magnitudes per impulse. The time for the accumulated charges on the surface of the void to decay, estimated in the literature between 1 to 2 ms, explains this behaviour [81], [82]. As the switching frequency increases, the impulse duration becomes shorter and hence less time is available for the charges to decay before the next impulse. The electric field from these charges opposes the direction of the applied field which lowers the electric field at the center of the void [81]. Accordingly, fewer PDs with lower magnitudes are associated with higher switching frequency settings. This impact of the switching frequency on PDs can be realized as well from the simulated electric field, especially during the off period as seen in region D in Figure 5.6 and Figure 5.7, where a higher switching frequency setting results in a shorter period and hence less time for E_s to decay before the next voltage impulse. This also agrees with the results shown in Figure 5.3, which demonstrates that while the average PD magnitude per impulse is reduced with a higher switching frequency setting, the average discharge rate due to the residual field from the space/surface charges increases.

5.2.2 Effect of the Waveform Rise Time

The effect of the rise time on the maximum electric field strength is not evident from the simulation results as its main impact is limited to the instant of time at which PD occurs [50]. Under slow varying AC voltage, the discharge conditions can be satisfied as soon as the applied field is high enough to cause a discharge as the time required for locating the initial electron to start the avalanche processes is shorter than the rate of change of the voltage waveform. This is not the case when the discharge is brought on by impulse voltages. Under impulse, there is a lag between a voltage high enough to trigger a breakdown and the actual time for a breakdown, Figure 5.8. This time is referred to as the impulse time lag [83], [84].

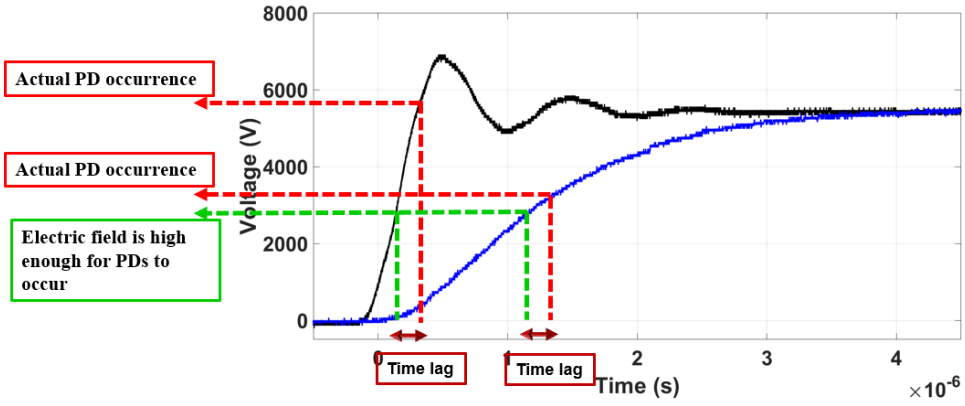

Figure 5.8 - Impact of the waveform rise time on the time incident of PD occurrence.

This time lag is divided into two components, the statistical time lag and the formative time lag. The statistical time lag is the time that lapses between the moment the field is high enough to initiate PD and the appearance of the initiatory electron [84]. Under fast rise time impulses, this time is considerable in comparison to the slew rate of the impulse which leads to the initiation of the ionization process at higher voltage levels. The initiatory electron appearance is usually considered to follow a statistical distribution [79]. After locating the initiatory electron, the time required for the ionization process to fully develop into a discharge is referred to as the formative time lag. The duration of the applied impulse must exceed the duration of both time lags for a discharge to occur, however, since the formative time lag is much shorter than the statistical time lag, the latter is usually what determines the incident of the discharge occurrence [83], [84]. Therefore, a shorter rise time promotes PDs at higher voltages which results in fewer PDs with larger magnitudes. From the experimental measurements, a larger number of PDs with lower magnitudes is found to be associated with waveforms of longer rise times. The average PD magnitude slightly reduces with longer rise times; whereas, the total sum of the PD magnitudes increases. Such results are in line with the findings reported in [31], [45] where, due to the PD time lag, shorter rise times cause PD to occur at higher voltages, triggering fewer PD with larger magnitudes. As can be seen from the simulated electrical field results in Figure 5.6, E_{cav} increases rapidly during the rise time of the waveform following the rate of increase in the applied voltage and hence the maximum electric field stress is almost the same at different rise time settings. On the other hand, the rate at which the electric field increases is not the same, and therefore, assuming a similar time lag, PD occurs at a higher stress level leading to higher PD magnitudes. Such behaviour also leads to higher accumulated surface charges, which affect the total number of associated PDs [71].

5.2.3 Effect of the Waveform Overshoot

The effect of overshoot on PD magnitude is obvious when comparing waveforms with equal step voltage since the overshoot causes the applied peak voltage to be higher across the cavity. Since the applied step voltage is the same, and the rise time and overshoot durations are very small compared to the impulse duration, the effect of the applied field on the charge accumulation is equivalent in both cases. A higher peak voltage will result in a higher electric field across the cavity during the overshoot and thus a higher PD magnitude. Alternatively, waveforms with overshoot still trigger higher PD even when both waveforms, with and without overshoot, have the same peak voltages. This is explained through the difference in the rate of charge accumulation and decay in the cavity in both cases. Waveforms with no overshoot exhibit a higher step voltage than those with an overshoot which leads to a higher charge accumulation and therefore a higher E_s opposing the applied field. In the absence of the applied field (during the off period of the waveform), the accumulated charges will decay over time. The strength of the electric field upon the next applied impulse depends largely on the residual field from the accumulated charges [40], [85]. Therefore, a higher residual field caused by the higher step voltage from the waveforms with no overshoot results in a lower E_{cav} at the center of the void upon the arrival of the next impulse. As a result, waveforms with overshoots cause higher discharge magnitudes than waveforms with no overshoots even at similar peak voltage applied in both cases. The effect of the residual field is also evident from the simulated E_{cav} of the first impulse as shown in Figure 5.6. As can be seen, the maximum electric field associated with the first impulse is higher compared to the subsequent impulses due to the absence of the surface charge effect at the first impulse. This also explains the significant interaction between the overshoot and the switching frequency as a higher switching frequency impacts the time required for the charges to decay which directly impacts the magnitude of the resultant electric field at subsequent impulses. Accordingly, fewer PDs with lower magnitudes are associated with higher switching frequencies as the additional stress caused by the overshoot is prompting a higher PD rate at a higher switching frequency.

5.3 Ageing Mechanism and the Impact of Tracking within Turn Insulation

The results of this research demonstrate that resin-rich mica-based insulation used in turn insulation is not immune to ageing under the application of repetitive impulse supply. The ageing mechanism and the life of turn insulation are found to be strongly correlated to the discharge rate. Therefore, it is anticipated that severe PD erosion and the initiation of tracking within the turn insulation are among

the main ageing factors affecting the life of turn insulation. Under a VSC, high dv/dt impulses contain high-frequency components that are blocked by the inductance of the motor coils. This results in the complete jump voltage appearing across the motor coil leading to a high turn-to-turn stress [15], [16]. The overlap and interface layers in the structure of turn insulation assume a major role in the failure process [77]. Turn insulation in a form-wound coil is typically wound in a layered structure by wrapping the resin-infused mica paper around the copper strands. The complete coil is then impregnated with epoxy resin through a vacuum pressure cycle and cured at high temperatures to form rigid insulation. During the manufacturing process, air voids can develop between the layers of the turn insulation. Insufficient penetration of the resin in the overlapped area due to the viscosity of the epoxy resin or the inadequate bonding between the resin and the layered insulation during the curing process are among the main factors contributing to voids in turn insulation [2], [77]. The organic resin in turn insulation tracks if the stress encountered during operation is high enough to ionize the air resulting in discharges in the trapped voids. Heat and ionization by-products generated from PD within voids can cause physical and chemical deterioration to the surface of the void [71], [72]. The overall result is a gradual deterioration of the insulation properties and dielectric strength. Continuous PD can lead to erosion of the epoxy resin and tracking. The ageing state of the cavity is mainly determined by the cavity surface conductivity [72], [81]. Therefore, to demonstrate the deterioration and tracking in an aged void, initial higher surface conductivity and limits are applied as per the values provided in Table 3.7 to simulate the condition of an aged void. Figure 5.9 demonstrates the effects and interactions of the studied factors as per the waveform settings provided in Table 4.6 for the simulated maximum electrical field in an aged void.

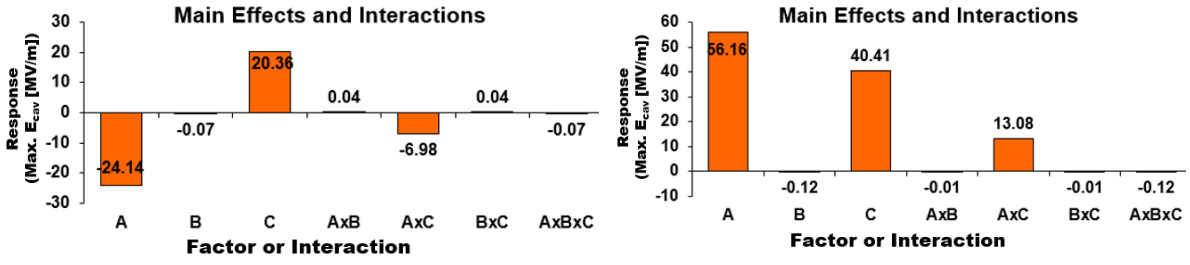

(a) (b)

Figure 5.9 - Analysis of the main effects and interactions based on the simulated maximum electric field in an aged void; (a) per impulse, (b) per unit time.

Unlike the unaged void conditions presented in Figure 5.5 (a) where the effect of the waveform overshoot was the highest followed by the switching frequency, for an aged void, the effect of the switching frequency (when adjusted for the repetition rate effect) becomes higher. This is explained through the impact of the tracking simulated through the increase in the void surface conductivity. Due to the initial higher surface conductivity for an aged void, the resultant electrical field decrements at a faster rate. This means that there is a lower impact of the waveform period, controlled through the switching frequency setting, on the resultant electrical field strength. Accordingly, the effect of the switching frequency is more evident through its impact on the number of cycles per second rather than its impact on the time for the charges to relax. A higher surface conductivity due to tracking around the cavity eventually acts as a shield reducing the strength of the electric field within the cavity or as an electrode extension if bridged to either side of the electrode transferring the maximum electrical stress to the corner of the cavity [72], [86], Figure 5.10.

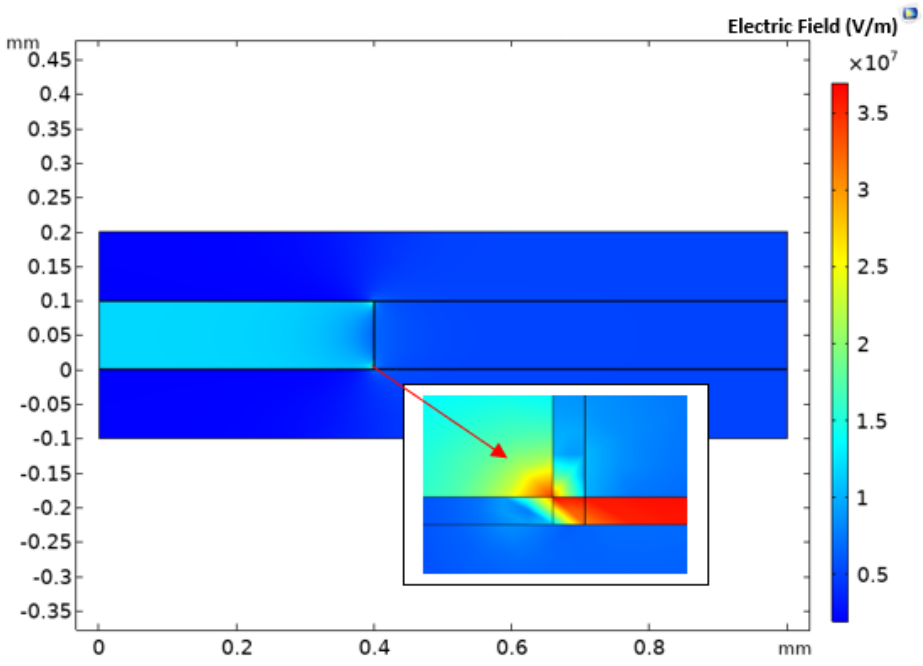

Figure 5.10 - Simulation results of the electrical field under the influence of tracking showing the maximum stress at the corner of the void.

As illustrated in Figure 5.10, tracking shifts the stress from the centre to the corner of the cavity resulting in the propagation of tracking along the interface layer. Therefore, based on the experimental observations and the results reported in Section 4.3, it is evident that incomplete impregnation of epoxy

resin leaving air cavities within the insulation layers is the reason for the initiation of the deterioration process. This is deduced from Figure 4.14 where tracks are observed mainly at the overlap of the insulation layers where trapped air voids are present. This also agrees with the findings reported in [77] where 7 out of 9 failed motors examined pointed towards a PD-related failure in the turn insulation. Further investigation revealed that these turn insulations contained voids created due to the lack of bonding in the insulation and/or the incomplete filling with impregnation resin. Voltage waveform shape and setting determine the electrical stresses and PD that these voids experience. Discharges in voids lead to the propagation of the tracks simultaneously and in opposite directions into the gaps and along the insulation surfaces as shown in Figure 4.17. The continuous discharge activity increases the conductivity of the area around the void leading to further erosion and expansion of the tracks. The localized field is strengthened as a result of erosion and tracking, which also cause the highest electrical stresses to be concentrated around the edges of the void. As the resin-rich mica-based insulation is a composite material (inhomogeneous) and due to the erosion caused by the high electrical stresses, the strength of the material surrounding the void is not the same. This leads to the initiation of several tracking paths, Figure 4.17 (c). The strength of the bulk material is higher than the surface layer and thus the development of tracks on the surface and interface layers rather than penetration through the mica tape [87], [88]. Penetration and electrical treeing can still occur if the tracking path is longer. The continuous and accumulative flow of the charges can lead to a high surface charge concentration at certain points (around the voids) which may cause a local breakdown of the material. Figure 5.11 demonstrates a schematic summarizing the stages of tracking growth between two cavities in a layered structure.

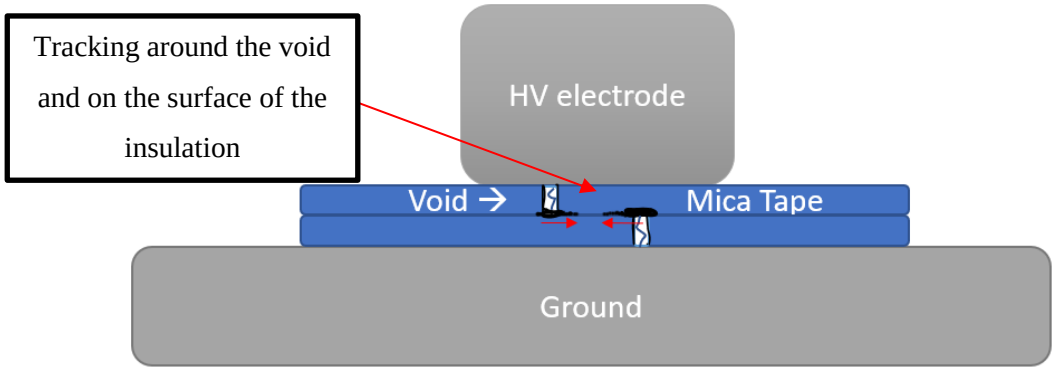

Figure 5.11 - Schematic of tracking growth between two cavities in layered insulation.

The stages of the tracking development between two cavities in layered insulation also agree with the experimental results and the dissected sections of the failed specimens presented in Section 4.3. In the back-to-back turn insulation samples, PDs within the trapped voids cause the surrounding surface to deteriorate. The localized heating at the discharge area causes the surface of the voids to track. Continuous electrical, thermal and mechanical stresses lead to the expansion of these tracks and the development of micro gaps between the electrode and/or the insulation layers by the removal of the bonding material and the increased separation between the layers, Figure 4.15. This leads to new voids and new sources of PDs. The continuous PD and charge injection leads to the slow growth of tracking between the mica flakes and between the insulation layers [87]. The localized enhanced electrical field further enhances the tracking expansion towards the weakest bond directed by the maximum electrical stress, until a full path between the electrodes is formed or the localized final electrical stress is high enough to puncture through the material and bridge the conductors, as per Figure 5.12.

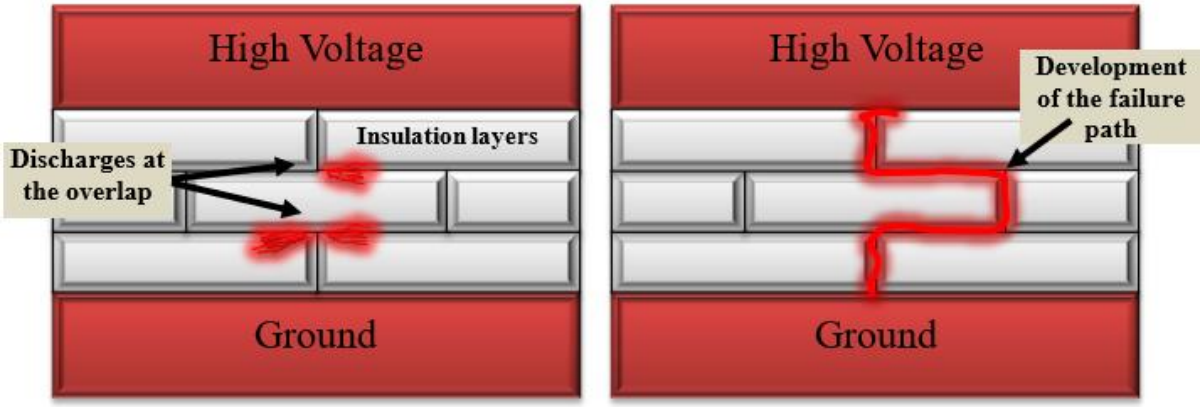

(a) (b)

Figure 5.12 - Schematic showing the stages of tracking development in a multilayer structure; (a) initiation of the discharges at the overlap areas, (b) full growth of the failure path.

Chapter 6
Conclusions and Suggestions for Future Work

6.1 Summary

The main purpose of this research is to provide a comprehensive understanding of the degradation and ageing process of rotating machine Type II form-wound coil turn-to-turn insulation under repetitive impulse energization that simulates an adjustable speed drive. This is done through voltage endurance studies and time-to-failure analysis to establish life plots. PD under various impulse features is measured to evaluate the importance and the role of the studied factors in the ageing process and how they affect the life of turn insulation. The impulse features include jump voltage, step voltage, switching frequency, rise time and overshoot. A full-factorial experiment design is utilized to investigate the role and importance of the studied factors and their interactions. Weibull statistical analysis and their confidence intervals are used to support the conclusions.

To ensure that the experimental work supports the objectives of this research, all samples are made to meet production standards using commercial materials and methods of vacuum pressure injection of epoxy resin frequently used in the manufacture of turn-to-turn insulation of form-wound coils. The additional layer of insulation at the crotch area of the samples reduces the PD activity at the point of separation of the parallel turns which increases the dielectric strength to avoid undesired failures at the crotch. Quality conformance tests of the samples prior to testing and examination of the failures to ensure failures are in the parallel section of the samples validate the proper collection and censoring of the experimental data. In the time-to-failure experiments, replacement of the failed samples with equivalent low inductance capacitors ensures identical load capacitance thereby maintaining the same rise time and overshoot components throughout the experiments.

Another important aspect of the experimental setup is to separate the effect of rise time from the overshoot component. Both factors, rise time and overshoot, are varied independently while investigating their influence on the life of turn insulation. This is very important since different test objects and cable lengths may create different overshoot components even within the same range of rise time. Moreover, depending on the range of the rise time, there may be insignificant changes to the overshoot while varying the rise time of the applied impulses. The embedded effect of the generated overshoot while varying the rise time would, therefore, cause a variation in the outcome of the

experimental work. Hence, the implemented setup ensures proper control of both rise time and overshoot while allowing an independent identification of the role of each factor in the acceleration of the ageing process.

In this work, phase-resolved PD measurements assist in understanding the behaviour of generated discharges by relating the changes in their features to the time-to-failure results in the voltage endurance tests. This is conducted as an independent study on separate samples of both back-to-back and single cavity layered insulation specimens to investigate the changes in the PD features in response to the changes in the switching frequency, rise time, and overshoot factors. The experimental results from both PD measurements and the time-to-failure experiments are used in identifying the significant factors in the ageing process as well as confirming the ageing mechanism involved. Finite element method simulations are used to help explain and support the experimental findings and to describe the ageing and failure mechanisms of the turn insulation in accordance with the experimental observations.

6.2 Conclusions

The findings in this research lead to the following conclusions:

- Contrary to the current IEC 60034-18-42 standard, accelerated ageing under sinusoidal voltage does not represent the life endurance of Type II turn insulation under unipolar repetitive impulse energization. The results presented in this work suggest a non-linear effect of the supply switching frequency on the life of turn insulation. Despite the fact that a linear relationship with frequency may hold under sinusoidal voltage stress, the same is not applicable under repetitive impulse voltages.
- The life of turn insulation is substantially influenced by the shape of the waveform applied. Particular emphasis is made toward the role of the overshoot as a major factor in the life assessment of turn insulation. Time-to-failure results show that even at similar jump voltages applied, waveforms that have a higher overshoot ratio exhibit a higher ageing rate on turn insulation resulting in a significant reduction in their life expectancy. Therefore, it is important to consider the overshoot as an independent factor from the jump voltage when evaluating turn insulation endurance.
- Based on the voltage endurance tests and the analysis of the average PD rate per unit time, research findings show that the jump voltage, switching frequency and overshoot of the

voltage waveform are among the main factors affecting the lifespan of machines turn insulation; whereas, the effect of the rise time is found to be minimal within the considered range. This impact of the rise time, although minor, was found to be consistent at steeper waveforms applied (less than 600 ns) which can be concerning as the drive industry is moving towards faster switching capabilities through the use of the next generation wide band-gap switching devices.

- Evidence presented in this research points toward a considerable interaction between switching frequency, jump voltage and the overshoot ratio on the life of turn insulation which may lead to considerable error in the estimation of the turn insulation endurance if otherwise ignored.

The following serve as the main contributions and outcomes of this research:

- Characterization of the influence of the voltage source converter supply features; in particular, switching frequency, rise time, jump voltage, step voltage, and overshoot, on the turn insulation life assessment which provides an in-depth understanding of the turn insulation ageing and failure mechanisms. This work contributes to the ongoing efforts to enhance our overall understanding of the stresses imposed by inverter drives and serves as a guideline in evaluating turn insulations under repetitive impulse supply which may support the further development of the current version of the IEC 60034-18-42 qualification standard.

- Creation of a life plot of Type II turn insulation under repetitive impulse switching supply as the current reference life plot provided by the IEC 60034-18-42 standard – and used by manufacturers who lack a reference lifeline with which to evaluate their machine insulation – is based on data collected under sinusoidal supply.

- Enables a foundation for the future application of wide band-gap fast switching devices in variable speed drives by identifying the interaction stresses of rise time and overshoot factors that are anticipated in the use of these devices.

- Introduces the waveform overshoot as an additional factor impacting the life of turn insulation; distinguishing it from the rise time and the jump voltage effect. While the IEC qualification standard identifies the jump voltage as a main factor impacting the insulation

life, it does not specify or signify the unique influence of the overshoot. This identification highlights a major factor which can be employed and utilized by manufacturers and drive system designers to enhance the performance of the machine insulation and improve the designs of their drive and machine systems.

- Identifies the correlation between partial discharges and the endurance of turn-to-turn insulation through the average discharge rate per unit time. This correlation serves as a guideline for designing long-term ageing experiments and identifying the main factors and interactions to be considered.

6.3 Suggestions for Future Work

The following are suggestions for future work:

- Full-size coil endurance studies are suggested to ensure the correlation between samples used in this study and those obtained from the endurance testing of back-to-back turn insulation specimens.
- Other factors such as the pulse polarity, duty cycle, or the number of inverter output levels may influence the performance of turn insulation. Investigating the effects of these factors and their interactions with other features of the converter supply constitute an important next step toward the full comprehension of the effects of VSC supply on machine turn insulation.
- Studying the performance of different insulation materials or the effect of changing the size of the strands, the number of insulation layers or the overlapping profile on the strength of the insulation is of great importance to machine manufacturers to improve their insulation designs.
- This research applies to machines operating at standard conditions of pressure, temperature and humidity. Machines operating at high altitudes with reduced atmospheric pressure, particularly in mines, may be subjected to accelerated ageing conditions even under normal operating voltages. Therefore, it would be of interest in such applications to include the impact of such extreme conditions on the ageing process and the performance of turn insulation.

References

[1] G. Stone, E. A. Boulter, I. Culbert and H. Dhirani, Electrical insulation for rotating machines: design, evaluation, aging, testing, and repair, Wiley-IEEE Press, 2004.

[2] S. U. Haq, A study on insulation problems in drive fed medium voltage induction motors, Ph.D. Thesis, University of Waterloo, Ontario, Canada, 2007.

[3] Rotating electrical machines - Part 18-41: Partial discharge free electrical insulation systems (Type I) used in rotating electrical machines fed from voltage converters - Qualification and quality control tests, IEC 60034-18-42:2019, Ed.1.1, 06, 2019.

[4] Rotating electrical machines - Part 18-42: Partial discharge resistant electrical insulation systems (Type II) used in rotating electrical machines fed from voltage converters - Qualification tests, IEC 60034-18-42:2020, Ed.1.1, 08, 2020.

[5] M. Ghassemi, "Accelerated insulation aging due to fast, repetitive voltages: A review identifying challenges and future research needs," *IEEE Transactions on Dielectrics and Electrical Insulation*, vol. 26, no. 5, pp. 1558-1568, Oct. 2019.

[6] M. S. Moonesan, A study of medium and high voltage form-wound coil turn-to-turn insulation of converter fed rotating machines, Ph.D. Thesis, University of Waterloo, Ontario, Canada, 2016.

[7] W. Yin, L. Durantay, L. Zhang, S. U. Haq and F. Vannay, "End winding protections improvements helping to downsize dV/dt filter for medium voltage machine fed by NPP multi-levels VSI drive," in *2018 IEEE 2nd International Conference on Dielectrics (ICD)*, Budapest, 2018.

[8] A. Contin, *Design and testing of insulation for adjustable speed drives*, France: T4-Part 1, International Conference on Electrical Machins (ICEM), September 2, 2012.

[9] M. Ghassemi, "High power density technologies for large generators and motors for marine applications with focus on electrical insulation challenges," *IET-High voltage*, vol. 5, no. 1, pp. 7-14, Feb. 2020.

[10] B. Lloyd, *Effects of modern variable speed drives on motor winding insulation,* Alberta, Canada: IEEE-NCS, IAS/PES, 2017.

[11] A. Naeini, A study of stress grading system of medium voltage motor fed by adjustable speed drives, Ph.D. Thesis, University of Waterloo, Ontario, Canada, 2019.

[12] F. Espino, Stress grading materials evaluation and performance, Ph.D. Thesis, Ontario, Canada: University of Waterloo, 2002.

[13] E. Sharifi, Analysis of electrical and thermal stresses in the stress relief system of inverter fed medium voltage motors, Ph.D. Thesis, University of Waterloo, Ontario, Canada, 2010.

[14] J. C. G. Wheeler, "Effects of converter pulses on the electrical insulation in low and medium voltage motors," *IEEE Electrical Insulation Magazine,* vol. 21, no. 2, pp. 22-29, March-April 2005.

[15] A. Krings, G. Paulsson, F. Sahlén and B. Holmgren, "Experimental investigation of the voltage distribution in form wound windings of large AC machines due to fast transients," in *2016 XXII International Conference on Electrical Machines (ICEM)*, Lausanne, 2016.

[16] M. Stranges, G. Stone and D. L. Bogh, "Progress on IEC 60034-18-42 for qualification of stator insulation for medium-voltage inverter duty applications," in *2007 IEEE Petroleum and Chemical Industry Technical Conference*, Calgary, Alta, 2007.

[17] G. B. Kliman, W. J. Premerlani, R. A. Koegl and D. Hoeweler, "Sensitive, on-line turn-to-turn fault detection in AC motors," *Electric Machines & Power Systems*, pp. 915-927, 28 10 2000.

[18] Mohan, Undeland and Robbins, Power electronics: converters, applications, and design, 3rd Edition, John Wiley & Sons Inc., 2003.

[19] M. Rashid, Power electronics: circuits, devices, and applications, 3rd Edition, Pearson-Prentice Hall, 2003.

[20] H. Abu-Rub, S. Bayhan, S. Moinoddin, M. Malinowski and J. Guzinski, "Medium-voltage drives: challenges and existing technology," *IEEE Power Electronics Magazine,* vol. 3, no. 2, pp. 29-41, June 2016.

[21] B. Wu, High-power converters and AC drives, IEEE Press Wiley Inter Science, 2006.

[22] A. Morya, M. Moosavi, M. C. Gardner and H. A. Toliyat, "Applications of wide bandgap (WBG) devices in AC electric drives: A technology status review," in *2017 IEEE International Electric Machines and Drives Conference (IEMDC)*, Miami, FL., 2017.

[23] Adjustable speed electrical power drive systems – Part 8: Specification of voltage on the power interface, Technical Specification, IEC/TS 61800-8, Edition 1.0 2010-05.

[24] F. Alferink, "meettechniek.info," [Online]. Available: https://meettechniek.info/compendium/signal-parameters.html. [Accessed 4 April 2020].

[25] P. Seri, G. C. Montanari and R. Hebner, "Partial discharge phase and amplitude distribution and life of insulation systems fed with multilevel inverters," in *2019 IEEE Transportation Electrification Conference and Expo (ITEC)*, Detroit, MI, USA, 2019.

[26] K. Wu, T. Okamoto and Y. Suzuoki, "Effects of discharge area and surface conductivity on partial discharge behavior in voids under square voltages," *IEEE Trans. on Dielectrics and Electrical Insulation*, vol. 14, no. 2, pp. 461-470, 2007.

[27] D. Manns, S. Galioto, K. Weeber and J. Yagielski, "High frequency life testing of stator coil insulation," in *Conference Record of the 2008 IEEE International Symposium on Electrical Insulation*, Vancouver, BC, 2008.

[28] A. Cavallini, D. Fabiani and G. C. Montanari, "Power electronics and electrical insulation systems - part 2: life modeling for insulation design," *IEEE Electrical Insulation Magazine*, vol. 26, no. 4, pp. 33-39, July-Aug. 2010.

[29] P. Wang, A. Cavallini and G. C. Montanari, "Endurance testing of rotating machines insulation systems: Do sinusoidal and square voltage waveforms provide comparable results?," in *2013 IEEE International Conference on Solid Dielectrics (ICSD)*, Bologna, 2013.

[30] B. Florkowska, J. Roehrich, P. Zydroi and M. Florkowski, "Measurement and analysis of surface partial discharges at semi-square voltage waveforms," *IEEE Transactions on Dielectrics and Electrical Insulation*, vol. 18, no. 4, pp. 990-996, August 2011.

[31] M. S. Moonesan, S. H. Jayaram and E. A. Cherney, "Time to failure of medium-voltage form-wound machine turn insulation stressed by unipolar square waves," *IEEE Transactions on Dielectrics and Electrical Insulation,* vol. 22, no. 6, pp. 3118-3125, December 2015.

[32] M. S. Moonesan, S. H. Jayaram and E. A. Cherney, "Study on form-wound machine turn insulation subjected to unipolar and bipolar square waves," *IEEE Transactions on Dielectrics and Electrical Insulation,* vol. 23, no. 6, pp. 3242-3248, Dec. 2016.

[33] E. Lindell, T. Bengtsson, J. Blennow and S. M. Gubanski, "Influence of rise time on partial discharge extinction voltage at semi-square voltage waveforms," *IEEE Transactions on Dielectrics and Electrical Insulation,* vol. 17, no. 1, pp. 141-148, February 2010.

[34] F. Sahlén, L. Ming, K. Johansson, E. Mårtensson and O. Koponen, "Investigation of mica based insulation for high voltage machines subjected to repetitive pulsed voltage," in *2010 IEEE International Symposium on Electrical Insulation*, San Diego, CA, 2010.

[35] F. Sahlén, G. Paulsson and E. Mårtensson, "Life-time investigation of mica-based insulation for high voltage machines subjected to converter-like voltages," in *2016 IEEE Electrical Insulation Conference (EIC)*, Montreal, QC, 2016.

[36] G. C. Montanari and P. Seri, "The effect of inverter characteristics on partial discharge and life behavior of wire insulation," *IEEE Electrical Insulation Magazine,* vol. 34, no. 2, pp. 32-39, 2018.

[37] G. C. Montanari, F. Negri and F. Ciani, "Partial discharge and life behavior of rotating machine wire insulation under PWM waveforms: The influence of inverter characteristics," in *2017 IEEE Electrical Insulation Conference (EIC)*, Baltimore, MD, 2017.

[38] G. C. Montanari, "Time behavior of partial discharges and life of type II turn insulation specimens under repetitive impulse and sinusoidal waveforms," *IEEE Electrical Insulation Magazine,* vol. 33, no. 6, pp. 17-26, November-December 2017.

[39] G. C. Montanari, A. Cavallini, F. Ciani and A. Contin, "Accelerated aging, partial discharges and breakdown of Type II turn-to-turn insulation system of rotating machines," in *2016 IEEE Electrical Insulation Conference (EIC)*, Montreal, QC, 2016.

[40] D. Fabiani, G. Montanari, A. Cavallini and G. Mazzanti, "Relation between space charge accumulation and partial discharge activity in enameled wires under PWM-like voltage waveforms," *IEEE Transactions on Dielectrics and Electrical Insulation,* vol. 11, no. 3, pp. 393-405, June 2004.

[41] D. Fabiani, G. Montanari and A. Contin, "Aging acceleration of insulating materials for electrical machine windings supplied by PWM in the presence and in the absence of partial discharges," in *ICSD'01. Proceedings of the 2001 IEEE 7th International Conference on Solid Dielectrics (Cat. No.01CH37117)*, Eindhoven, Netherlands, 2001, 2001.

[42] P. Wang, A. Cavallini and G. C. Montanari, "The influence of impulsive voltage frequency on PD features in turn insulation of inverter-fed motors," in *2014 IEEE Conference on Electrical Insulation and Dielectric Phenomena (CEIDP)*, Des Moines, IA, 2014.

[43] P. Wang, A. Cavallini and G. C. Montanari, "The effect of impulsive voltage rise time on insulation endurance of inverter-fed motors," in *2015 IEEE 11th International Conference on the Properties and Applications of Dielectric Materials (ICPADM)*, Sydney, NSW, 2015.

[44] L. Benmamas, P. Teste, E. Odic, G. Krebs and T. Hamiti, "Contribution to the analysis of PWM inverter parameters influence on the partial discharge inception voltage," *IEEE Transactions on Dielectrics and Electrical Insulation,* vol. 26, no. 1, pp. 146-152, Feb. 2019.

[45] P. Wang, A. Cavallini, G. C. Montanari and G. Wu, "Effect of rise time on PD pulse features under repetitive square wave voltages," *IEEE Transactions on Dielectrics and Electrical Insulation,* vol. 20, no. 1, pp. 245-254, 2013.

[46] K. Kimura, S. Ushirone, T. Koyanagi, Y. Iiyama, S. Ohtsuka and M. Hikita, "Study of PD behaviors on a crossed sample of magnet-wire with repetitive bipolar impulses for inverter-fed motor coil insulation," in *CEIDP '05. 2005 Annual Report Conference on Electrical Insulation and Dielectric Phenomena*, Nashville, TN, USA, 2005.

[47] W. Yin, "Failure mechanism of winding insulations in inverter-fed motors," *IEEE Electrical Insulation Magazine,* vol. 13, no. 6, pp. 18-23, Nov.-Dec. 1997.

[48] S. Grzybowski, E. Feilat and P. Knight, "Accelerated aging tests on magnet wires under high frequency pulsating voltage and high temperature," in *1999 Annual Report Conference on Electrical Insulation and Dielectric Phenomena (Cat. No.99CH36319)*, Austin, TX, USA, 1999.

[49] T. J. Å. Hammarström, "Partial discharge characteristics within motor insulation exposed to multi-level PWM waveforms," *IEEE Transactions on Dielectrics and Electrical Insulation*, vol. 25, no. 2, pp. 559-567, April 2018.

[50] T. J. Å. Hammarström, "Partial discharge characteristics at ultra-short voltage risetimes," *IEEE Transactions on Dielectrics and Electrical Insulation*, vol. 25, no. 6, pp. 2241-2249, Dec 2018.

[51] R. Leuzzi, V. G. Monopoli, F. Cupertino and P. Zanchetta, "Active ageing control of winding insulation in high frequency electric drives," in *2018 IEEE Energy Conversion Congress and Exposition (ECCE)*, Portland, OR, 2018.

[52] T. Hammarström, "Multi-rise time PWM: A way to reduce PD exposure in motor windings," *IEEE Transactions on Dielectrics and Electrical Insulation*, vol. 27, no. 2, pp. 613-621, April 2020.

[53] D. E. Moghadam, J. Speck, S. Grossmann and J. Stahl, "Parameters affecting the turn insulation lifetime and durability," *IEEE Transactions on Dielectrics and Electrical Insulation*, vol. 25, no. 2, pp. 516-523, April 2018.

[54] S. U. Haq, S. H. Jayaram and E. A. Cherney, "Evaluation of medium voltage enameled wire exposed to fast repetitive voltage pulses," *IEEE Transactions on Dielectrics and Electrical Insulation*, vol. 14, no. 1, pp. 194-203, Feb. 2007.

[55] W. Chen, G. Gao and C. A. Mouton, "Stator insulation system evaluation and improvement for medium voltage adjustable speed drive applications," in *2008 55th IEEE Petroleum and Chemical Industry Technical Conference*, Cincinnati, OH, 2008.

[56] D. C. Montgomery, Design and analysis of experiments, Eighth Edition, John Wiley & Sons, Inc, 2013.

[57] "American national standard for magnet wire, ANSI/NEMA MW 1000-2018," National Electrical Manufacturers Association, 1300 North 17th Street, Suite 900 • Rosslyn. VA 22209, 2019.

[58] I. M. Jarrar, E. A. Cherney and S. H. Jayaram, "Switching wave characteristics affecting the life of Type II machine turn insulation," *IEEE Transactions on Dielectrics and Electrical Insulation,* 2022.

[59] I. M. Jarrar, E. A. Cherney and S. H. Jayaram, "Ageing and the life curve of Type II turn-to-turn insulation under repetitive impulse energization: effect of switching frequency," in *2021 IEEE Conference on Electrical Insulation and Dielectric Phenomena (CEIDP)*, 2021.

[60] "Rotating electrical machines - Part 27-1: Off-line partial discharge measurements on the winding insulation," *IEC Standard 60034-27-1: Edition 1,* 2017-01.

[61] "IEC/IEEE guide for the statistical analysis of electrical insulation breakdown data (Adoption of IEEE Std 930-2004)," *IEC 62539 First Edition 2007-07 IEEE 930,* 2007.

[62] I. M. Jarrar, E. A. Cherney and S. H. Jayaram, "Effect of repetitive impulse waveform characteristics on partial discharges in Type II turn-to-turn insulation," *IEEE Transactions on Dielectrics and Electrical Insulation,* vol. 29, no. 3, pp. 1183-1190, June 2022.

[63] Y. Yu, Design and development of IGBT based pulse voltage generator for insulation testing, M.S. Thesis, Waterloo, ON: University of Waterloo, 2009.

[64] R. Aldrian, G. C. Montanari, A. Cavallini and Suwarno, "Statistical analysis for internal and surface discharges identification in XLPE insulation under AC voltages," in *in 2017 Int. Conf. High Volt. Eng. and Power Syst. (ICHVEPS)*, 2017.

[65] High-voltage test techniques – Partial discharge measurements, IEC 60270, Edition 3.1, 2015-11.

[66] R. Abernethy, The new Weibull handbook (5th edition), Abernethy, 2006.

[67] "Quality tools; design of experiment," American Society for Quality (ASQ), available on www.ASQ.org, April 2020.

[68] D. C. Montgomery and R. G. C., Applied statistics and probability for engineers, Sixth Edition ed., WILEY, 2014.

[69] AC/DC module user's guide, COMSOL Multiphysics® v. 5.6, COMSOL AB, Stockholm, Sweden, 2021.

[70] "Conductofol 2371 Data Sheet," ISOVOLTA AG . High Voltage, 2355 Wiener Neudorf, Austria, 2008-12-01.

[71] H. Illias, G. Chen and P. L. Lewin, "Partial discharge behavior within a spherical cavity in a solid dielectric material as a function of frequency and amplitude of the applied voltage," *IEEE Transactions on Dielectrics and Electrical Insulation,* vol. 18, no. 2, pp. 432-443, April 2011.

[72] L. Niemeyer, "A generalized approach to partial discharge modeling," *IEEE Transactions on Dielectrics and Electrical Insulation,* vol. 2, no. 4, pp. 510-528, Aug. 1995.

[73] C. Forssen and H. Edin, "Partial discharges in a cavity at variable applied frequency part 2: measurements and modeling," *IEEE Transactions on Dielectrics and Electrical Insulation,* vol. 15, no. 6, pp. 1610-1616, December 2008.

[74] John R. Rumble, ed., CRC handbook of chemistry and physics, 103rd Edition (Internet Version 2022), CRC Press/Taylor & Francis, Boca Raton, FL.

[75] T. Hammarström, "A measurement set-up method to evaluate motor winding quality and winding insulation by exploring discharge characteristics," in *2018 21st International Conference on Electrical Machines and Systems (ICEMS)*, 2018.

[76] M. Florkowski, "Accumulative effect of partial discharges at impulse voltage wave tail," *IET Science, Measurement & Technology,* vol. 14, no. 5, pp. 505-513, 2020.

[77] G. C. Stone, B. K. Gupta, M. Kurtz and D. K. Sharma, "Investigation of turn insulation failure mechanisms in large AC motors," *IEEE Transactions on Power Apparatus and Systems,* Vols. PAS-103, no. 9, pp. 2588-2595, Sept. 1984.

[78] A. Rumi, J. G. Marinelli, A. Cavallini and P. Seri, "Can corona resistant wires ensure reliability in aerospace machine insulation?," in *2022 IEEE Electrical Insulation Conference (EIC)*, 2022.

[79] R. J. Van Brunt, "Stochastic properties of partial-discharge phenomena," *IEEE Transactions on Electrical Insulation,* vol. 26, no. 5, pp. 902-948, Oct. 1991.

[80] S. Morsalin, B. T. Phung and A. Cavallini, "Measurement and modeling of partial discharge arising from different cavity geometries at very low frequency," *IEEE Transactions on Dielectrics and Electrical Insulation,* vol. 27, no. 4, pp. 1110-1118, Aug. 2020.

[81] F. Gutfleisch and L. Niemeyer, "Measurement and simulation of PD in epoxy voids," *IEEE Transactions on Dielectrics and Electrical Insulation,* vol. 2, no. 5, pp. 729-743, Oct. 1995.

[82] H. A. Illias, M. A. Tunio, H. Mokhlis, G. Chen and A. H. A. Bakar, "Determination of partial discharge time lag in void using physical model approach," *IEEE Transactions on Dielectrics and Electrical Insulation,* vol. 22, no. 1, pp. 463-471, Feb. 2015.

[83] B. Fruth and L. Niemeyer, "The importance of statistical characteristics of partial discharge data," *IEEE Transactions on Electrical Insulation,* vol. 27, no. 1, pp. 60-69, Feb. 1992.

[84] E. Kuffel, W. Zaengl and J. Kuffel, High voltage engineering fundamentals, Butterworth-Heinemann, 2000.

[85] M. S. Moonesan, S. H. Jayaram and E. A. Cherney, "Impact of charge accumulation on insulation films subjected to unipolar and bipolar square waves," *IEEE Transactions on Dielectrics and Electrical Insulation,* vol. 24, no. 4, pp. 2626-2632, 2017.

[86] C. Calebrese, D. Smith, L. Zhang and W. Zhong, "Resistively graded insulation system for next-generation converter-fed motors," General Electric, Global Research Center, Niskayuna, NY (United States), 2018.

[87] Y. J. Kim and J. K. Nelson, "Assessment of deterioration in epoxy/mica machine insulation," *IEEE Transactions on Electrical Insulation,* vol. 27, no. 5, pp. 1026-1039, Oct. 1992.

[88] R. Vogelsang, T. Farr and K. Frohlich, "The effect of barriers on electrical tree propagation in composite insulation materials," *IEEE Transactions on Dielectrics and Electrical Insulation,* vol. 13, no. 2, pp. 373-382, April 2006.